The Thesis Committee for Sarah Blake Bateman
Certifies that this is the approved version of the following thesis:

Earliest Turbidite Emplacement (~6.3 -5.6 Ma) in the Newly Opening Gulf of California (Fish Creek-Vallecito Basin)

APPROVED BY
SUPERVISING COMMITTEE:

Supervisor:

Ronald J. Steel

David Mohrig

Cornel Olariu

Kitty L. Milliken

Earliest Turbidite Emplacement (~6.3 -5.6 Ma) in the Newly Opening Gulf of California (Fish Creek-Vallecito Basin)

by

Sarah Blake Bateman, B.S.

Thesis

Presented to the Faculty of the Graduate School of

The University of Texas at Austin

in Partial Fulfillment

of the Requirements

for the Degree of

Master of Science in Geological Sciences

The University of Texas at Austin

May 2015

Dedication

To my parents, Inga and Skip, and my sister and brother, Ashley and David.

Acknowledgements

First, I would like to thank my supervisor, Ronald steel, for his insight and guidance throughout my graduate career. Thank you to Cornel Olariu for your help in the field as well as in the office, you always took the time to help me out no matter how busy you may have been. Thank you to David Mohrig for sharing your knowledge and providing me with advice and direction throughout the thesis writing process. A special thanks to Kitty Milliken for your guidance along the way as well as spurring my interest in petrography through my favorite class at UT, Siliciclastic Petrology.

A special thanks to Lyn Murray for all of your help with sample collecting and permitting, and being an insightful contact at Anza-Borrego Desert State Park. I especially enjoyed learning about the Park's rich history and touring its paleontology collection with you.

I greatly appreciate all of the input from Dynamic Stratigraphy group, both in the office and at our weekly meetings at Double Dave's. I am especially grateful for all of the guidance and introspect I received out in the Borrego Desert from Jeremy Slaugenwhite and Rattanaporn Fongern while collecting data. A special thanks to Michael Cloos, for all of the support both in the field and during the thesis writing process, I couldn't have come this far without you.

Thank you to the Riomar Consortia and Jackson School of Geosciences for providing me the means to study out in the California Desert for the past two years.

Finally, I would like to thank my parents, Inga and Skip, for all of their support along the way. Although they may not be familiar with sedimentology or even know what a turbidite may

be, they have offered their unconditional support. I could not have possibly achieved any of this without them.

Abstract

Earliest Turbidite Emplacement (~6.3 -5.6 Ma) in the Newly Opening Gulf of California (Fish Creek-Vallecito Basin)

Sarah Blake Bateman, MS Geo Sci

The University of Texas at Austin, 2015

Supervisor: Ronald J. Steel

The Fish Creek-Vallecito Basin chronicles late Miocene through Pleistocene sedimentation into the newly rifting Gulf of California. Initial rifting in the basin began around 8.0 Ma, subsequently followed by sedimentation of locally derived alluvial fan conglomerates. Subsequent deepening of the basin created conditions for deposition of subaqueous gravity flow deposits. The deposition of the initial marine sediments is known lithostratigraphically as the Lycium Member turbidites (~6.3 to 5.6 Ma) of the Latrania Formation, comprising a thick succession of coarse-grained sediment up to 115m in thickness. Sedimentation and facies distribution throughout the system is a direct result of the tectonically derived topography in this rift basin environment. Detailed study of the facies distribution and nature of the sediment fill allows for realization of models of facies variability in rift basin environments.

Deposition of this turbidite succession is somewhat problematic. A significant run-out distance as well as water depth is needed to deposit a turbidite succession of this magnitude and although there is currently no field evidence of a transitional shoreline or delta system previous detrital zircon analysis suggests a possible more northerly source. This study aims to seek out the processes which led to a thick turbidite succession in an early rift basin sequence and provide a complete picture of source-to-sink deposition.

In depth analysis of turbidite architecture variability was conducted using over 500 m of outcrop logged section taken laterally throughout the 7 km outcrop belt. Lithofacies and architectural variability, reconstructed and imaged using correlation of high resolution sections and photo panel interpretations, show a transition from a proximal to distal basin floor fan environment. Provenance data, constrained through petrographic inspection of samples taken systematically throughout the system, indicate that the initial marine sediments deposited in the Miocene-Gulf of California are derived from the neighboring Peninsular Range Batholith. In depth stratigraphic analysis coupled with provenance study allows us to decipher the depositional history and basin paleogeography during initial marine inundation into the newly formed Gulf of California. A paleogeographic model of the Late Miocene (~6.3 to 5.6 Ma) is proposed. Sediment was transported from the northwest to the southeast along the West Salton Detachment Fault, depositing in a basin floor fan system.

Table of Contents

List of Figures

1. INTRODUCTION

The Fish Creek-Vallecito Basin of southern California exposes the infill of the Late Miocene to Pleistocene Gulf of California which was deposited in an extensional rift basin setting. Late Miocene marine deposits of the Fish Creek-Vallecito Basin represent the earliest marine deposits that entered the paleo-Gulf of California. At this early stage very locally derived boulder-rich debris flow deposits interfingered with a coarse-grained, sand-rich turbidite system that had entered, also locally, but from farther north and west. Previous workers recognized these sediments as marine turbidite deposits but did not focus on the lateral and vertical heterogeneity of the system, nor on paleogeographic or source-to-sink context of the turbidites.. The present study's main objective is to:

(1) define the main architectural elements and the processes which contributed to the development of the thick, Lyceum submarine fan system and,

(2) make the first attempt at a paleogeographic reconstruction for the Latrania Formation (~ 6.3 Ma), in this segment of the early Gulf of California rift basin, using provenance (15 samples) and paleocurrent data to infer the transport direction of sediment into the basin and further constrain its source. This is important because the Lycium turbidites are coming from farther afield than the associated alluvial fans and the mass transport complexes.

1.2 GEOLOGIC BACKGROUND

1.2.1 Geologic Setting

The Fish Creek-Vallecito Basin records late Miocene through Pleistocene sedimentation into the newly rifted Gulf of California. The basin is currently located to the west of the Salton Trough that is bordered on its east side by the San Andreas Fault. Dextral movement along the San Andreas Fault during the last 1My transposed the Fish Creek-Vallecito Basin far to the north of its Miocene position in the Gulf of California. The basin is one of many in the Gulf Extensional Province in which late strike-slip faulting created small depocenters in areas of transtension (Dorsey et al., 2011). Accommodation in the Fish Creek-Vallecito Basin was originally created by extreme extension along the low-angle West Salton Detachment around 8 Ma. The Miocene basin, with an infill, consisting of terrestrial and marine sediments sourced from local basement rocks, is therefore classed as a supra-detachment basin. After the early, irregularly shaped basin was partially infilled by local sources, it was still low-lying and covered by some 4-500m of marine, Gulf of California seawater. By about 5.4Ma the submarine Fish Creek area of the Gulf was being encroached from the north by a thick sedimentary prism driven largely by the newly arrived Colorado River (Rebecca J. Dorsey et al. 2011; Shirvell et al. 2009). The sedimentary prism was not just a large deltaic and river pile of sediment, it was an entire deep water shelf margin with submarine fan deposits (Wind Caves), overlain by deep water slope deposits (Mud Hills), overlain by shelf platform deposits (Yuha), overlain by Colorado River Delta deposits (Camels Head), and finally overridden by the distributaries of the Colorado River itself. The whole southward migrating Colorado sedimentary prism was nearly a 1km high with respect to the submarine Fish Creek basin floor fans. Subsequent episodes of abandonment of the area by the Colorado River occurred from the Late Pliocene through Pleistocene and resulted

in deposition of local basement-sourced sediment in fluvial and lacustrine settings across the Fish Creek region. A Pleistocene fanning dip interval marks a halt to the extension leading to short-term wrench tectonism which has since exhumed the sediments of the Fish Creek-Vallecito Basin in the last 1 Ma. At present, the basin is bound to the northwest by the Vallecito Mountains and the Fish Creek Mountains to the east. (Dorsey et al. 2012; Winker 1987)

Miocene

Sedimentation into the Fish Creek-Vallecito Basin began during the Early Miocene with deposition of eolian sands filling the chaotic paleotopography attributed to the erosion of the peninsular ranges batholith (Dorsey 2010). These sandstone deposits were then overlain by the volcanics of the Middle Miocene Alverson formation Dorsey 2010). During the Mid to Late Miocene minor regional extension caused the formation of high-angle normal faults (Winker and Kidwell, 1996), this extension was most likely induced by early movement along the West Salton Detachment Fault (Axen and Fletcher 1998). Between 7 and 6 Ma, rapid marine incursion throughout the Salton Trough region took place (Dorsey 2010) (Fig. 1-1). Cause for this rapid flooding is still debated. Early workers suggested it was the result of a major tectonic change in the region. Dorsey et al.(2007) hypothesized that rapid marine incursion was the result of 'accelerated basin subsidence and crustal thinning related to initiation of the active plate boundary in the Salton Trough' coupled with a global rise in sea level (Dorsey 2010). Later Dorsey et al (2011) showed that there was no real increase in the subsidence rate of this region at this time, and no documented global sea-level rise either. We suggest that the early Fish Creek Basin was simply very low-lying and below sea level, and that a barrier into the region was discontinuously breached to allow first the Fish Creek Gypsum to accumulate in the basin, then the Lycium turbidites, prior to the arrival of the Colorado shelf margin prism.

Pliocene to Early Pleistocene

Continuous subsidence, driven by the relative plate motion in the northern Gulf-Salton Trough and further slip along the West Salton Detachment Fault, coupled with marine incursion and transgression influenced Colorado River delta progradation through the area (Dorsey 2010). The transition from deep water marine sediment to distal prodelta deposits took place throughout the Pliocene (Dorsey et al., 2007, 2010). During the late Pliocene to Early Pleistocene, abandonment of the Colorado River caused a transition from marine to nonmarine sedimentation and deposition was controlled by locally sourced alluvial fans and braided streams around the basin margin (Winker and Kidwell 1996; Dorsey 2010).

Pleistocene to Modern

Around 1 Ma, slip on the West Salton Detachment Fault halted and a major tectonic reorganization initiated movement along the San Jacinto and Elsinore faults (Dorsey et al. 2011). During this reorganization, subsequent uplift of the Fish Creek-Vallecito Basin took place, exhuming Mio-Pliocene sediments (Dorsey et al. 2011). Strike-slip faulting attributed to movement along the Elsinore and San Jacinto Faults allows for present exposure and uplift of these older deposits. The modern Fish-Creek Vallecito Basin is somewhat chaotic, with modern strike-slip faulting and northwestern trending ridges (Dorsey 2010).

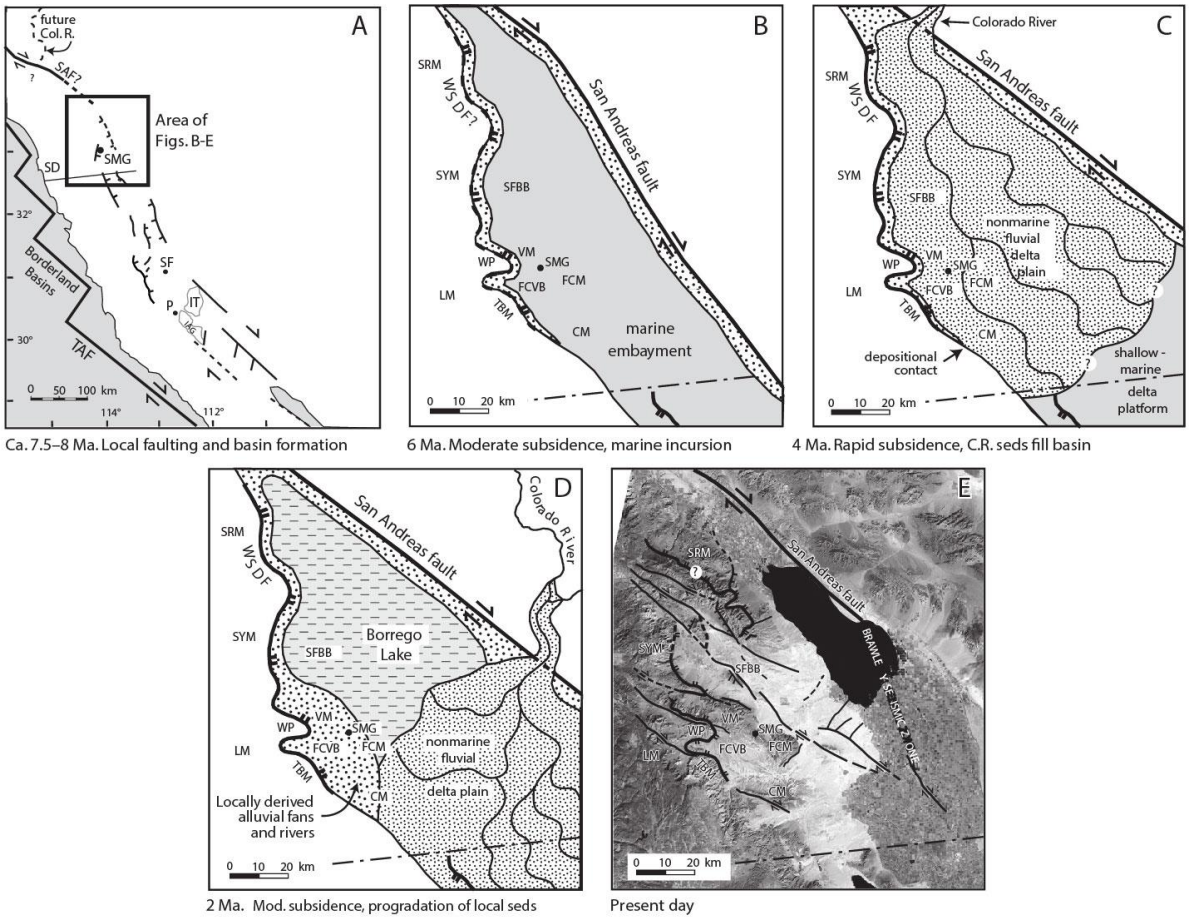

Figure 1-1: Paleogeographic reconstructions of the Salton Trough and surrounding region at 7.5 to 8, 6, 4 and 2Ma. (From Dorsey et al. 2011)

1.2.2 Stratigraphic Background

The stratigraphy exposed in the Fish Creek-Vallecito Basin near Split Mountain Gorge consists of three major lithostratigraphic units organized into groups based on depositional setting, these groups are illustrated in Figure (1-2). Designation of individual groups, and subgroups within, are based on the terminology used by (Winker and Kidwell 1996), which was later revised by Dorsey et al. (2007). These units include the Split Mountain, Imperial and Palm Spring Groups and record sedimentation of the Fish Creek-Vallecito Basin from the Middle Miocene to Late Pliocene. Further subdivision of the lithostratigraphic groups was based on both depositional environment and lithologic variations.

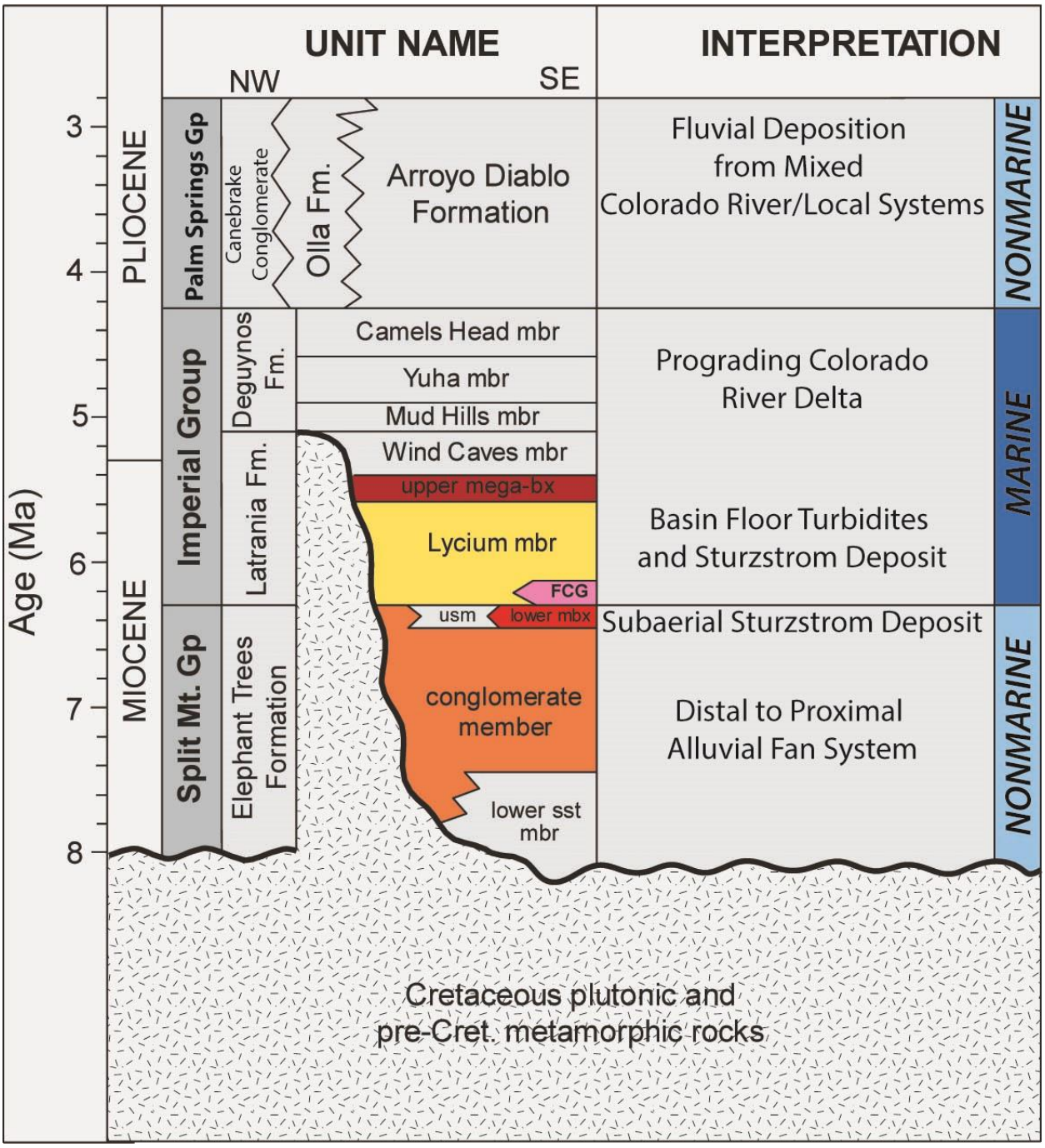

Figure 1-2: Stratigraphic units present in the Fish Creek-Vallecito Basin. The major units pertaining to the study are highlighted (i.e. upper mega breccia, Lycium Member, Fish Creek Gypsum, Lower Mega Breccia and the Elephant Trees Formation); Marine and nonmarine units are also highlighted. (Modified from Dorsey et al., 2011)

The lowermost unit, the Late Miocene Split Mountain Group (~8 to 6.3 Ma), is comprised of the non-marine Elephant Trees Formation and Lower Mega-Breccia. Accumulation of coarse-grained basement detritus derived from the uplifted Vallecito Mountains and the Peninsular Ranges to the north and west, and deposited as sub-aerial debris-flow dominated alluvial fans formed the coarse-grained sandstone and conglomeratic Elephant Trees Formation (Kerr 1984; Kerr 1982). In the Split Mountain Gorge area, the Elephant Trees is capped by the Lower Mega breccia. In the Mid-Miocene (around 6.4 Ma) the Vallecito Mountains stood high to the northeast of the basin. Strong tectonic pulses resulting from active rifting triggered massive rock falls from the heavily fractured Vallecitos, culminating in large scale subaerial sturzstrom events(Dorsey et al. 2011; Abbott et al. 2002). These sturzstrom deposits, referred to as the Lower Mega breccia, increased topographic complexity of the basin during the Mid-Miocene.

During the Late Miocene (~6.3 Ma), the basin underwent an abrupt change from a sub-aerial to subaqueous marine environment (Abbott et al. 2002) resulting in the deposition of the marine Imperial Group, which is further subdivided into the Latrania and Deguynos formations. The Latrania Formation is dominated by subaqueous sediment gravity flow deposits, comprised of coarse-grained sands, deposited in water depths of up to 200m. (Winker and Kidwell 1996; Winker 1987). The sediment gravity flow deposits of the Latrania Formation are divided into an upper and lower turbidite succession by a subaqueous mass-transport complex (~5.3 Ma). Deposits of relatively pure gypsum are also included in the early Latrania Formation (Dorsey et al. 2011).

The Deguynos Formation (~5.1 to 4.2 Ma) depicts a vertical succession of a prograding deep-water slope and an overlying marine delta (Winker & Kidwell, 1996) and is subdivided into the Mud Hills, Yuha and Camels Head Members. The Mud Hills Member is composed of marine

siltstones and claystones, indicative of a deep water slope environment, which is dominated by marine rhythmites (Dorsey et al. 2012). Overlying the Mud Hills Mbr. is the Yuha Mbr., a mix of fossiliferous sandstone and mudstone deposited on the marine delta platform (Dorsey et al. 2011). The uppermost unit of the Deguynos Fm. Is the Camels Head Mbr., comprised of marginal marine sandstones and siltstones accumulated in the tidal flats and marginal-marine Colorado Delta front (Winker and Kidwell 1996; Dorsey et al. 2011). The uppermost limit of the Deguynos formation marks a well-defined conformable transition from marine sediments to the fluvial deposits of the Arroyo Diablo Fm. of the Palm Springs Group. (Dorsey et al. 2011)

Around 4.2 Ma, deposition in the basin transitioned from the marine to the non-marine portion of the prograding Colorado River Delta, forming the Palm Springs Group (Dorsey et al. 2011). The basal unit of the Palm Springs Group is the Colorado River-deposited Arroyo Diablo Formation; consisting of well-sorted, fine-grained fluvial sandstones and mudstones (Dorsey et al. 2011). The Arroyo Diablo Fm. interfingers with the laterally equivalent Olla and Canebrake Conglomerate formations, derived from local alluvial and fluvial systems. Additional units of the Palm Springs Group, the Tapiado and Hueso formations (~2.8 to 0.95 Ma) are not observed in the study area.

1.2.3 Latrania Formation

The main focus of this study is the Latrania formation, ~6.3 to 5.1 Ma, the lowermost unit of the Imperial Group. The formation contains clastic marine deposits consisting of sediment gravity flows, a subaqueous sturzstrom deposit and a deposit of relatively pure gypsum. This formation marks the introduction of marine waters into the paleo-Gulf of California. Initial sediment is sourced from nearby local basement but transitions abruptly to Colorado River derived sediments in the upper most member of the unit.

Four unique members comprise the Latrania Fm.: the Fish Creek Gypsum, Lycium Member turbidites, Upper Mega breccia and Wind Caves Member turbidites. Thickness measurements are difficult to obtain due to complexity in the field, but previous work by Dorsey et al. (2011) and Winker (1987) constrain the total formation thickness to be ~300m. The oldest marine deposits in the formation are the coarse-grained Lycium turbidites which account for 75 m of the total formation thickness and interfingers laterally with the Fish Creek Gypsum. The Upper Mega breccia overlies the Lycium Mbr. and accounts for approximately 17m of the total thickness (Abbott et al. 2002). The youngest unit is the Wind Caves Mbr., a 200m succession of sandy to muddy turbidite deposits. (Dorsey et al., 2011; Winker, 1987)

The Fish Creek Gypsum is an isolated deposit located just east of Split Mountain Gorge, and lies at the boundary between the nonmarine Split Mountain Group and the marine Imperial Group (Dorsey 2010).Origin of the gypsum is somewhat problematic, previous work has concluded a marine origin but the type of marine environment has not been agreed upon. Interpretations of depositional environment range from a restricted shallow marine basin to a hydrothermal vent precipitation of gypsum in a marine basin (Dorsey 2010; Dean 1988).To this day, there is still considerable uncertainty relating to the origin of the Fish Creek Gypsum, but it is proven to be marine.

Coarse-grained, normal and inverse to normally graded beds are characteristic of the locally derived sediment gravity flows of the Lycium member turbidites. These turbidites are arkosic, biotite-rich sandstones and conglomerates(Winker 1987). Previous work by Winker (1987) suggests that the Lycium member was deposited as a slope apron, sourced by the coeval Elephant Trees alluvial fan system with paleo-flow direction to the east. There is no field evidence for an intermediate shoreline or delta system, possibly indicating that a ‘true shelf-slope

morphology was probably not developed' at the time of deposition (Winker, 1987). Paleoecology of the Lycium suggests deposition in water depths less than 200m (Winker, 1987). The present sedimentological and paleocurrent analysis argues that the thick turbidite succession was not sourced from the alluvial fans but originated from a NW-SE oriented valley running parallel to the edge of the West Salton Detachment Fault, debouching into the Fish Creek Basin to the east northeast, with locally derived alluvial fans from the Vallecito Mountains separately spilling into Fish Creek from local slopes along strike from the turbidite feeder system. Unfortunately, the outcrop distribution and present complexity of the outcrop do not exhibit a complete proximal to distal facies relationship in the system and must be inferred indirectly (Winker, 1987).

The Upper Mega breccia was deposited as a subaqueous sturzstrom event (~ 5.6 Ma) overlying the Lycium Member turbidites. The Mega breccia consists of pervasively fractured metamorphic clasts (ranging from gravel to house size boulders) with an olive-grey matrix (Abbott et al. 2002). Large folds and injections significantly deform the underlying turbidites. Work by Winker and Kidwell (1996) shows northeast to southwest fold axes alignment which Abbott et al. (2002), believe is aligned with the transport direction of the sturzstrom event. The inferred transport direction coupled with compositional similarities to the Fish Creek Mountains indicate that the Fish Creek Mountains are the source area for the Upper Mega breccia. (Abbott et al. 2002)

Locally derived sediment makes up the very thin, basal portion of the Wind Caves turbidites and is similar in character to that of the Lycium Mbr. Higher in the stratigraphy, the sediment source shifted from the coarse-grained locally derived sediment to the finer grained sediment of the Colorado River delta. The Wind Caves Member proper marks the introduction of the prograding Colorado River delta into the paleo-Gulf of California. The Colorado River

sourced sediments show are striking contrast to the locally derived wind cave turbidites, mud content increases as well as overall grain size and composition (Winker, 1987).

2. METHODS AND DATA

This study focuses on the Lycium Member of the Latrania Fm. In the Fish Creek-Vallecito Basin, a 400 km2 area, located near the town of Borrego Springs in southern California (Fig. 2-1). Impressive, up to 100 m thick outcrop belts provide an exceptional setting to study the earliest marine sedimentation into the paleo-Gulf of California.

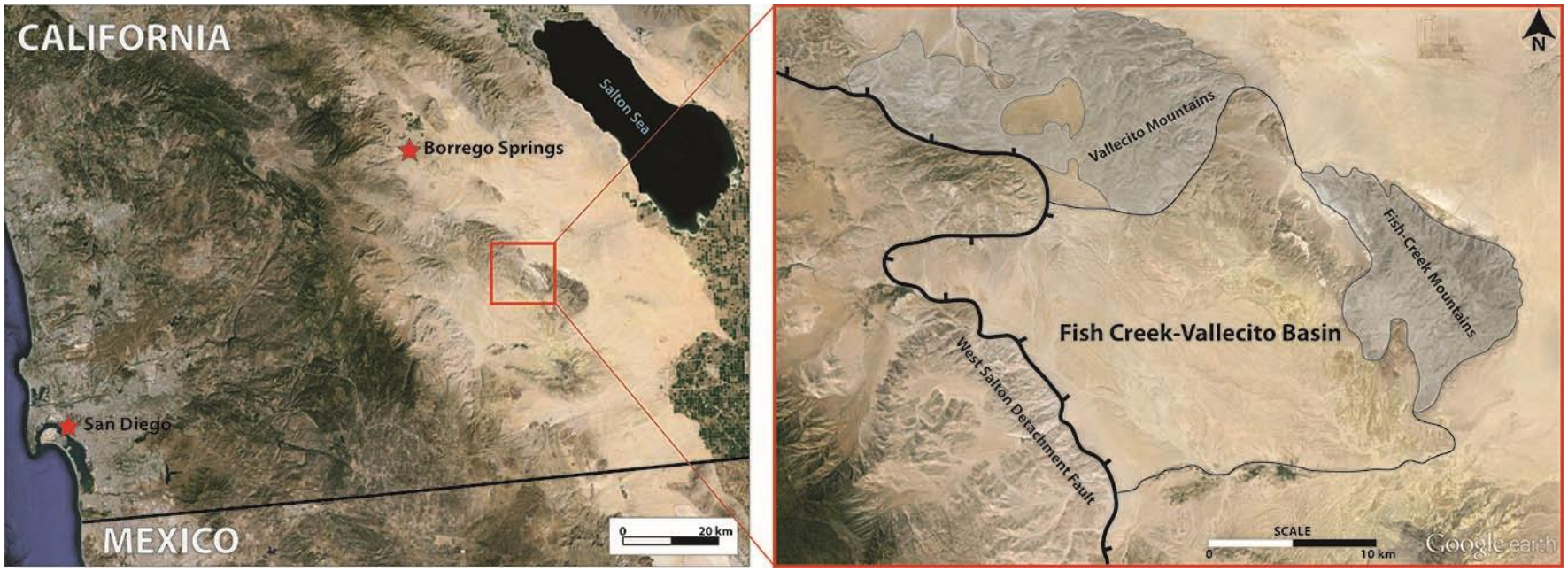

Figure 2-1: LEFT: Google earth image outlining study area in southern California just west of the Salton Sea; RIGHT: Zoomed in view of study area illustrating major attributes.

2.1 Measured Section

Outcrop logged sections were the chief investigation method in this study. A total of 10 outcrop measured sections, comprising approximately 540 m of measured section, were logged over a distance of 6 km along the northwest to southeast direction. Section locations were strategically placed at an oblique transect in order to aid in identifying lateral and vertical trends throughout the unit. Outcrops are focused in the northwestern portions of the system and become less abundant to the southeast of Crazy Cline Canyon. Complex faulting throughout the basin allowed for good exposure of outcrop belts but increased the complexity of the system, making it difficult to correlate sections over any distance.

Outcrop measurements focused on recording lithology, bed thickness, grain size, sedimentary structures and paleocurrent directions. Thickness measurements were taken using a Jacobs's Staff and Brunton compass to provide accurate measurements and account for dipping strata. The sedimentary descriptions and interpretations taken from logged sections were used to map and identify distinctive lithofacies types throughout the system. These lithofacies types were then grouped into facies associations in order to better interpret process and deposition of the system. Paleocurrent indicators were scarce, but when found they were measured on flute and groove casts at the base of beds and indicated an overall E-SE flow direction.

2.2 Facies and Grain Size Distribution

System variability was analyzed using Matlab software in order to map facies, bed thickness and grain size distributions. Scripts were used to quantify grain size and bed thickness distributions from each outcrop logged section. The data extracted using the software was then plotted into histograms highlighting lateral variability. The results for each section were then

normalized and compared. First, histograms of grain size and bed thickness were created and compared for each vertical section. Secondly, lateral correlation of facies proportions was made in order to map and more quantitatively image the facies variability in space and time..

2.3 PHOTO-PANEL ANALYSIS

High resolution imagery was used to construct photo-panels of large scale outcrops within different segments of the submarine complex. These detailed photo mosaics were used to identify the architectural-element geometries on the larger scale, as well as the depositional boundaries of the Lycium member. Five photo-panels were constructed along the following elements: debris flow lobes, amalgamated channel complexes, and channel-lobe complexes. Architectural variations were distinguished based on facies associations coupled with bedding geometries. Geometrical discontinuities and erosional relief along basal surfaces were used to distinguish channels from lobes bodies. Due to the outcrop complexity and distribution, photo-panels were then analyzed in detail to support vertical measured section correlations and create diagrams illustrating the architectural elements of the system.

2.4 PETROGRAPHY

A total of 15 thin sections were made from coarse-grained samples that were strategically collected from different locations throughout the Lycium Member turbidites in order to attain an even distribution of samples throughout the system. Thin sections were impregnated with blue-dyed epoxy for ease of identifying pore space. K-rhodizonate and Na-cobaltinitrite were used to stain the samples in order to aid in identifying feldspars and feldspar types. Using J-Microvision, long-axis measurements were taken from 100 grains per sample in order to evaluate grain-size distribution and sorting.

In order to assess provenance, thin sections were point counted using the Gazzi-Dickinson method (Dickinson 1985; Gazzi 1966), in which all crystals > 62.5 μm are counted as individual grains regardless of whether or not they occur as a monocrystalline grain or as part of a lithic fragment. A petrographic inspection of 250 points, randomly distributed throughout each thin section, was used to conduct a modal analysis of each sample. The types of grains counted were monomineralic fragments and lithic fragments (refer to Appendix A for full listing of components counted). Lithic fragments were further subdivided based on source-type. Relative abundances of quartz, feldspars and lithic fragments were then used to classify each sample based on Folk's classification (Folk 1980). Secondary porosity created by dissolution pores in feldspar grains was not used in restoring Feldspar values because it did not make a significant impact on bulk Q-F-L classification.

3. RESULTS

3.1 FACIES AND FACIES ASSOCIATIONS OF THE LYCIUM MEMBER

Outcrop observations coupled with vertical measured sections revealed five lithologic facies that make up the Lycium Member turbidites. Process-based interpretation of deposition was made for each lithologic facies, within four separate facies associations (i.e., amalgamated channelized turbidites, alluvial-fan fed debris flows, sheet turbidites and turbiditic heterolithics). These facies and associations aid in characterizing both lateral and vertical variations throughout the Lycium Member turbidite succession.

3.1.1 Lithofacies Descriptions

Well-bedded Turbidite Sandstones (Lithofacies 1)

The Lycium Member is dominated by spectacular and abundant well-bedded, fine to coarse-grained sandstones that are interpreted as sandy , submarine sediment gravity flows (turbidites) because of the flute casts along the soles of some of the beds, their sharp and sometimes slightly erosive bases and the common graded nature of beds. These turbidites can be subdivided into: normally graded sandstone beds, inversely graded sandstone beds and inverse-to- normally graded sandstone beds.

Lithofacies-1A) Normally Graded Sandstones

Tabular, normally graded sandstone beds are prevalent throughout the Lycium member. Average bed thickness is 20 cm, with a maximum thickness of 45 cm. ‘Beds’ thicker than 45 cm are generally an amalgamation of several thinner ones. Individual beds are poorly to moderately

sorted and grade vertically from coarse to medium-grained sand up to a very-fine sand capping. Occasional plane parallel lamination is focused in the upper portion of the bed. (Fig. 3-1A)

The normal grain-size grading from coarse to very fine sand is indicative of a turbulent suspended load during flow and leads to a selective dumping of the coarser grain sizes and a decrease in flow energy during deposition of the entire bed. These flows were likely deposited from decelerating flows (see Talling et al., 2012). As flow energy decreased the grains transitioned from being in suspension to being carried in traction, thus creating laminations. The tabular, sheet-like deposition, and lack of scouring strongly suggests distal or off-axis unconfined deposition, out from a channelized flow (Talling et al. 2012)

Transitional flow deposits (Kane & Ponten, 2012) are also present in the system but make up less than 5% of the well-bedded sandstones and are thus not included as a major bed type, but are similar in character to the normally graded sandstones. The transitional flow deposits in the Lycium Member are comprised of medium sandstone beds with basal grading topped with a mud clast horizon within a muddier matrix. These transitional beds, also termed linked debrites (Haughton et al., 2003)represent turbulent flows which entrain finer sediments through deceleration thus increasing near-bed clay content and transition from turbulent to laminar flows (Kane and Ponten, 2012). These flows may be indicative of flow expansion at the channel-lobe transition and are usually described from the fringes of fans. (Kane and Ponten 2012)

Lithofacies-1B) Inversely Graded Sandstone beds

Inversely graded sandstone beds are interspersed throughout the section, with bed thicknesses ranging from 5 to 20cm. Beds grade crudely from medium or coarse grained at the base to very coarse sand and even pebbles higher in the bed. . Beds have irregular bases

suggesting scour into the underlying substrate. (Fig. 3-1B). The inverse grading and generally associated slightly coarser grain size suggest that these beds represent flows with a higher sediment concentration and higher density than the normally graded beds associated with highly turbulent currents.

These beds may represent grain-flow deposits where the inverse grading forms through a kinetic sieving process, or where dispersive stress within the bed causes larger grains to move upwards during the flow (Hampton, 1979). The erosive contacts between the beds suggest erosion or scouring by the overlying bed, indicating an erosive or high-energy flow (Lowe, 1982)

Lithofacies-1C) Inverse to Normally Graded Sandstone beds

Inverse to normally graded sandstone beds are also scattered throughout the Lycium Member. Average bed thickness is 44 cm, with a maximum thickness of 80 cm. These beds are interspersed within thick, normally graded sandstone intervals. The basal portion, bottom 2/3, of the bed grades from medium or coarse sand and gravel, which then rapidly grades to medium sand in the upper 1/3 portion of the bed and then is capped with fine silty sand. Occasional ripple laminae are found in the fine sand/silt capping. (Fig. 3-1C)

These deposits also represent high density turbidity flows, like the inversely graded beds, and possibly correspond to Lowe's S2 and S3 divisions (Lowe, 1982). The basal, very coarse sand and gravel rich, portion moved along as a traction carpet for the more dilute overlying turbidity flow. Kinetic sieving or dispersive stress in the basal portion of the flow, formed the observed inversely graded portion of the bed. The overlying turbulent part of the flow was then deposited out of suspension, forming the normally graded top of the bed. (Lowe, 1982; Talling et al., 2012)

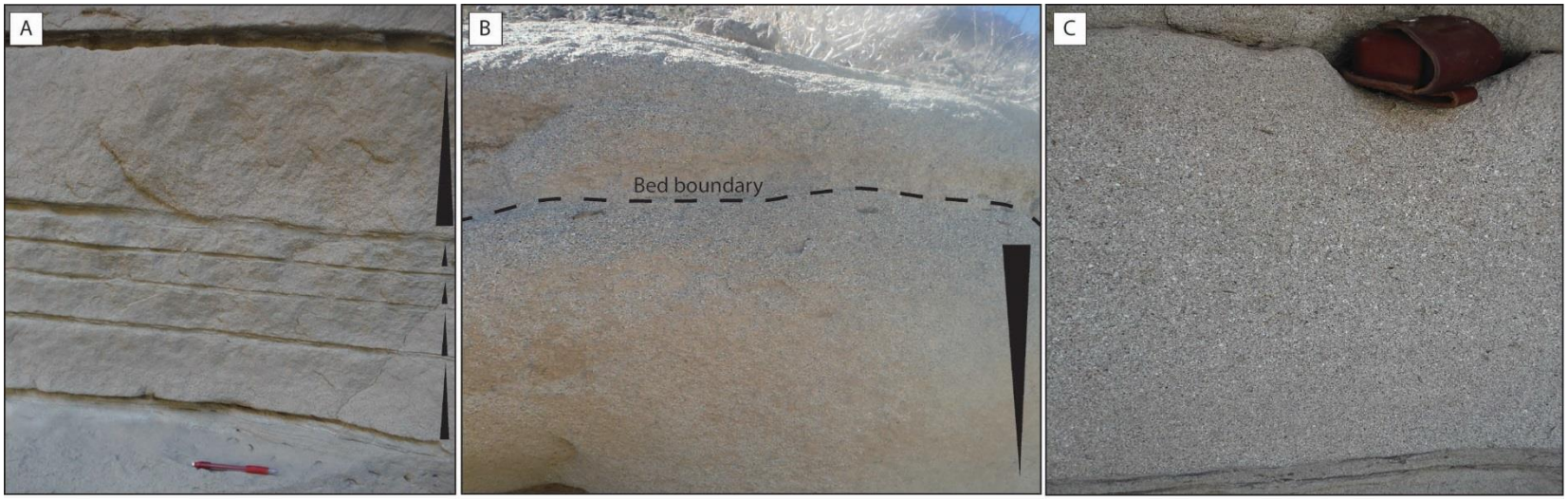

Figure 3-1: Well Bedded Sandstones; A) Normally graded sandstone bed (LF-1A), beds generally have flat, unscoured bases; B) Inversely graded sandstone (LF-1B), grades from medium/coarse at base to very coarse gravel at top of bed ; C) Inverse to normally graded sandstone (LF-1C), beds grade from medium to very coarse gravel sand at the middle, and then normally grade from very coarse to medium sand in the upper portion of the bed.

Thick Amalgamated Sandstone Units (Lithofacies 2)

Thick, amalgamated, sandstone units (>0.5 m) are abundant in sections measured throughout the Lycium Member. Average thickness of component beds in the amalgamated unit is 80 cm, but can reach up to 2m in places. Amalgamated units can reach up to 15m in thickness, with mud clasts or grain size changes separating individual flow events. Individual beds in the units are poorly to moderately sorted and commonly grade from gravel or coarse sand at the base, to medium or fine sand at the top of the bed. Occasional planar laminations, outsized mud clasts (up to 7 cm) and boulder inclusions (up to 60 cm) are observed. (Fig. 3-2). A very common feature of amalgamated sandstone units is the presence of internal scour erosion surfaces, both at the base of the amalgamated unit and at the base of individual beds within this unit.

Planar laminations observed towards the base of beds, termed 'spaced' laminations by Talling (2012), probably correspond to Lowe's S2 division (1982) and Talling's T_{B-3} division (2012). Individual 'laminae' average ~10cm in thickness and show inverse grading from medium to coarse sand. Hiscott and Middleton 1980 interpreted these structures to be formed by traction carpets beneath high density flows. (Hiscott and Middleton 1980)

Talling (2012) interpreted amalgamated facies similar to those described here to be deposited from high density turbidity currents. He suggested that spaced laminations in the basal portion of the bed signify high density turbidity flows; higher sediment concentrations decrease turbulence towards the base of the bed allowing for kinetic sieving. Normal grading coupled with amalgamation indicates a decelerating flow deposited in an axial position of the flow. The occurrence of outsized mud clasts along a discreet horizon further indicates deposition out of a

decelerating flow (Talling et al., 2012). The occurrence of such thick-bedded turbidites amalgamating in zones with thinner-bedded turbidites lateral to them, suggests that this facies developed in the main system channels. The erosive base and edges of the channels can occasionally be seen but sometimes channel ‘edges’ are less obvious.

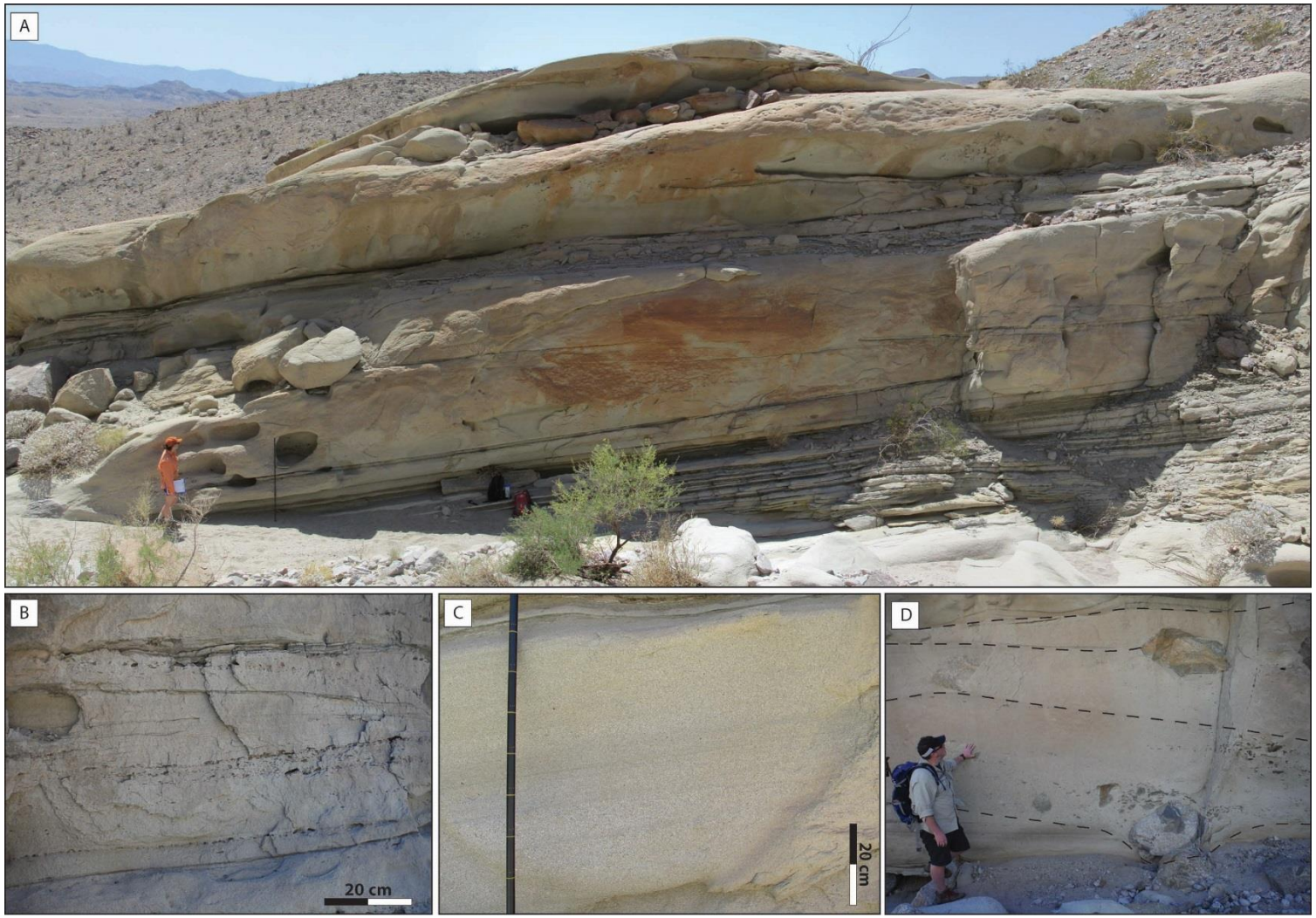

Figure 3-2: Thick-bedded amalgamated sandstone units(LF-2); A) Outcrop scale, amalgamated sandstones; B) Mud clasts highlighting amalgamation surfaces; C) Spaced laminations (~10 cm thick); D) Amalgamated beds with boulder inclusions (up to 1m).

Sandy Debris Flow Beds (Lithofacies 3)

Beds characterized by poor sorting and dispersed clasts are interpreted as submarine debris flows and are interspersed throughout the Lycium Member. These beds are less common than turbidite beds but are interspersed within thick, normally graded sandstone beds or amalgamated sandstone intervals. There are two distinctive types of debris flows found in the Lycium Mbr.: sandy debris flows with clasts up to boulder size and sandy debris flows with abundant mud clasts.

Lithofacies -3A. Sandy, Boulder Rich, Debris Flow beds

These deposits are abundant in the upper portions of the Lycium Member from Lycium Canyon to Split Mountain Gorge (location on map). Average bed thickness is 1.8 m, with a maximum thickness of 4 m. Beds are poorly sorted with abundant clasts up to boulder size and a coarse to medium-grained, graded sand matrix. Boulder diameters range from 5 to 95 cm. The base of these beds is erosive, cutting into underlying strata while the tops are capped with normally graded, coarse to fine sand. These beds rapidly thin laterally within 10s of meters. (Fig. 3-3A, 3B))

The poor degree of sorting as well as outsized (0.5m and up) igneous and metamorphic clasts, in beds of moderate thickness suggest a flow that is cohesive with a moderate strength to support such large clasts. The sandy capping suggests a turbulent, late stage settling of sand grains above the main body of the debris flow. The erosive reaches of the base of the flow probably indicate an axial location within the flow (Talling et al., 2012)

Lithofacies-3B Sandy Debris Flow with Mud Clasts

Beds of this type are also poorly sorted and structureless. Grain size ranges from very coarse to coarse sand. Mud clasts, with diameters ranging between 0.5 and 12 cm, are common and tend to be randomly dispersed throughout the bed. These beds also rapidly thin laterally and have erosive bases. The lack of vertical grading, chaotic distribution of outsized mud clasts and lack of structure again indicates 'en masse' or 'plug' deposition of a cohesive flow with moderate matrix strength to support clasts (Talling et al., 2012) (Fig. 3-3C,3D)

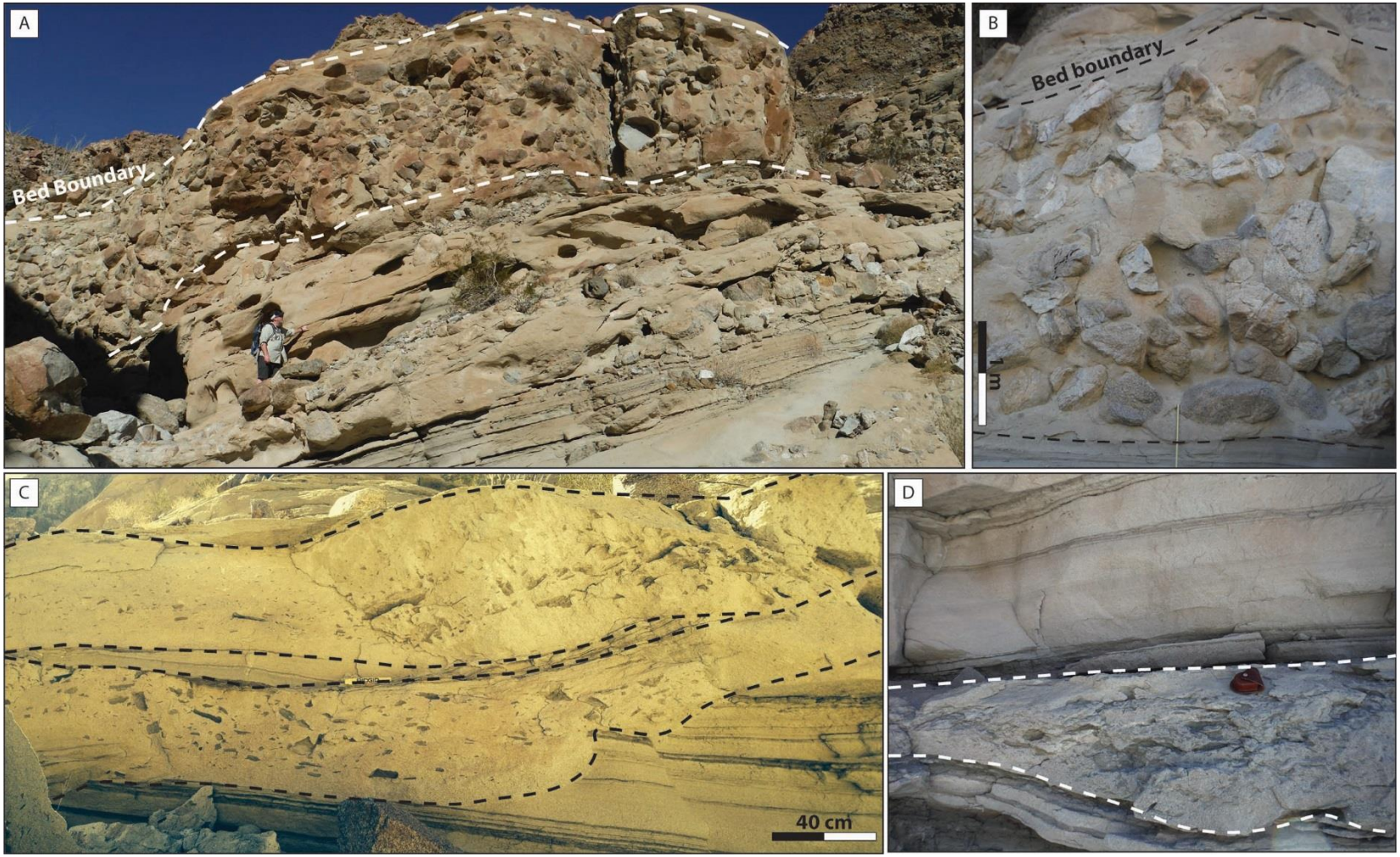

Figure 3-3: Sandy debris flows; A) Outcrop scale boulder rich debris flow with large boulder clasts (average 0.6m) chaotically distributed throughout multiple beds; B) Single debris flow bed (some boulders reach >1m) with sand capping; C) Beds have highly erosive, scoured bases, with chaotic distribution of mud clasts (2-10 cm); D) Beds tend to thin laterally and abruptly and are associated with normally graded sandstone beds.

Sandstone Dominated Heterolithics (Lithofacies 4)

Some parts of the turbidite Lycium Member succession are dominantly heterolithic and composed of normally graded, thin sand beds (up to 10 cm) interbedded with thin layers (<2cm) of silty mudstone; these occur in heterolithic intervals of up to 10 m. The sandstone beds are most commonly medium-grained sandstone but some very-coarse sandstone beds are also observed. Parallel lamination and ripple lamination are common towards the top of the otherwise structureless sandstone beds. The deposition of this unit is interpreted to have been distal to or off-axis from the main channelized flows, allowing for deposition of more dilute and less competent turbidity currents. The preservation of very fine sand and siltstone also indicates a generally lower energy environment. (Plink-Björklund, Mellere, and Steel 2001)(Fig.3-4A,4B)

Siltstone- Dominated Heterolithics (Lithofacies 5)

The siltstone-dominated heterolithic unit is comprised of very fine grained sand to silty mudstone beds up to 10 cm thick, interbedded with lenticular medium to coarse grained sandstone beds up to 5 cm thick. Parallel lamination and minor ripple-lamination is common in the sandstone beds of the unit. This facies may represent overbank deposits from channels or distal/off-axis deposits of lobes. The preservation of very fine sand and silt indicates a lower energy environment. (Plink-Björklund, Mellere, and Steel 2001)(Fig. 3-4C,4D)

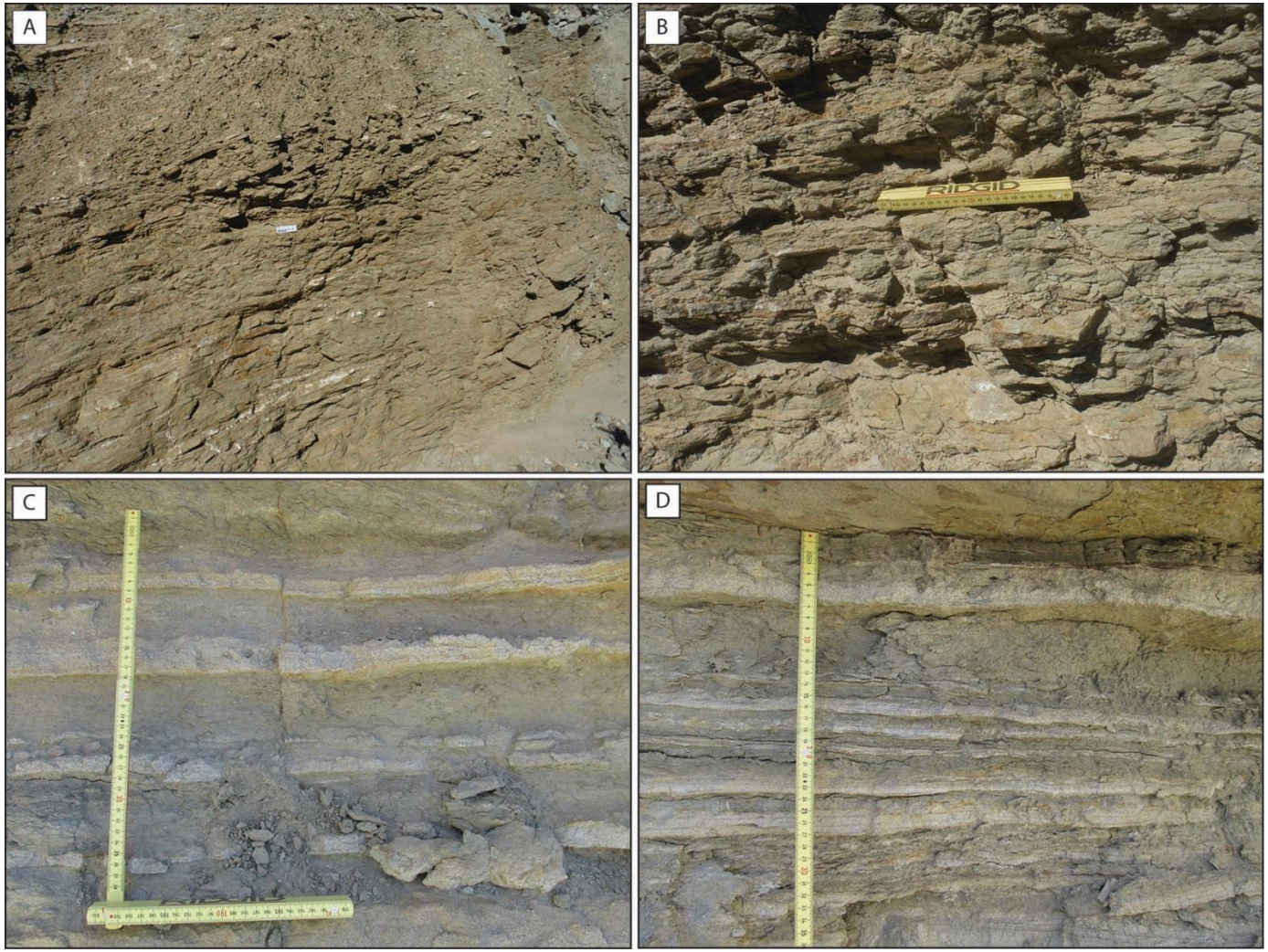

Figure 3-4: Heterolithics; A+B) Sand dominated heterolithics, 5 cm sand beds interbedded with thin silt layers; C+D) Silt-dominated heterolthics; normally graded sandstone beds (avg. 5cm) are interbedded with very find sand/silty intervals up to 10 cm thick.

3.1.2 Facies Associations

Facies Association 1: Channelized turbidites

This channelized turbidite association, the most laterally variable of all in the Lycium Mbr., consists of thick, amalgamated turbidite beds (LF-2, LF-3A, and LF-3B) and some debris-flow beds. The channelized units are clearly visible from a distance because of their great thickness relative to laterally equivalent thinner turbidite beds. Such channelized units vary in thickness from 1 to 4 m. Channelized turbidites are most common in the northwestern portion of the basin (thickness up to 15m) but there are also a few channel complexes (<5m thick) in the southeastern portions too. (Fig. 3-5)

These channelized zones with thick to very thick turbidite sands are the result of scoured erosion, followed by focused aggradation of sediment from channelized turbidity currents and debris flows along a channelized-axis of sediment accumulation. Lateral to the channels the turbidite beds are thinner, so it looks like channels are cutting down into and through slightly older sheetlike turbidite bed accumulations. Sections in the northwest of the basin, where this association is common, represent the more proximal deposits closest to the slope or bathymetric exit point, whereas portions in the southeast were most likely the result of larger flows with longer run out(see also Galloway, 1998;Talling, 2012) The channelized, amalgamated turbidite units are interpreted as representing turbidity-current conduits on the deep subaqueous slope, sometimes with the channels emerging also onto the flatter basin floor area. It is unclear whether all of the sheetlike turbidites on the basin floor represent the unconfined flows that emerged from these conduits, or whether some of the sheetlike turbidites also represent subaqueous continuation of debris-flow lobes.

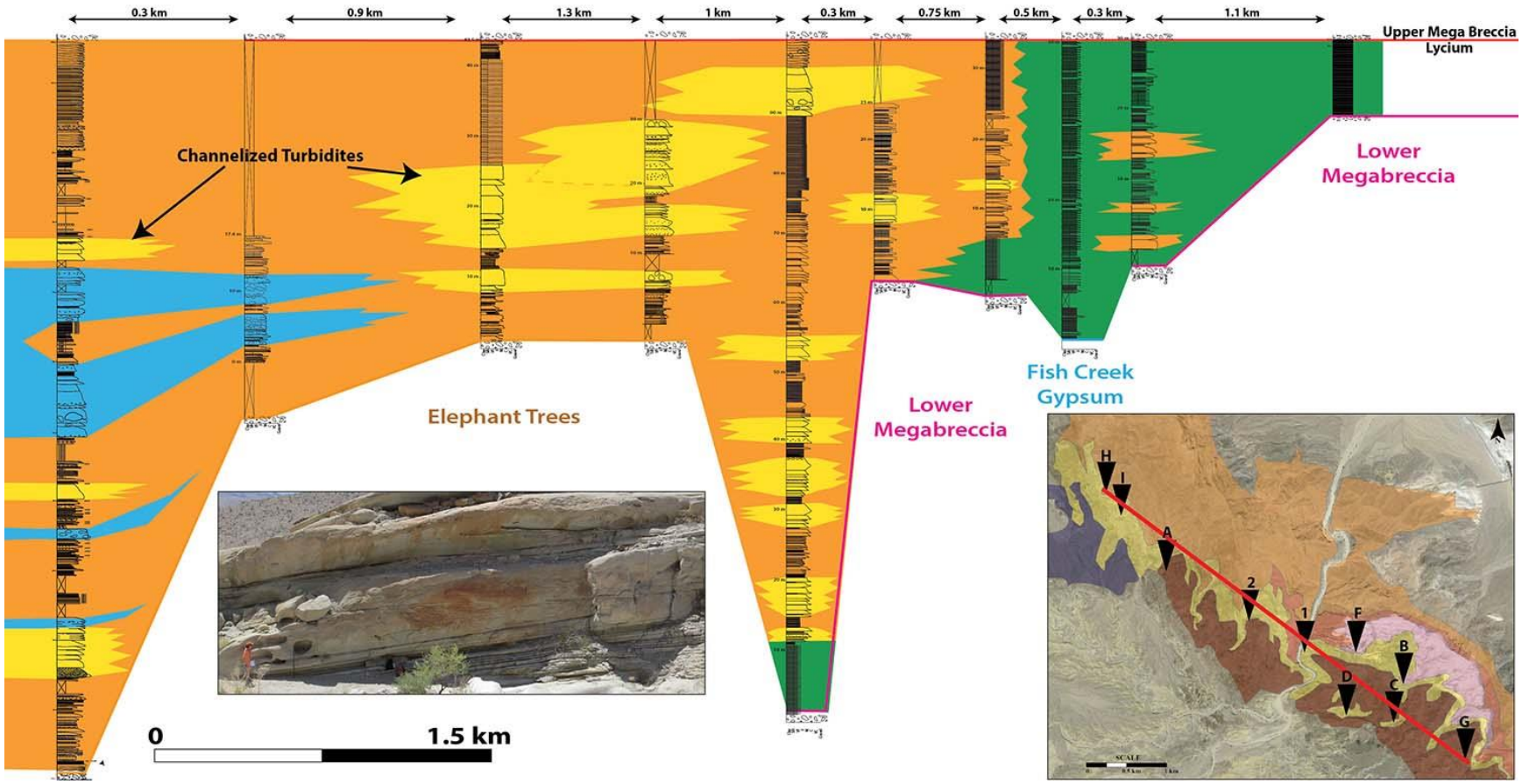

Figure 3-5: Section correlation highlighting Facies Association 1- Channelized Turbidites. Channelized turbidites are common throughout the NW (Lycium Canyon) and medial portions of the system (Split Mountain Gorge) and are absent in the SE (Cairn Canyon).

Facies Association 2: Subaqueous fan delta debris-flow lobes

Subaqueous debris flows are found in the northwestern portions of the basin and are absent east of Split Mountain Gorge. Such units are composed of lithofacies 3A-B: mud-clast and boulder-rich debris flows. Interfingering between the debris flow beds and channelized turbidite units is common in Lycium Canyon and Oyster Shell Wash-2. The coeval alluvial fans, now high on the slopes, dispersing sediment down into the main turbidite fairways is a likely source for the debris flows though debris flows could also originate from the same drainage as the turbidite channels, produced for example by slope collapse into the turbidite fairway. As regional extension and rifting continued in Fish Creek Basin, input from both potential debris-flow sources remained active, triggering massive debris flows that bypassed the inherited upper slope and deposited down into the active turbidite basin (see also Galloway, 1998). (Fig. 3-6)

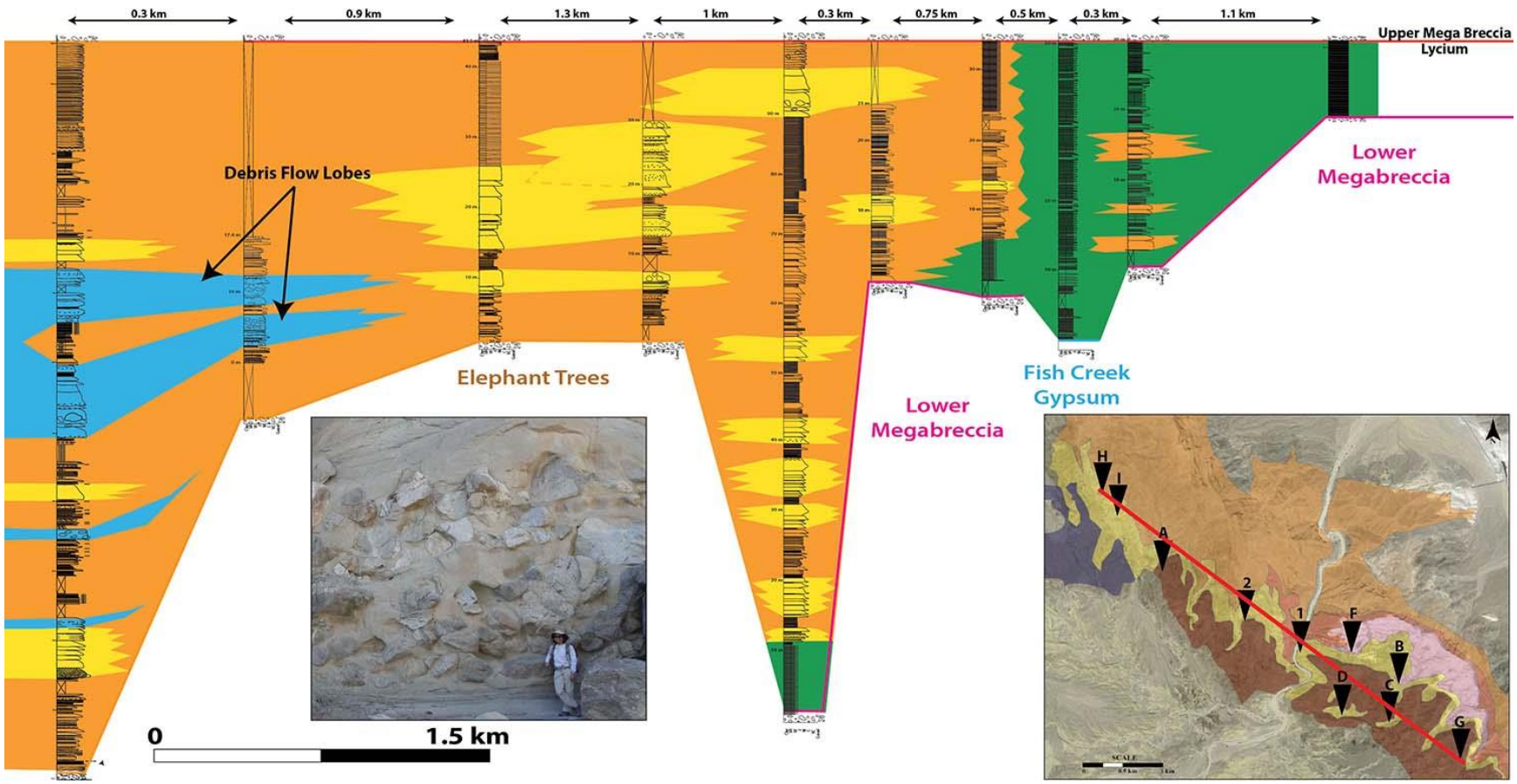

Figure 3-6: Section correlation highlighting Facies Association 2- Debris Flow Lobes. Debris Flow lobes are only found in the NW portions of the system, specifically Lycium Canyon and Oyster Shell Wash 2.

Facies Association 3: Sheet Turbidites

Sheet turbidites are the dominant facies association in the Lycium Mbr., the unit is comprised of lithofacies 1A-C: normal, inverse and inverse to normally graded turbidite sandstone beds. The sheet turbidites are widespread throughout the basin, they are thickest in the northwest and become thinner and slightly finer grained to the southeast in the basin. Highly stratified successions are seen throughout the basin, displaying well-bedded sandy turbidites. In unconfined areas, the succession of sheet turbidites grades laterally, from the NW to SE, into basin plain finer grained sand beds alternating with silty mudstones. Irregular bathymetry created by the underlying mega breccia created depressions where the turbidites ponded and onlapped the edges of the underlying mega breccia. Deposition of the sheetlike, relatively course-grained turbidite units strongly suggests a high supply and delivery of subaqueous sand into the basin, allowing for the deposition of widespread, unconfined sediment gravity flows. (Fig. 3-7)

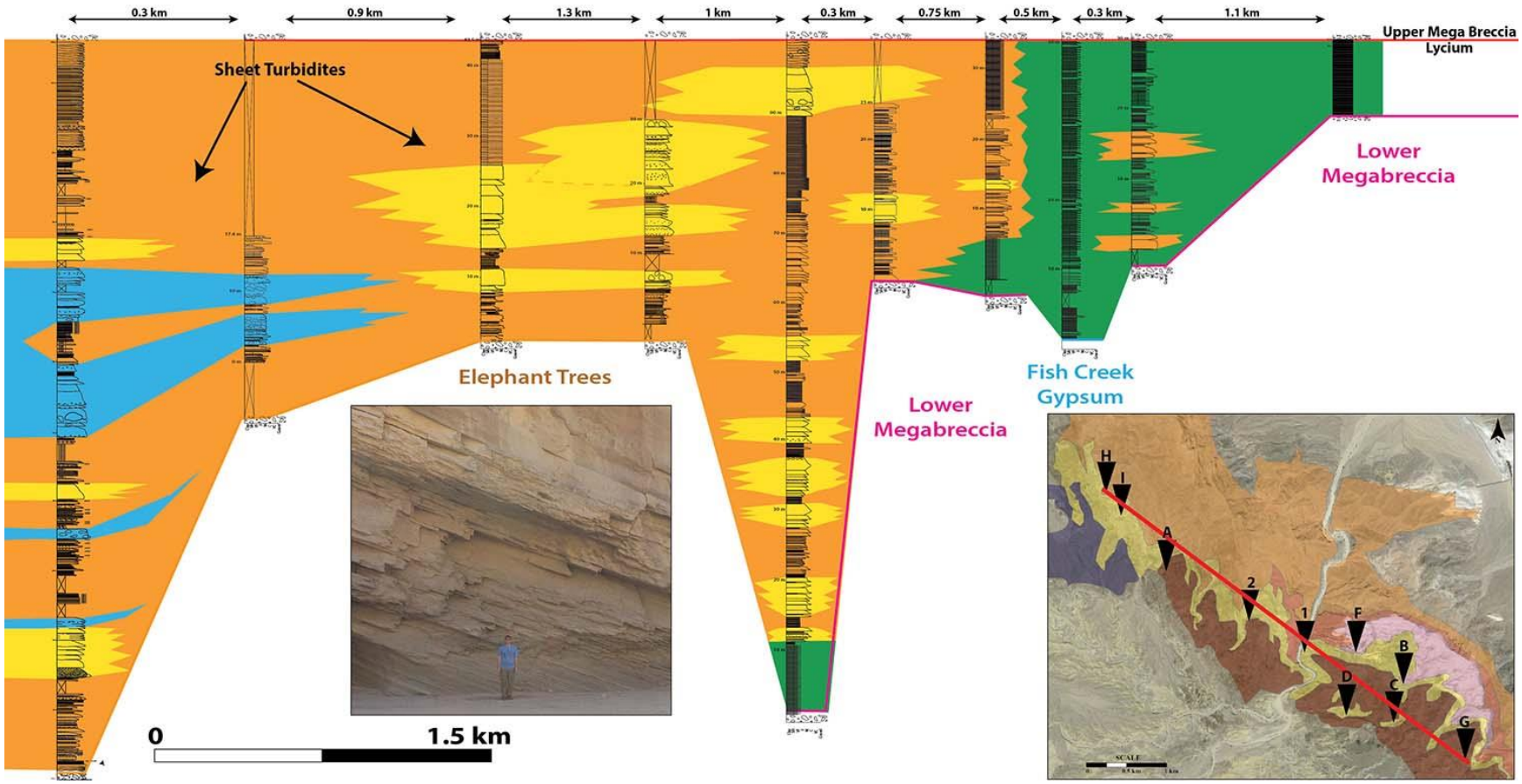

Figure 3-7: Section correlation highlighting Facies Association 3- Sheet Turbidites. Sheet turbidites are the most common facies association throughout the system, they interfinger with debris flow lobes, channelized turbidites and heterolithics.

Facies Association 4: Heterolithic Interbedded Sandstones and Siltstones

This association is composed of heterolithic units of very thin beds of sandstone and siltstone (LF-4, LF-5). It occurs predominately in the southeastern or distal reaches of the basin but thin intervals of such heterolithics (up to 1m thick) are dispersed throughout most of the basin. These deposits are interpreted to represent off-axis turbidity flows which infill both interchannel areas and the most distal reaches of the channel-lobe complexes. (Galloway, 1998) (Fig. 3-8)

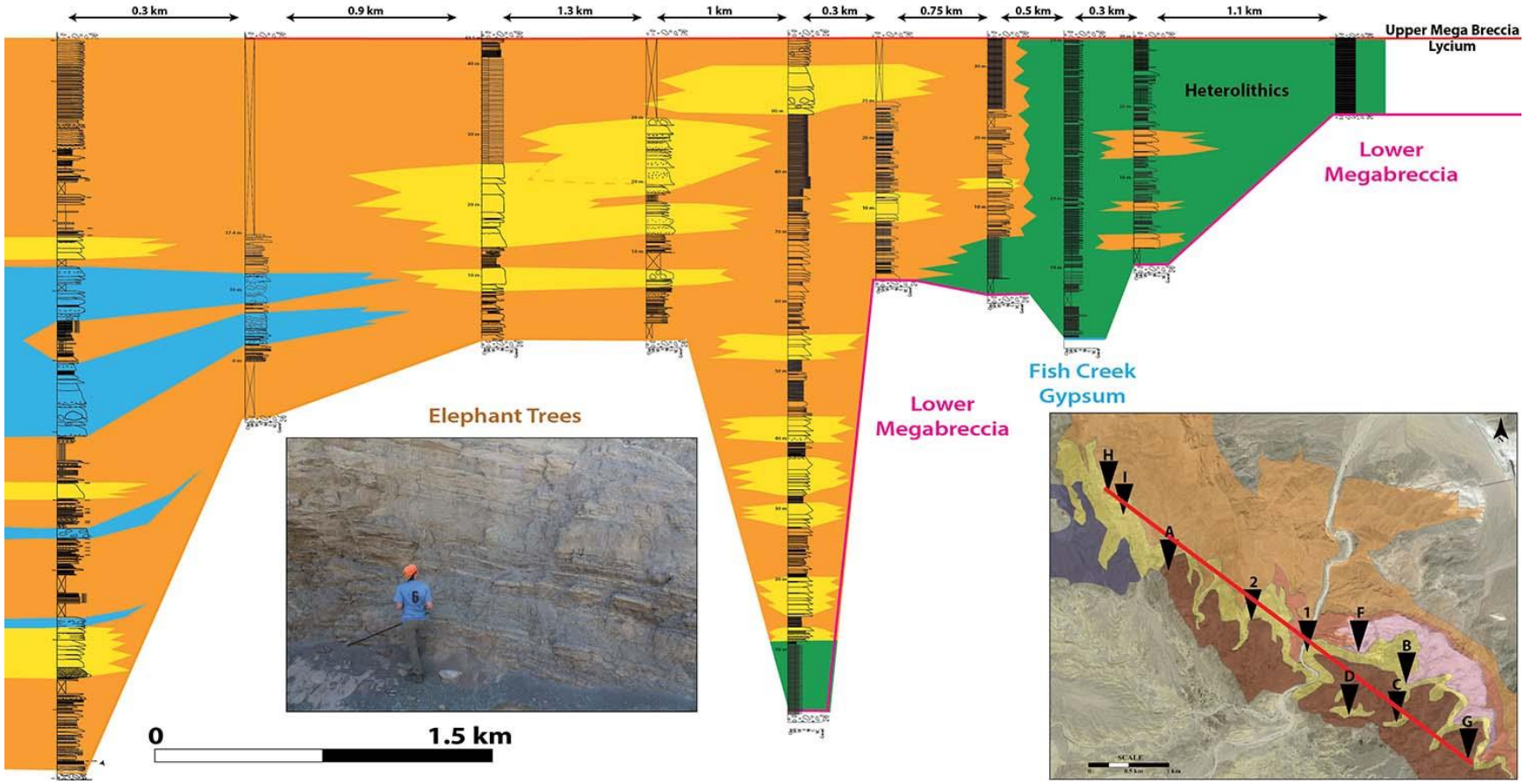

Figure 3-8: Section correlation highlighting Facies Association 4- Heterolithic interbedded sandstones and siltstones. Facies Association 4 is most common in the southern most portions of the system (Cairn Canyon) and can be seen at the base of Section 1 in Split Mountain Gorge.

3.2 FACIES VARIABILITY OF THE LYCIUM MEMBER

3.2.1 Bed Thickness and Grain Size

Within the Lycium unit, we see an overall decrease in average bed thickness (from 16 cm to 1.3 cm) in the NW to SE direction (Fig. 3-9). In the northwestern portion of the system (Section H through Section 1) individual bed thicknesses exceed 2 meters with an abundance of coarser grain sizes (medium to very coarse sand or gravel) (Fig. 3-10). Directly south of Split Mountain Gorge maximum bed thickness decreases to approximately 1.6 meters along with a dominance of very fine sandstones. . In the most southeastern portions of the system bed thicknesses thin to <2cm with alternations of coarse and fine sandstones with siltstones.

In the northwestern portion of the system, the vertical profile shows an overall thickening upwards trend of beds with thinner bedded sands in the most basal portions of the unit, sometimes grading into amalgamated, thick sands and debris flows. The upward-thickening vertical profile continues to near the most distal portions of the system in the southeast, where thin fringe deposits of interbedded sands dominate the profile.

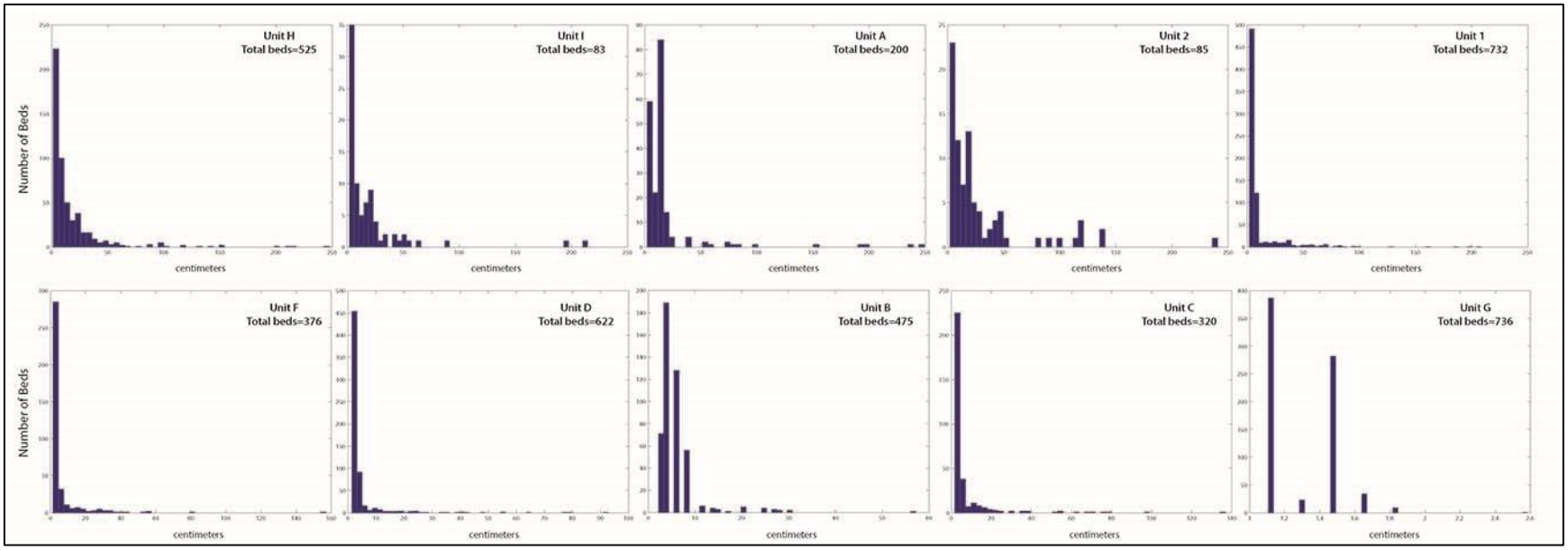

Figure 3-9: Bed thickness distribution of all outcrop measured units; Bed thickness show an overall decrease from NW to SE with beds thinning out to less than 2 cm in thickness in the most southeastern portions of the system

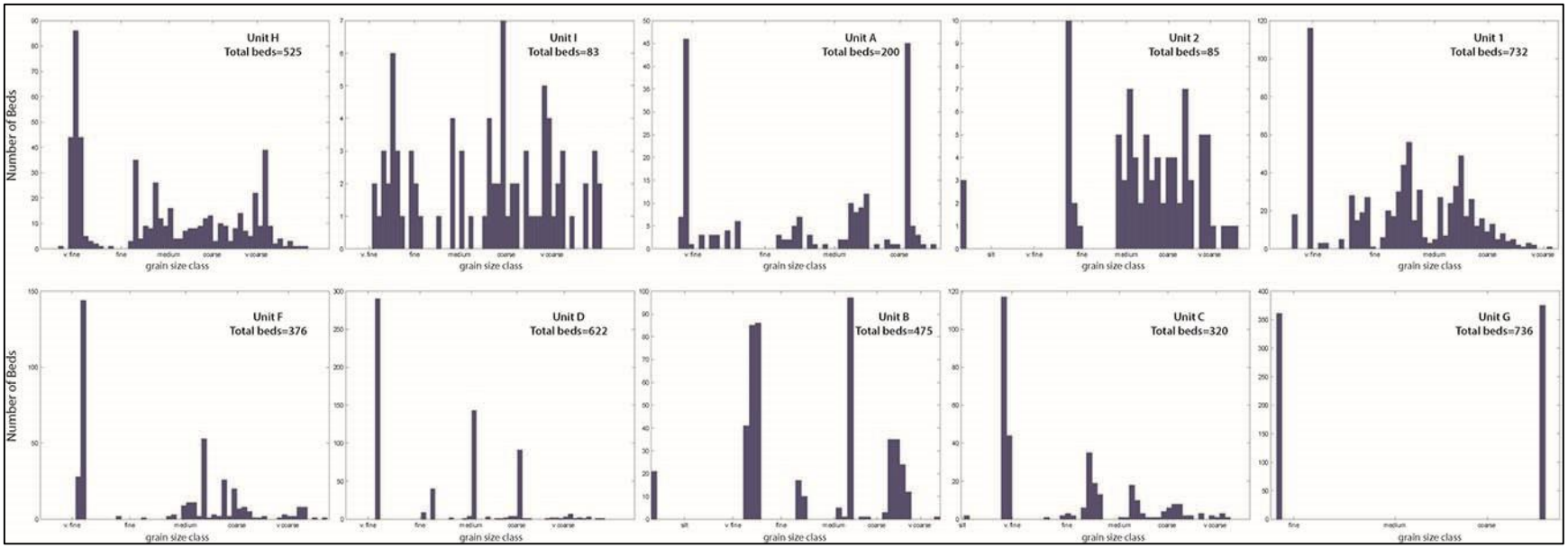

Figure 3-10: Grain size distribution of all outcrop measured units; Grain sizes are steadily coarser in the northern portion of the system (Unit H through 1) whereas fines become more abundant in the southern half (unites F through G)

3.2.2 Facies Distribution

Significant vertical and lateral variation in facies can be seen throughout the outcrop extent of the Lycium Member. Using Matlab, the facies distribution of each measured section was plotted along a NW to SE transect (Figure 3-11) in order to highlight the dominance and trends of the different lithofacies throughout the system. The transect has an oblique-to-depositional dip orientation.

The northwestern portions of the system (Section H and I) are dominated by well-bedded turbidite sandstones, debris flows and thick amalgamated turbidite sandstones (around 80%) with minor amounts of heterolithics. Southeastwards along the NW-SE transect to Section A, the sandy, boulder-rich debris flows (LF-3A) disappear and the proportion of sandstone dominated heterolithics increases to around 40%. Further to the southeast Section 1, located in Split Mountain Gorge, is dominated by both normally graded and thick amalgamated turbidite sandstones (around 75%) with minor amounts of heterolithics. When you reach Section D, the thick, amalgamated sandstone units (LF-2) pinch out and we are left with approximately 60% sandstone dominated heterolithics and 40% normally graded sandstones. In the most southeastern portions of the system, Lithofacies 1 through 4 dissipate and we are left with 100% siltstone dominated heterolithics.

Transitioning from the NW to the SE, we see a significant decrease in sandstone content coupled with an increase in heterolithics. This transition represents a change from a more proximal to distal locality of the channel-lobe complex. Thick, amalgamated channels and debris flows are interpreted to be axial fairway deposits in the most proximal setting of the channel lobe complex. Well-bedded thinner sandstones (LF-1A, 1B, 1C) are interpreted as off-axis proximal

and medial deposits of the system. The heterolithic units (LF 4 and 5) represent off-axis and distal-fringe deposits of the channel-lobe system.

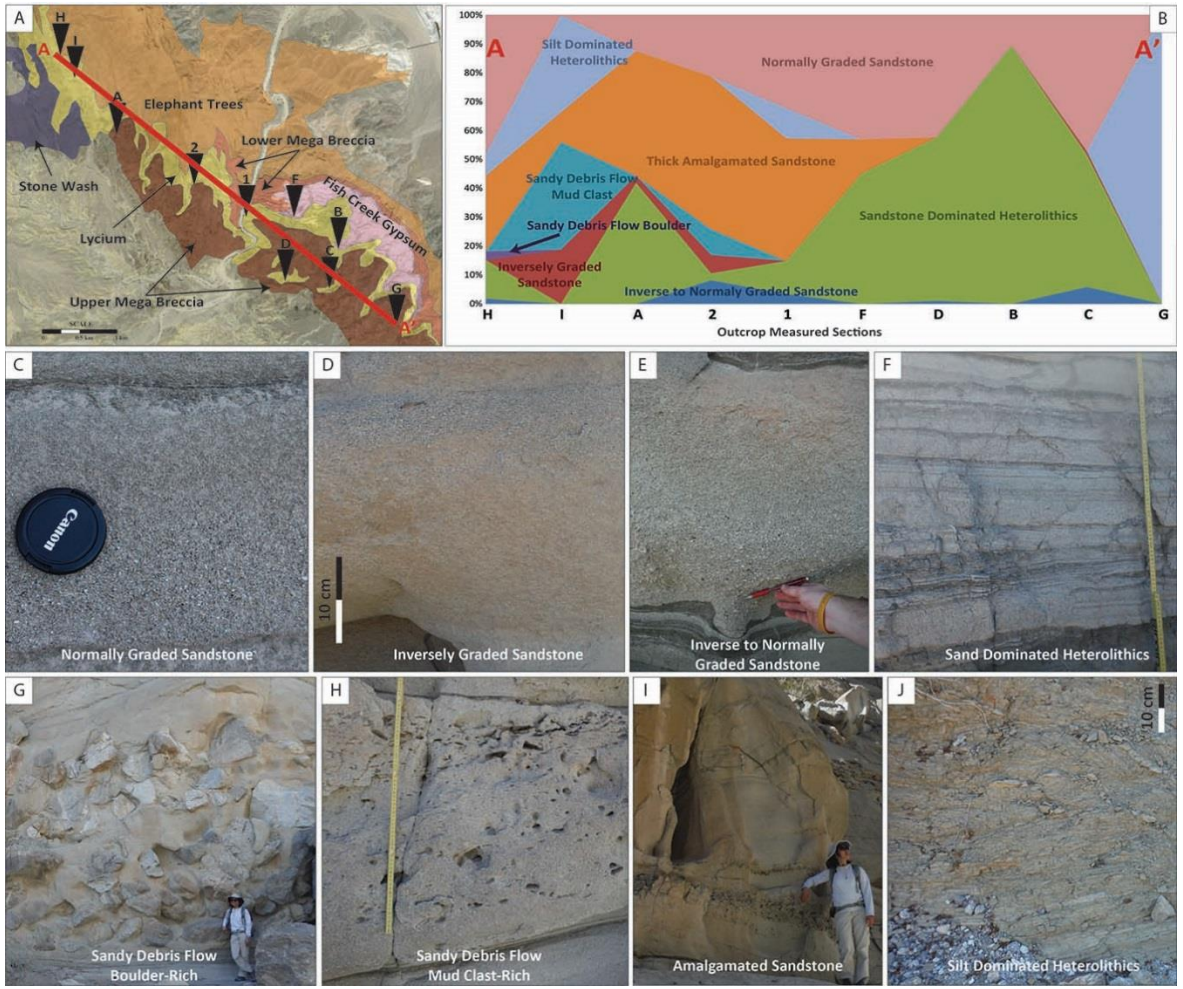

Figure 3-11: Facies variability of the Lycium Member turbidite system; A) Location of outcrop measured sections and NW to SE transect; B) Distribution plot of lithofacies throughout the 10 outcrop measured sections; C) Normally graded sandstone bed (LF-1A); D) Inversely graded sandstone (LF-1B); E) Inverse to normally graded sandstone (LF-1C); F)Sandstone dominated heterolithics (LF-4); G)Sandy debris flow, boulder rich (LF-3A); H) Sandy debris flow, mud clast rich (LF-3B); I) Amalgamated sandstone (LF-2); J) Siltstone dominated heterolithics (LF-5)

3.3 DEEP WATER ARCHITECTURE OF THE LYCIUM MEMBER

The Lycium Member is composed of an unusual system of channel and lobe complexes. The unusual aspect is the sand-rich character of the turbidite system and the relative lack of mudstones, in a setting that appears to be partly deep water slope and partly basin floor. From the NW to SE of the Fish Creek-Vallecito Basin, we move from more proximal to more distal reaches of the channel-lobe complex because, as we traverse in this direction the general facies changes are consistent with a dominant southeastern paleo-flow direction (Fig. 3-12). Observations made during field mapping, coupled with high resolution photo imagery, were used to separate the sand bodies into four main types: debris flow lobes, turbidite-filled channel complexes, turbidite lobe complexes and lobe fringe deposits.

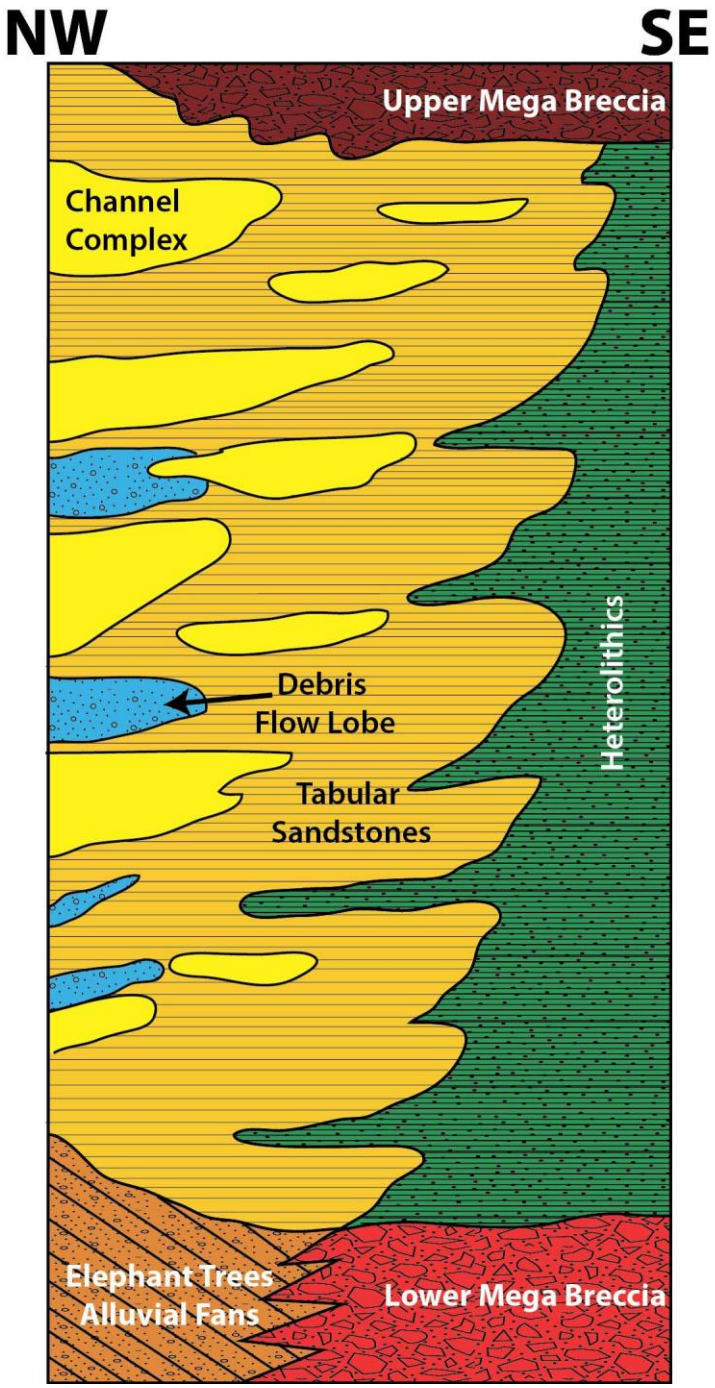

Figure 3-12: Composite section showing variation of interpreted environments within the Lycium Member turbidites.

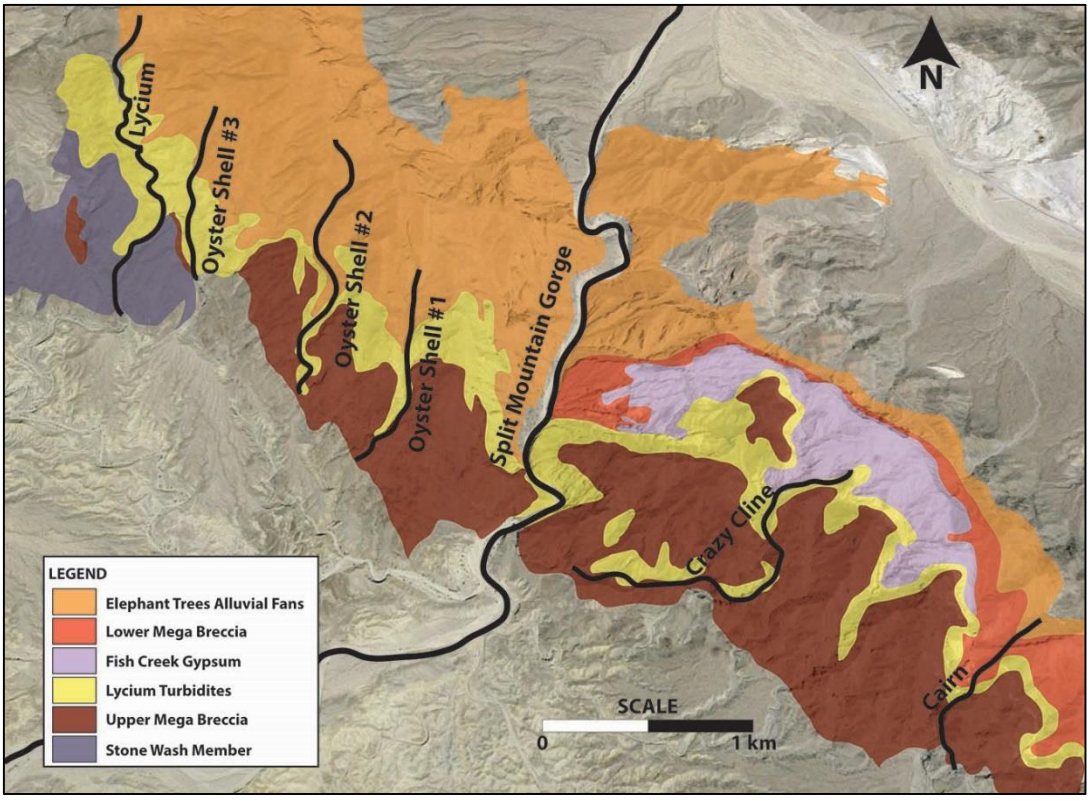

Figure 3-13: Map of Fish Creek Vallecito Basin illustrating formations and locations of studied canyons

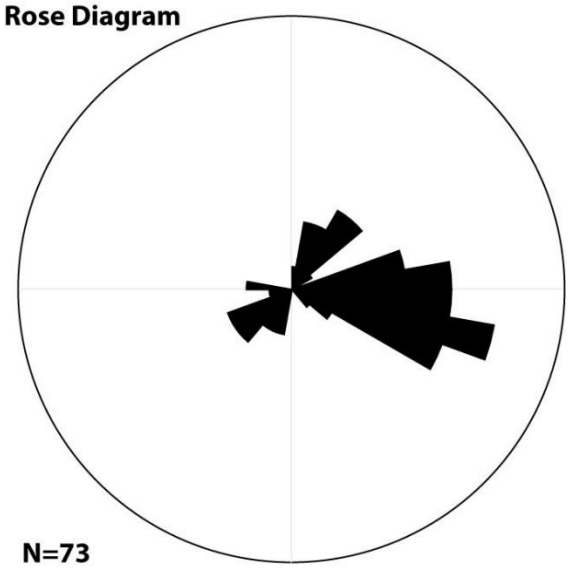

Figure 3-14: Rose diagram of measured paleo currents from flute clasts distributed throughout the Lycium Member turbidites. Dominant transport direction is E-SE.

3.3.1 Debris Flow Lobes

Description

Debris flow lobes occur preferentially in the northwestern portion of the system, and are recognized by their thick, wedge-shaped geometries, generally poorly sorted and chaotic character and abundant boulder inclusions. Stratigraphically, they are located in the upper portions of the Lycium Member and they extend laterally into Lycium Canyon and Oyster Shell Canyon #2 (Fig. 3-13) where they interfinger with sandy channelized turbidites.

The geometry of these deposits is blocky, with a thick, pluglike aspect that shows rapid lateral pinchout. The bodies are composed of boulder-rich debris flows (LF-3A, 3B). In the more proximal locations, beds tend to be thicker (up to 8 m) and are clast supported, but with distance from the source beds tend to thin, and sand content increases and clast populations decrease. The base of each package is slightly erosive, scouring into the underlying thinner bedded turbidite flows. Lack of paleocurrent indicators make it difficult to discern paleo flow direction but bed thinning and compositional changes show a general NW to SE paleo-flow direction.

The thickness of units of these deposits reaches up to 8 m and they can extend up to 20 meters laterally (aspect ratio 2:5). Aspect ratios (height: width) are high when compared to those of the sandy channel-lobe complexes in the basin.

Interpretation

The individual beds of this type are debris flows, as already described, and the observed groups of debris flows (bodies) often with a somewhat erosional base, are interpreted as lobes. The proximal to distal facies relationships of the debris flow lobes in the Lycium Mbr. are comparable to those described by Reading and others (1994) in gravel-rich submarine ramp

systems. Proximal areas are dominated by conglomerates and breccias, with sand content increasing within the medial to distal portions of the basin (Reading,1994) The course-grained, conglomeratic nature of the debris flows limits deposition and run out distances, causing formation of thick plug geometries. Because competence of debris flows decreases with transport distance the large clasts are focused in the more proximal areas of the system while sand content increases down flow. These observations are similar to those seen in the Blanca Turbidites System. (McLean and Howell 1985)

Due to their marked contrast with the turbidite sandstones in the Lycium Mbr., a second, separate source may be hypothesized for these debris flows. The grain size and abundance of outsized clasts is similar to the coeval Elephant Trees alluvial fan deposits, and both of these are likely to have had a similar source. Alluvial fans forming alongside a faulted margin, in this case the West Salton Detachment, may have caused subaerial debris flows to cascade from fault controlled line sources along the edge of the basin and to form subaqueous debris aprons in the deep water (McLean & Howell, 1985;Reading, 1994).

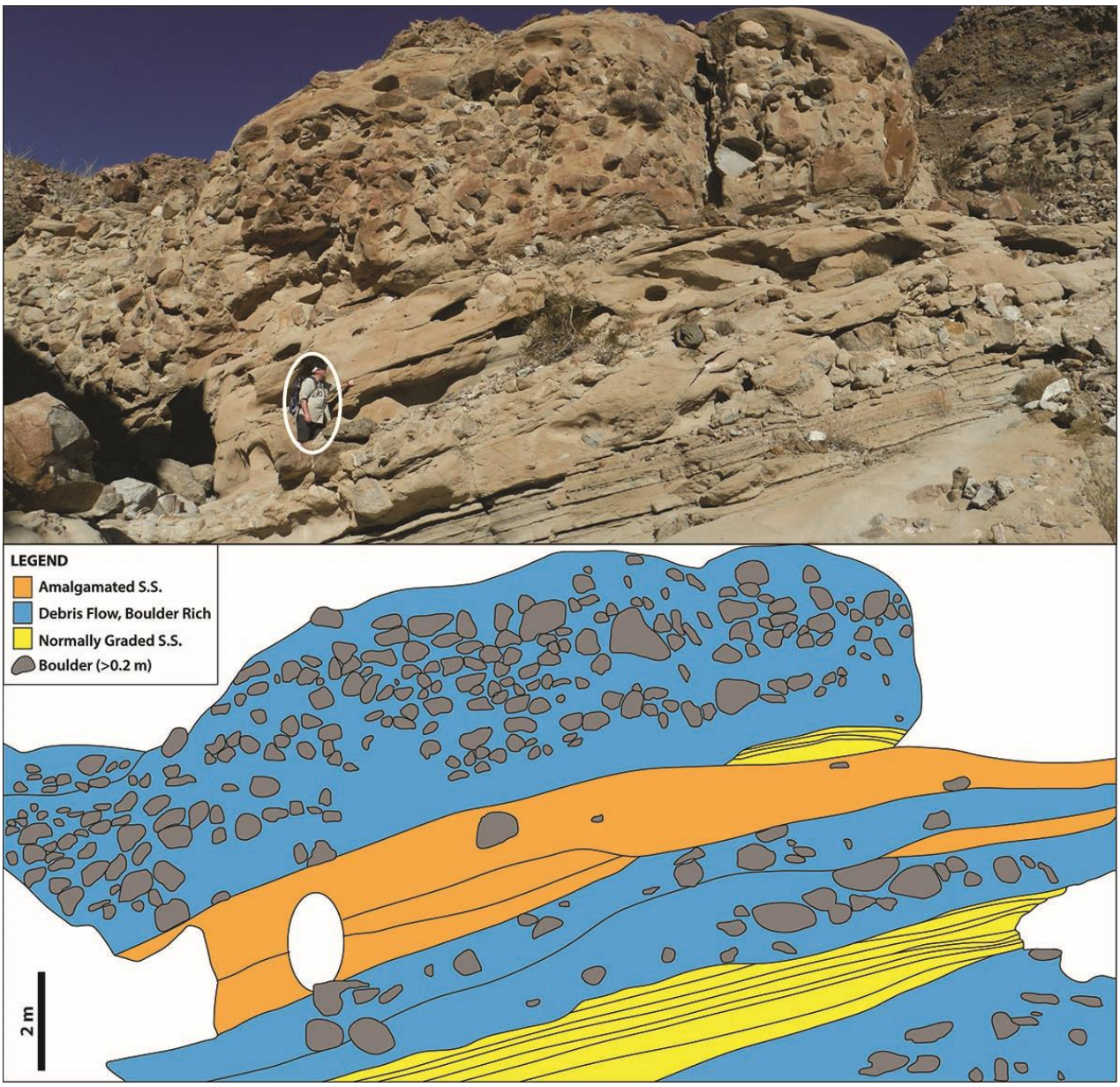

Figure3-15 : TOP) Outcrop image of debris flow lobe; BOTTOM) Illustration of bed type distribution in the above image. Thick debris flow beds are intermixed with amalgamated sandstones. Boulder inclusions are large and can reach sizes greater than 1 meter in diameter. Debris flow beds are plug like, with rapid lateral pinchout and thinning.

3.3.2 Channel Complexes

Channels represent a long lived pathway for sediment transport and are expressed in outcrop as negative relief created by confined turbidity flows in the deep water (Johnson et al., 2001). Channel-fill sequences tend to be complex, comprised of variable sediment facies. Mutti and Normark (1987) split channel types into three separate categories: depositional, erosional and mixed depositional and erosional. A series of stacked channels make up a channel complex. In this study, we encounter both depositional and slightly erosional channel forms making up thick channel complexes. Turbidite-filled channel complexes vary throughout the system and are preferentially located in the middle to upper sections of the Lycium Member. They are dispersed laterally throughout the system in the north and are absent in the most southeastern portion of the system.(Mutti and Normark 1987)

In Lycium Canyon, thick channel complexes (>10m) interfinger with debris flow lobes. These channelized turbidites comprise multiple flows, and sometimes multiple smaller channels which range in thickness from 5 to 9m. Complexes extend laterally for 10s of meters, with low aspect ratios (1:10) when compared to the debris flow lobes. Channels tend to be mildly erosional, with minor scouring into the underlying strata.

From a geometrical standpoint, the channel complexes have broad, sheetlike sand body geometries which contain amalgamated sandstones and some debris flow beds (LF-1, 2, 3). Amalgamated sand bodies are focused along the main axis of the channel bodies with thin -bedded sandstones located at the channel margins. Some lateral accretion

packages are prominent in the sand-rich channel bodies (Fig. 3-17). Individual flows are composed of normally graded beds (up to 0.5m) accreting at the margins of these sand-rich channels with packages up to 9m thick. Direct paleocurrent measurements were not recorded due to the lack of sole marks in beds. (Figure 3-16) The presence of lateral accretion packages (LAPs) suggests slight channel sinuosity in a lower energy environment. During lateral and down-dip channel migration, systematic erosion at the outer banks of the channel coupled with deposition along the inner-bend allows for the formation of these accretion packages (Abreu et al. 2003). (Fig. 3-17)

In Split Mountain Gorge, channel complexes tend to be broader and less erosive then those found further to the north in Lycium Canyon. The complexes tend to be interspersed with tabular sheet-like sandstones (Fig. 3-18) and increase in thickness as you move up in section. In outcrop, channel complexes increase from 4 m in thickness at the base to approximately 10m at the top with aspect ratios remaining at 1:10. Channel bases are more planar and less scouring than those found further to the north. Channel-fill is less complex than the channel fill in Lycium Canyon, it is predominantly normally graded sandstones with some inverse to normally graded beds (LF-1C, 1A).

The high-density turbidity flows in these bodies indicate deposition in a confined channelized setting. In a fan setting, channel confinement is generally restricted to proximal parts of the fan system such as the upper to mid fan regions. The high degree of channelization suggests deposition in the medial-axial fan setting (Grundvåg et al. 2014). The erosive character and thicker complexes found in Lycium Canyon suggest a more

proximal locality than the broader complexes found in Split Mountain Gorge. Deposits in Lycium Canyon appear to be more axial and further up the mid-fan setting than that of the deposits found in Split Mountain Gorge. In moving southwards across the basin, a progressive thinning of beds and shallowing of the channels is observed thus defining the transition from channel to lobe deposits. Further support for a mid-fan setting is the presence of erosional, multiple-event channel fill with amalgamated turbidites focused at the channel axis with heterolithics at the channel margin (Reading and Richards, 1994).

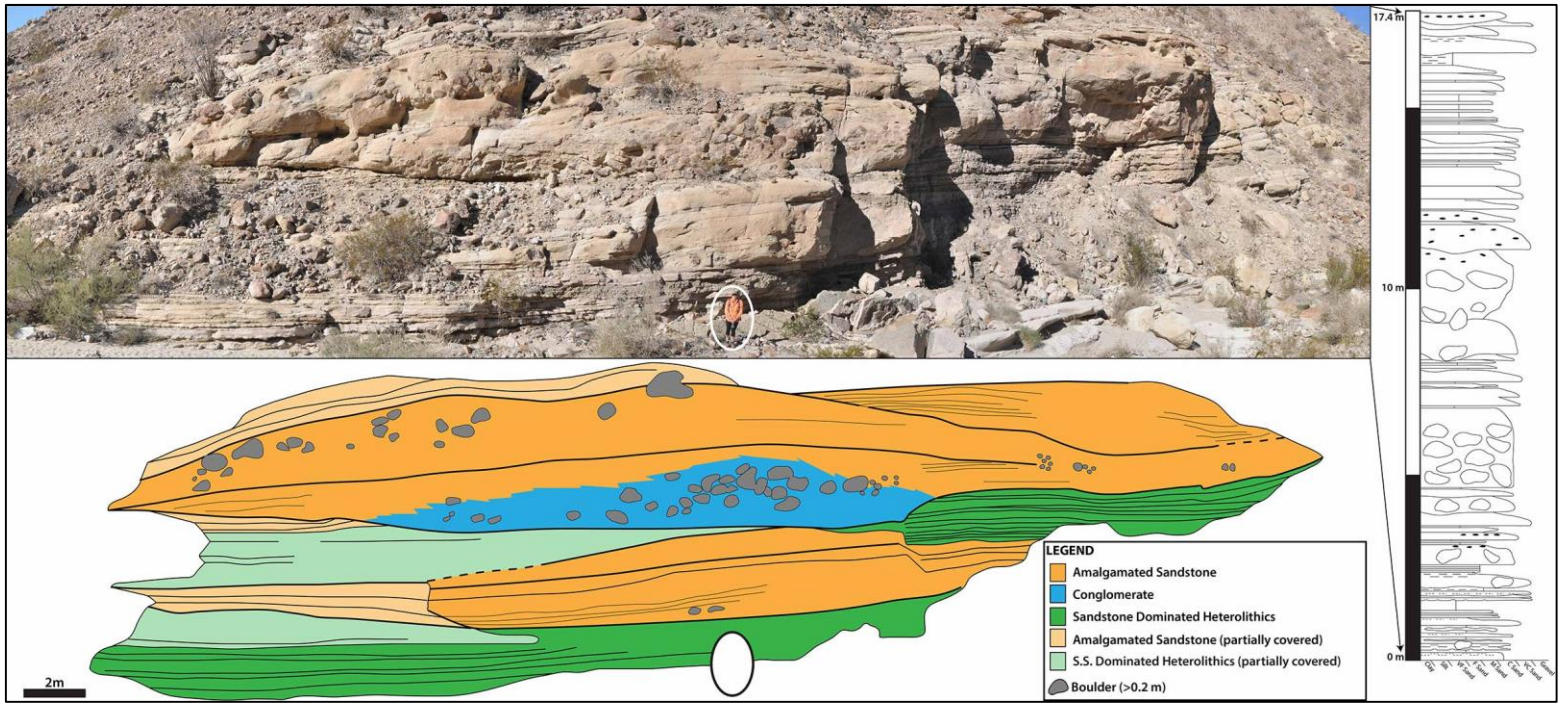

Figure 3-16: TOP) Outcrop image of channel complex; BOTTOM) Illustration of bed type distribution in the above image. Thick amalgamated sandstones are interbedded with conglomeratic debris flows and sandstone dominated heterolithics. Channel bodies are broad and lenticular with minorly scouring bases.

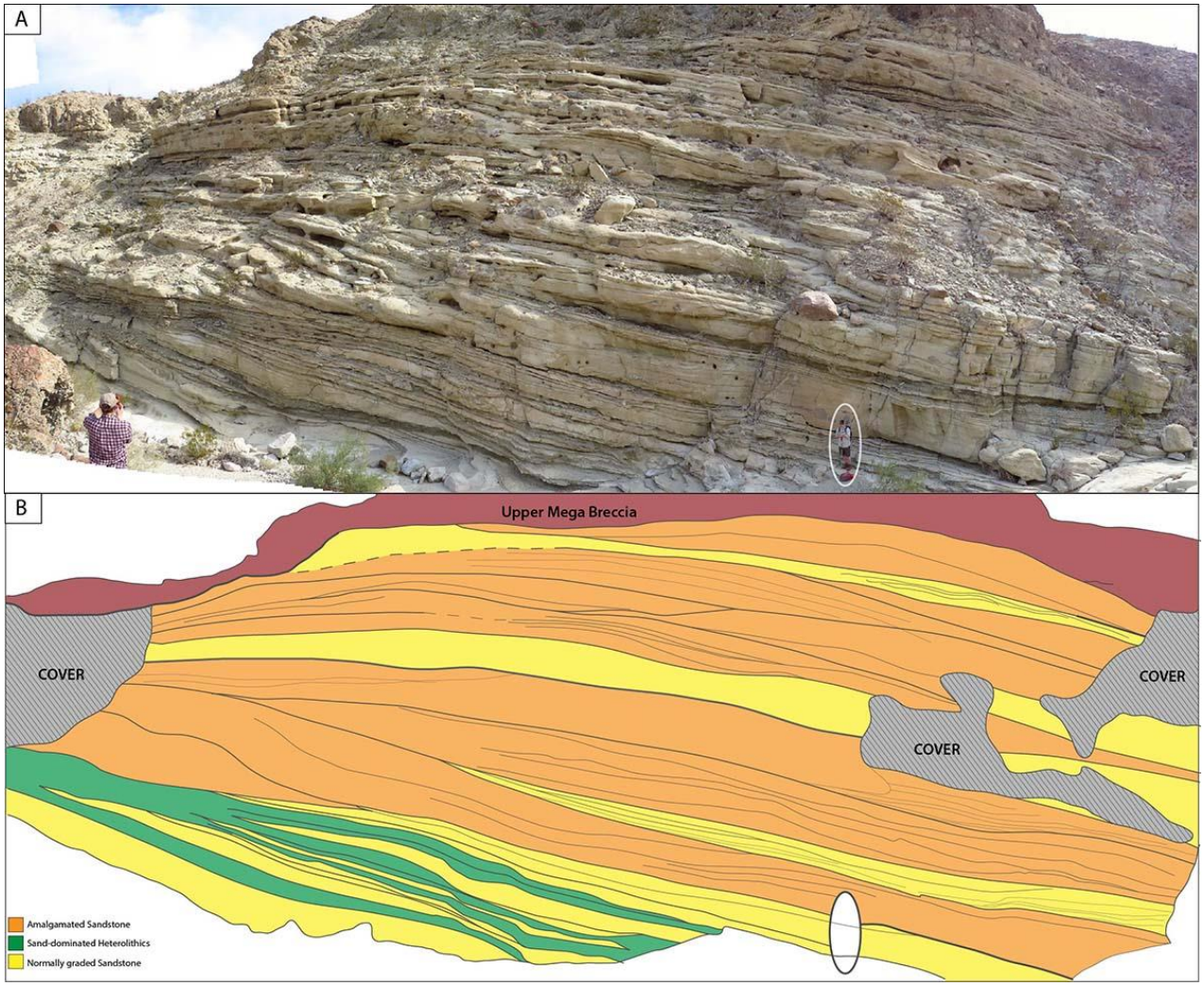

Figure 3-17: A) Outcrop example of lateral accretion packages found in Lycium Canyon; B) Illustration of bed type distribution throughout the outcrop example. Lateral accretion packages (LAPs) suggest slight channel sinuosity in a lower energy environment.

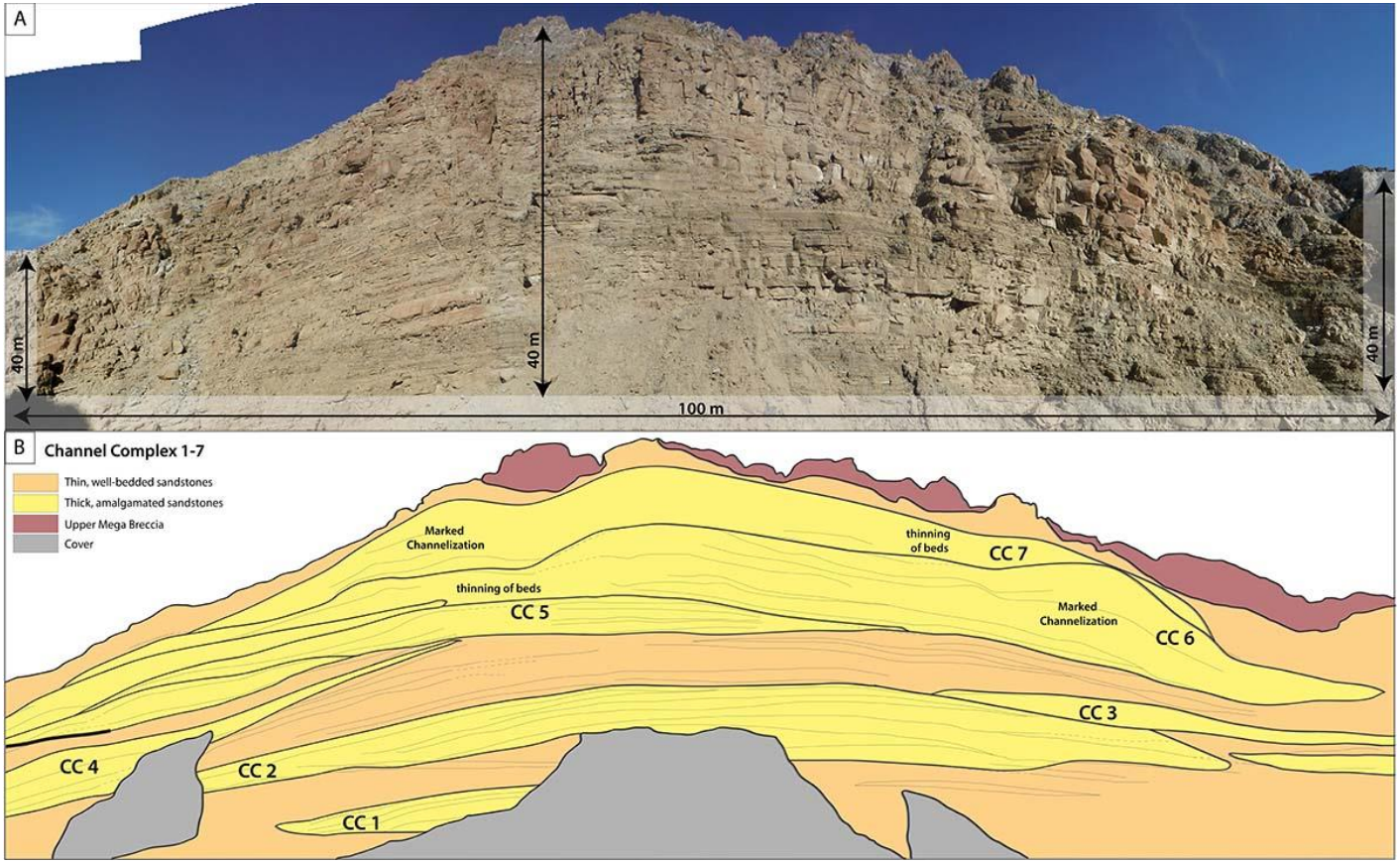

Figure 3-18: A) Outcrop image of steep cliff face in Split Mountain Gorge; B) Illustration of bed type distribution throughout the panorama. There are 7 identified channel complex packages. Packages widen and thicken as you move up in section. The top of the unit is capped by the Upper Mega Breccia. Complexes are broad and less erosive than those found in Lycium Canyon and feed into lobe complexes. Thin-bedded normally graded sands are found in between channel packages.

3.3.3 Lobe Complexes

Description

Extensive tabular, sheet-like sand bodies with only occasional, broad shallow channels comprise the lobe complexes of the Lycium Member turbidites. These lobe complexes are common to areas of submarine fans where the flow changes from a confined to unconfined nature (Johnson et al. 2001). This architectural style is similar to the transitional units described for the Skoorsteenberg Formation in the Karoo Basin (Johnson et al., 2001) and the Ross Formation of Western Ireland (Chapin et al. 1994).

Prominent in both the upper and lower Lycium Mbr., tabular sheet-like sand bodies are recognized by planar upper and lower surfaces and are predominately composed of layered sheets. They are organized into thickening and coarsening upward packages with a higher degree of bed amalgamation in the upper portions of units. They are laterally distributed throughout the basin and transition into finger grained lobe-fringe deposits towards Cairn Canyon (Fig. 3-13) in the southern most portions of the system. The lobe deposits interfinger with the channelized sand complexes and debris flows in the northwest and become the dominant architectural element in the mid to distal portions of the system.

The gently channelized sandstones of the lobe complex are composed of minor erosional channels which transition laterally into sheetlike over bank deposits and are predominant in the northern portions of the system. Thick, amalgamated sandstones (LF-

2) make up the channel fill of these packages. Average channel package thickness is approximately 5m, and extends laterally for up to 10s of meters, providing low aspect ratios when compared to the larger channel complexes in other portions of the system. Moving from the northwest (near Lycium Canon) to the southeast (Crazy Cline Canyon) individual bed thickness, and channel package thicknesses decrease.

Tabular, sheetlike sand bodies with planar top and bottom surfaces are found lateral to the channel deposits. These deposits are comprised of well-bedded turbidite sands, predominately normally graded sandstones with minor inversely and inverse-normally graded sandstones (LF-1). Individual bed thicknesses average 0.2m in the medial portions of the system and can be locally traced for 10s of meters (Fig. 3-18). Flute casts are common in the tabular sands and show a general E-SE paleo flow trend (Fig. 3-19). Beds tend to be heavily bioturbated with abundant cruziana trace fossils on exposed bedding surfaces (Fig. 3-20).

Interpretation

Lobe complexes were generated during focused aggradation of unconfined sediment gravity flows. Off-axis and deceleration of the turbidity currents at channel mouths resulted in a more wide-spread distribution of coarse-grained sediment (Galloway 1998). The laterally consistent sheetlike deposits with minor channelization are characteristic of the channel-lobe transition zone, where the flow changes from channelized to unconfined. The broad, gently scouring channels composed of amalgamated sandstones represent more axial lobe deposits. In coarse-grained systems

the lobe deposits tend to pile up, forming mounded lobes that have a somewhat restricted areal distribution. (Galloway 1998; Gardner et al. 2003)

In the off-axis, medial to distal portions of the fan we see a decrease in the presence of mounded lobe packages. Progressive decrease in bed thickness as well as an overall fining in grain size supports the interpretation of off-axis, medial to distal fan deposition.

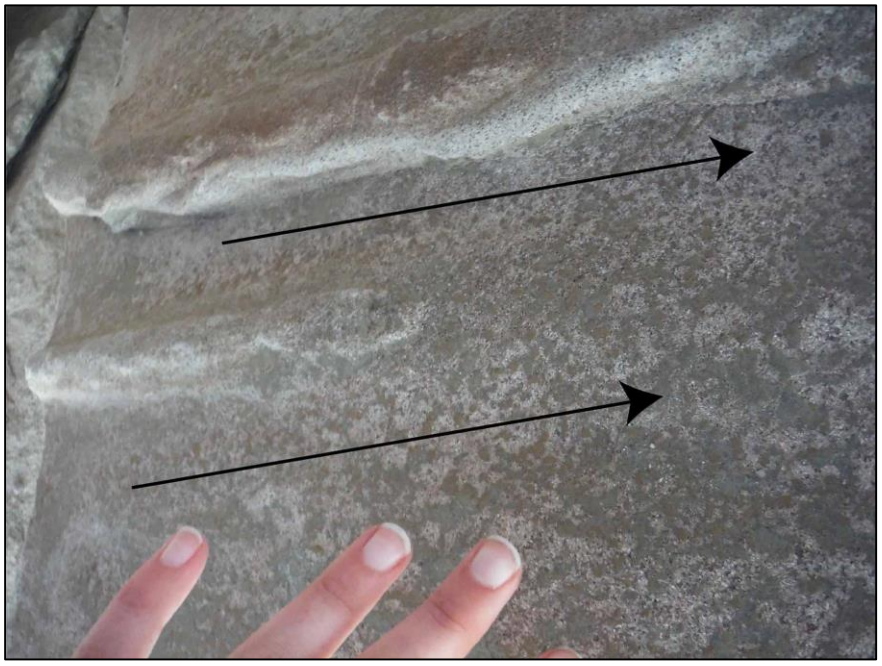

Figure 3-19: Flute casts on base of turbidite bed indicating paleo flow direction.

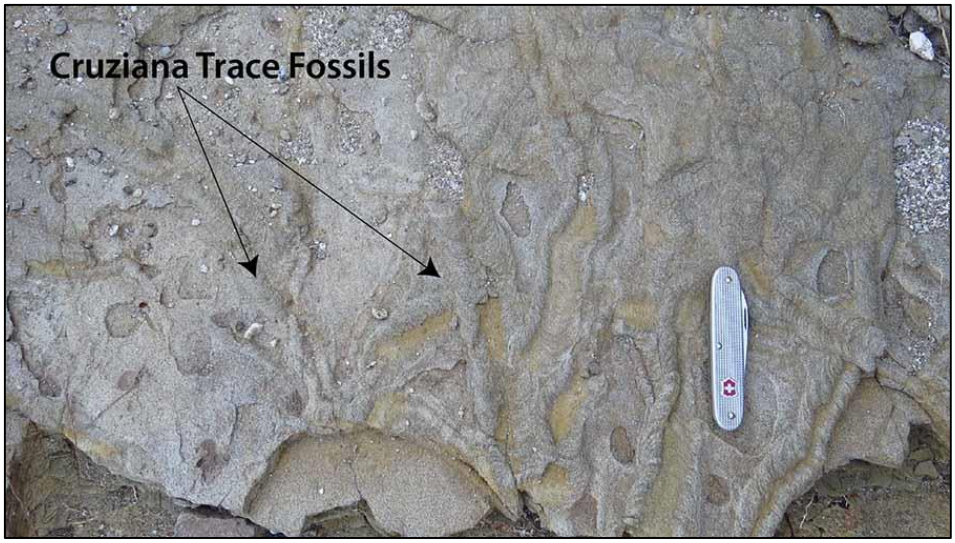

Figure 3-20: Cruziana trace fossils found on top of turbidite bed.

3.3.4 Lobe Fringe

In the most distal portions of the system, especially toward the southeast of the basin, we see a relative increase of fine-grained sandstone and siltstones interpreted as lobe fringe deposits. An abundance of fine sediments, interbedded with thin sheetlike beds of medium to coarse grained sands defines the distal fringes of the lobe complex (LF-5). The thickness of units of this type of deposit reaches up to 15 m and is composed of thin (up to 5 cm) beds interbedded with siltstone. The lobe fringe is located in the southern most areas of the basin, specifically Cairn Canyon (Fig. 3-13). Degradation of the outcrop makes it difficult to differentiate distinct beds as well as paleocurrent indicators. (Fig. 3-21)

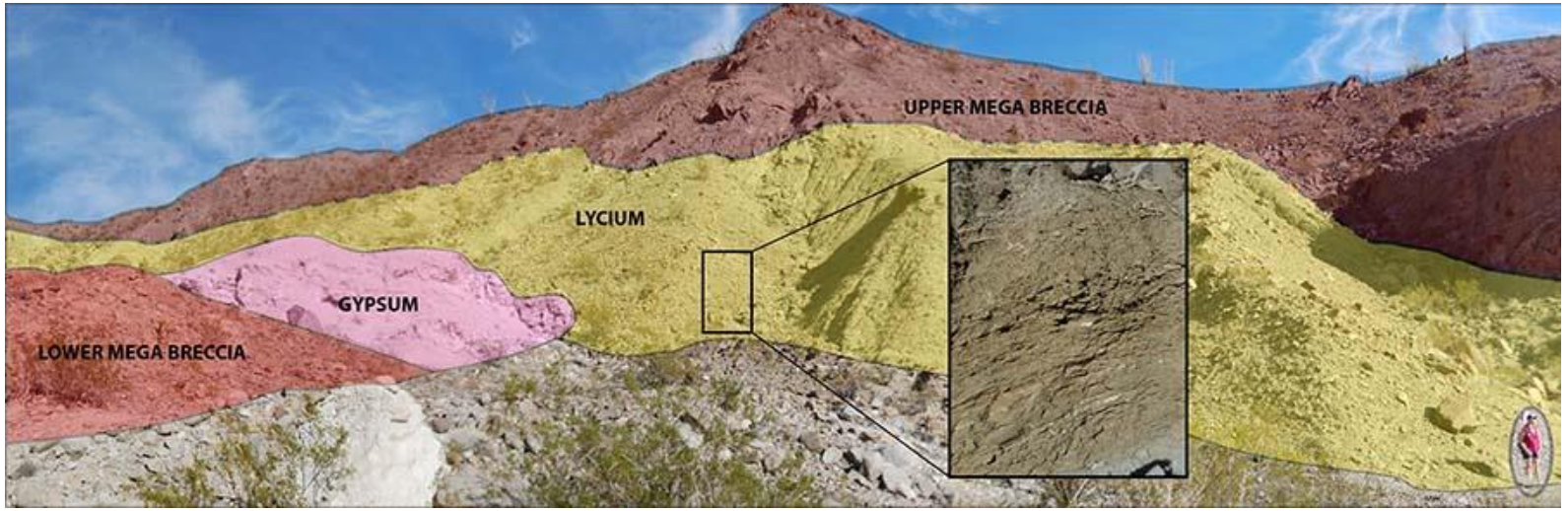

Figure 3-21: Outcrop image of lobe fringe; bound below by Lower Mega Breccia and Fish Creek Gypsum; bound above by the Upper Mega Breccia. The zoomed in section of the lobe fringe shows the fine sand and thin character of beds at this locality.

3.3.5 Architecture Element Distribution

A schematic map and fan model has been made for the highlighted architectural elements in the Lycium Member turbidites (Fig. 3-22). The model illustrates the interpreted location for each highlighted and outcrop example in a submarine turbidite fan. The most proximal mid-fan deposits, in Lycium Canyon, are characterized by thick channel complexes which are broad and mildly erosive with some observable lateral accretion packages (fig. 3-17). Moving further down-dip but still in the mid-fan setting, we see broader less erosive channels interfingered with thinner normally bedded sandstones interpreted as the channel lobe transition zone (Fig. 3-18). The fines found in Cairn Canyon represent the lobe fringe of the system (Fig. 3-21).

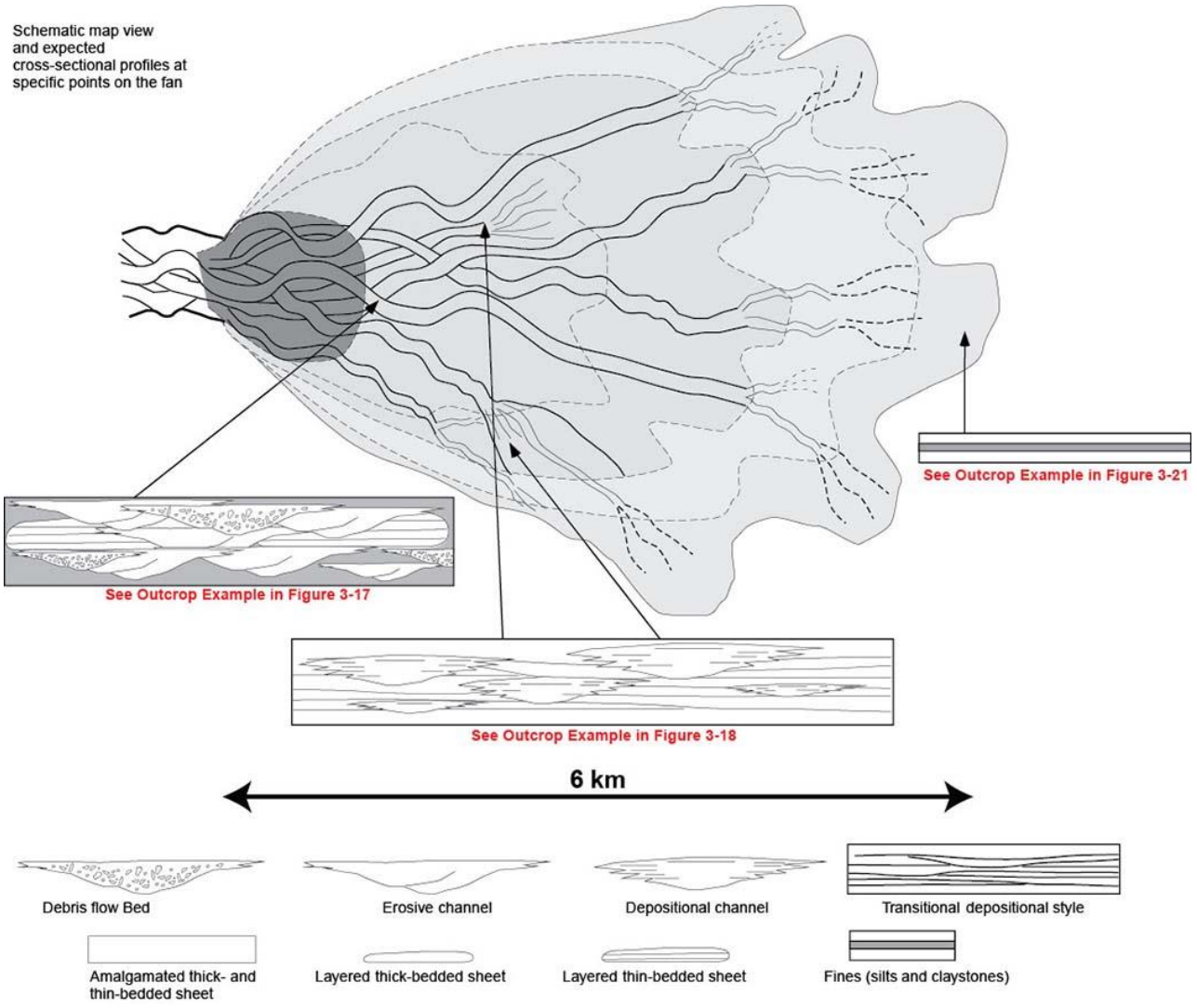

Figure 3-22: Model for basin-floor fan systems developed from outcrop data. Modified from Johnson et al., 2001.

3.4 PETROGRAPHY

The turbidite sandstones of the Lycium Mbr. comprise a range of coarse-grained, poorly-sorted arkoses consisting of 24-40% feldspar, 25-41% quartz, up to 22% biotite and subordinate lithic fragments. Diagenetic alterations vary throughout the sampled

sandstones; compaction is the most dominant process with variable concentrations of cementation throughout the studied sands. Composition was plotted and summarized on standard Q-F-L, Qm-F-Lt and Qm-P-K diagrams in order to assess provenance. Point-count data and statistics are documented in Appendix A.

3.4.1 Composition and Textures

Framework grain composition of the Lycium Member turbidites consists of feldspar, quartz, and biotite with subordinate plutonic lithic fragments and heavy minerals. The sampled sands fall into the arkose division of Folk's (1980) sandstone classification scheme. Sub-equal quantities of quartz and feldspar are observed with feldspar being the slightly dominant framework grain type. Biotite is the dominant non-QFL framework grain, with abundancies reaching up to 22%. Dominant grain sizes fall into the range of $328\mu m$ and $485\mu m$, corresponding to medium-grained sandstones. All samples are poorly sorted with angular grains.(Folk, 1980)

Plagioclase makes up 73% of the total feldspar population with K-feldspar comprising only 27%. P/K ratios average 3:1. Some degree of twinning is found in the majority of plagioclase grains and little to no visible twinning is observed in K-feldspar grains (Fig. 3-23).

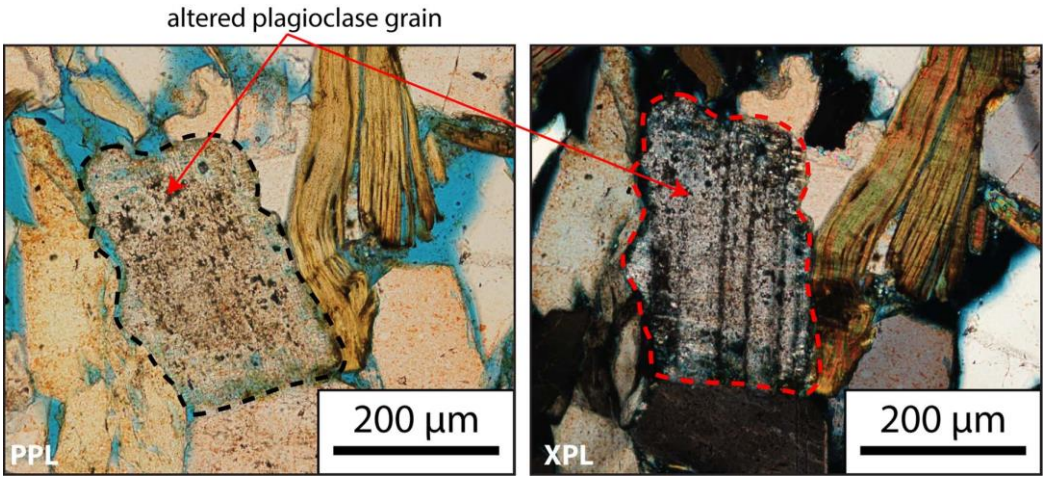

Figure 3-23: Photomicrograph of common feldspar vacuolization observed in samples. The image on the left is in plane-polarized light and the image to the right is the corresponding cross-polar image.

The quartz populations in the sampled sands are predominately monocrystalline with subordinate polycrystalline grains. Recycled quartz overgrowths are also observed throughout the sampled sands, but no quartz cement related to the most recent cycle of burial is observed.

Porosity values are highly variable throughout the sampled sands, ranging between 0.4 to 17%. Primary porosity is generally composed of intergranular pores and macropores whereas secondary porosity is attributed to dissolution of feldspars and both intragranular and circumgranular fractures. (Fig. 3-24)

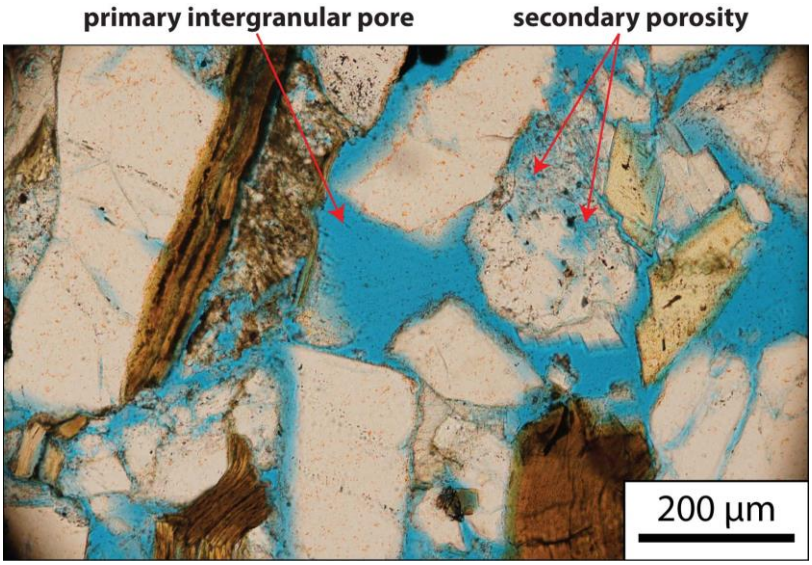

Figure 3-24: Pore network observed throughout the samples. Primary intergranular pores make up the majority of the porosity network in the samples. Significant amounts of secondary porosity is observed in leached feldspar grains. Plane-polarized light.

3.4.2 Diagenesis

Diagenesis is of interest due to the high degree of alteration in the studied samples, but was not a major of focus of this study but is important for documenting the validity of provenance data based on grain abundances. Diagenetic alterations vary throughout the studied samples but follow a general theme.

Varying degrees of alteration were observed in the feldspar grains of the sampled sands, with most feldspar grains featuring some degree of alteration. K-feldspar appears to be more resistant to alteration with a fresher, less-altered appearance than the plagioclase grains. Plagioclase alterations range from minor dissolution and replacement to heavy seritization and the presence of skeletal feldspar grains (Fig. 3-23).

Intergranular values (IGV) range between 9.5% and 22.4%, averaging 13.35%. Compactional Porosity Loss (COPL) values average 23.25% and range between 15.34% and 36.1%, indicating that compaction played a major role in alteration of the sample. (Lundegard, 1992; Ehrenberg, 1995) The most significant alteration resulting from resulting from compaction is intergranular porosity loss, with subordinate circumgranular fracturing and intragranular fracturing (Fig. 3-25). Other diagenetic processes include minor intergranular cementation (averaging 5.1%) and calcite grain replacement. Calcite and zeolite are the most common intergranular cements reaching modal percentages as high as 16%. Recycled diagenetic features include quartz cement overgrowths and seriticized feldspar grains.

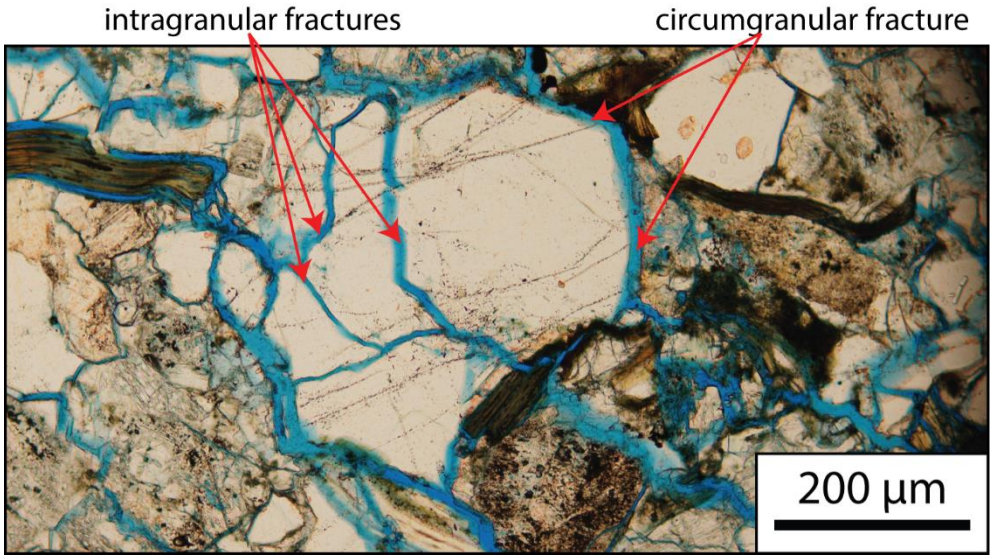

Figure 3-25: Photomicrograph illustrating fracturing observed in samples. Intergranular fractures are commonly seen throughout the studied sands. Circumgranular fractures are also observed in the samples.

3.4.3 Comparison to Previous Work

Previous work has focused on differentiating the source between local basement derived sediment and Colorado River derived sediment in the Fish Creek Basin. Winker termed these two separate compositional fields as "L-suite" for locally derived sediment from the Peninsular Range and "C-suite" for Colorado River derived sediment. Initial work by Merriam and Bandy (1965) recognized these two compositional fields and suggested a classification scheme to differentiate the two based on composition, present fossils, lithic types and relative abundance of biotite, hornblende, augite and plagioclase (Winker, 1987; Merriam & Bandy, 1965). In 1973, work by Van de Kamp focused on modern sands in the Salton Trough region. He recognized a compositional range between a local plutonic basement end member and a local volcanic basement end member (Winker, 1987; Van de Kamp, 1973).

The studied sands fall into Winker's "L-suite" classification for locally sourced, pre-Colorado River sediment. Previous work on Gulf of California sediments exhibits similar results to those of this study though a lack of standardization in sample analysis makes it difficult to directly compare statistical results from other studies. Winker (1987) has synthesized data from previous studies (i.e., Van De Kamp 1973, Merriam and Bandy 1965) and adjusted it to fit into the Gazzi-Dickinson approach. Compositional percentages from this study coincide with Dickinson's (1985) Qm-F-Lt and Q-F-L divisions for basement uplift and transitional continental sediment. These results fall in line with those from Winker's (1987) (Fig. QFL) as well as Van de Kamp's (1973) data

from local plutonic basement. Compositional percentages from this study do not completely fall in line with those of Merriam & Bandy (1965); samples from this study show higher percentages of K-feldspar. Variations in K-feldspar percentages between this study and work by Merriam & Bandy (1965) could be a result of staining, if samples from the previous study were unstained, the untwined K-feldspar grains may not have been accounted for. According to previous work, locally derived sediment or "L-suite" exhibits approximately a 1:1 quartz to feldspar ratio with a dominance of plagioclase over K-feldspar. These locally derived sediments are indicative of basement uplift and transitional continental sediments according to Dickinson's (1985) classification. (Dickinson 1985; Van de Kamp 1973; Merriam and Bandy 1965; Charles David Winker 1987)

4. DISCUSSION

4.1 COMPARISON WITH ANALOG SYSTEMS

The Lycium Member turbidites of the Latrania Formation show characteristics that stray from the standard submarine fan model, for instance: 1) relatively coarse-grained sands deposited over a relatively short period of time (~6.3 to 5.6 Ma); 2) mildly erosional beds and a dominance of sheet-like beds; 3) an absence of levee development; and 4) a lack of mud and clay. By comparing the results of this study with that of analog ancient systems we can better understand the depositional environment and processes behind the deposition of the Lycium Member turbidites.

The Repetto and Pico Formations in Ventura Basin, California show similar sedimentological and stratigraphic traits to those of this study. The Repetto and Pico formations are composed of sand-rich, coarse grained, and mud poor submarine gravity flows deposited in a rapidly subsiding elongate trough environment confined on three sides (Rotzien and Lowe, 2014). A study by Rotzien and Lowe (2014) noticed that the successions lack well developed channels, levees and lobes in relatively coarse-grained, laterally continuous, thick-bedded and scoured sand rich strata. Rotzien and Lowe (2014) hypothesized that these formations represent a type of deep-water braided environment and tested the hypothesis by comparing these deep water sediments to that of terrestrial braided systems.

Findings from his study show similar traits between both terrestrial braided systems and the Pico and Repetto formations. Rotzien and Lowe (2014) term the environment as 'braided lobe complexes' and classifies these complexes as having 3 main lithofacies associations: 1) highest energy, laterally continuous, thick-bedded mud clast-rich and gravelly sandstone which represents the most axial and proximal portions of submarine-fan lobes; 2) moderate energy deposits of laterally continuous thick to medium bedded sandstone with thin mudstone layers that represent off-axis and medial portions of the lobes; 3) Low energy deposits of thin to very thin bedded sandstone that represent distal lobe deposits and abandonment (Rotzien and Lowe 2014). Braided lobe complexes show disorganized stacking patterns which indicate a frequent shift of lobe depocenters as well as actively sought topographic lows (Rotzien and Lowe 2014). A lack of deep incisions, and lack of wedge-shaped channel architectures indicative of a channel-levee system further support the hypothesis of a braided lobe complex.

Lithofacies descriptions from Rotzien and Lowe show some similarities to the Lycium Member turbidites, with conglomeratic beds, thick and thin bedded sandstones and minor heterolithics and mudstones. Architectural elements of the sand successions are markedly similar as well, with broad, slightly erosional beds in proximal settings with sheetlike geometries in the more medial to distal portions of the system. Rotzien and Lowe identify disorganized stacking patterns in the Repetto and Pico formations, with alternating fining and coarsening upwards patterns. Some disorganization is seen in the stacked packages of the Lycium Member but is not as prevalent as the Pico and Repetto

Fms. The major similarities between the two systems are: 1) deposition of coarse sand onto a mud poor substrate; 2) lack of deep channel incisions; 3) depocenters switching; 4) lack of levee development. Aside from the major similarities between the Lycium Member and the Pico and Repetto Formations, the Lycium does show a higher degree of channelization in the most proximal portions of the basin suggesting a possible variation from Rotzien and Lowe's braided lobe complexes.

The Upper Carboniferous Ross formation in Ireland also shares some similar characteristics with the Lycium Member. It is a sand-rich system with low-sinuosity channel systems with spillover deposits and no evidence of muddy levees (Lien et al., 2003).The Ross formation consists of sand-rich sediment gravity flows. The main lithofacies of the Ross formation are thick and thin bedded sandstones and subordinate mudstones. Previous work by Lien et al. (2002) divides the Ross formation into the Upper and Lower Ross Formation, with the upper being more tabular with no defined channels and thickening or thinning packages and the lower being more channelized.

The character of the Upper Ross Formation is similar to that of the Lycium Member of this Study. It is composed of thickening upwards packages of amalgamated thick bedded sandstones interfingering with thin-bedded turbidites, similar to the deposits found in both Lycium Canyon and Split Mountain Gorge. Some lateral accretion deposits are observed in the system similar to that of the Lycium. But the overall character is of thick amalgamated sandstones forming broad channels.

Previous work has interpreted the Upper Ross Fm. as a prograding fan system within a rapidly subsiding basin (Chapin et al. 1994) but Lien et al. (2003) interprets the deposition of these deposits to be intimately related to channels and may be the result of lateral channel migration and aggradation (Lien et al. 2003; Chapin et al. 1994). Lien et al. have proposed a two stage model of channel filling and migration that would account for the character of the deposits in the Upper Ross Formation: 1) avulsion of a channel into a new area, the development of sinuosity and the beginning of lateral accretion at channel bends; and 2) vertical aggradation and channel filling (Lien et al., 2003). The two phases of Lien's model account for the observed vertical succession without needing large distances of lateral migration to form the same aggrading character. (Lien et al., 2003)

Each of the studied analogs share both similarities and differences with the Lycium Member turbidites. The Pico and Repetto Formations show a tabular, amalgamated, sand-rich and mud poor system similar to the deposits of this study but there is an clear lack of channelization in these formations that are present in the Lycium Member. The Ross Formation is markedly similar to the Lycium with both similar architectural elements and lithofacies, thus providing as the better analog for this study. Therefore Lien et al.'s two phase model for deposition of the Upper Ross Formation may also apply to the Lycium Member, suggesting that deposition was in a somewhat confined system with low-sinuosity channel systems and spill-over deposition.

4.2 PROVENANCE

4.2.1 Thin-Section Petrography

Winker identified four end member compositions in order to characterize the Neogene sandstones of the Salton Trough and Gulf of California: 1) Colorado River end members; 2) Plagioclase-rich arkosic end member; 3) Litharenite end member and 4) Arkosic end member (Winker, 1987). The four end members comprise a range of feldspar-rich plutonic and volcanic sands.

Samples from this study fall into composition #2, the plagioclase-rich arkosic end member. In Winker's study, samples in this category are deemed "L-suite" and their interpreted source is "readily attributed to granodiorites, quartz diorites and tonalities of the peninsular ranges" (Winker, 1987) which includes the neighboring Vallecito Mountains as well as the neighboring Peninsular Range rocks in the footwall of the West Salton Detachment Fault. By aligning Winker's classifications with the compositional statistics from this study, the source of the Lycium Member turbidites can be narrowed down to the near-by Peninsular Range batholith. Whether or not the sediment is derived from the upper or lower plate of the batholith is still in question and cannot be determined through petrographic inspection alone due to the overall homogenous character of the batholith.

Petrographic work by Kerr (1982), assessing provenance of the Elephant Trees alluvial fan deposits, which underlie the Lycium turbidites, indicates a plutonic

provenance interpreted to be the locally derived basement. Although both the Elephant Trees alluvial fan debris-flow deposits and Lycium Member turbidites are interpreted as derived from the same plutonic source, the compositional statistics of the two systems differ. Kerr's description of the alluvial fan deposits shows a feldspar to quartz ratio greater than 3:1, this study, along with previous work from Winker indicates a sub equal feldspar to quartz ratio for samples derived from local plutonic basement (Winker, 1987; Kerr, 1982). Winker suggests the statistical differences in the data to be caused by a lack of standardization in point count methodology and recalculated Kerr's data in order to better compare it to his study. After Winker's reassessment of Kerr's data, by recalculating lithic fragments as 40% quartz and 60% feldspar, Kerr's data falls in line with the results of this study as well as the previous work by Winker. (Winker, 1987)

From a petrographic standpoint data from Kerr, Winker and this study show that the Elephant Trees alluvial fans share a similar source with the overlying Lycium Member turbidites, the neighboring Peninsular Range batholith. When comparing the two formations on a larger scale, the idea of a shared source seems plausible but variations in character of the formations raises the possibility that the two systems are sourced from different areas within the Peninsular Range Batholith. (Fig. 4-1)

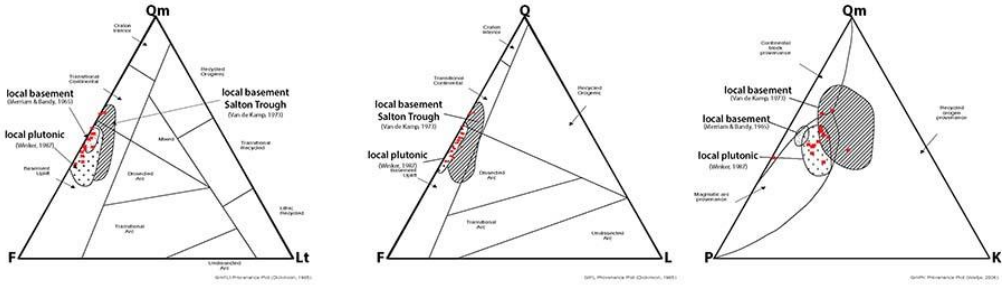

Figure 4-1: A) Q-F-L Diagram comparing results from this study to that of previous studies. Results of this study are highlighted in red.

4.2.2 Detrital Zircon as a proxy for provenance

Previous detrital zircon U-Pb and (U-Th)/He geo- and thermochronometry has been utilized in order to assess provenance of Mio-Pliocene sediment in the Fish Creek-Vallecito Basin. The detrital zircon U-Pb and (U-Th)/He ages obtained in the study by Cloos (2014) for both the Elephant Trees alluvial fan deposits and Lycium turbidites provide another proxy for provenance constraint of sediment dispersal into the Miocene Gulf of California. By combining previous detrital zircon work with both petrographic and stratigraphic data from this study, the sediment source for the Lycium Member turbidite sandstones can be further constrained.

Detrital zircon U-Pb ages of individual grains obtained by Cloos (2014) were used to identify sediment source areas which contained crystalline rock of known age. These source terranes could have shed sediment into systems which ultimately deposited into the Mio-Pliocene Gulf of California. The (U-Th)/He age of zircon was also determined for certain grains which had U-Pb ages previously obtained. This analysis provided the

"cooling age" of the zircon, or age since the grain cooled below 180 C. This temperature is reached when the zircon grain is at a shallow crustal level, generally between 5-7 km depth (Rahl et al. 2003). Combining crystallization age with cooling age can provide timing for when zircon was formed at deep levels in the crust and the tectonic event associated with exhuming it to a shallow crustal level. Obtaining these ages for grains from sedimentary rocks can help to identify sediment source areas with known tectonic histories. (Cloos, 2014)

Relative distributions of detrital zircon U-Pb ages for the Elephant Trees alluvial fans and Lycium turbidites both contained a similar age peak around 95 Ma. However, the Lycium also contained another age peak not present in the Elephant Trees around 162 Ma. This indicates the possible addition of a new sediment source terrane which began shedding sediment that was then deposited into the basin during Lycium deposition. If this is the case, the onset of Lycium deposition was not only a time of marine transgression, but also of new drainage capture for a headward eroding fluvial system from the north.

Detrital zircon (U-Th)/He cooling ages of grains range from 39.8 +-3.2 Ma to 72.6+-5.8 Ma. Crystalline basement with this thermal history is seen over a broad area of the Cretaceous Peninsular Range and Sierra Nevada batholith as flat-slab subduction during Laramide orogenesis leading to exhumation to shallow crustal levels (Grove et al., 2003).

U-Pb and (U-Th)/He ages from Cloos (2014) are similar to crystallization and cooling ages for the Peninsular Range batholith, which occurred in two pulses from 140 to 80 Ma with cooling during Laramide unroofing (Silver and Chappell 1988; Grove et al., 2003). As mentioned before, these ages make up a large percentage of detrital zircon ages for Elephant Trees and Lycium samples. The 162 Ma U-Pb age peak seen in Lycium samples predates emplacement of the Peninsular Range batholith but could be sourced from rock crystallized during early Sierra Nevada batholith emplacement. Zircon U-Pb ages from Cecil et al. (2012) give evidence for a Late Jurassic arc 167-145 Ma in age which makes up a portion of the northern Sierra Nevada (Cecil et al. 2012). Cordilleran arc accretion began in the Middle Jurassic in central California and moved south to present day Mexico in the Early Cretaceous (Dickinson, 2004).While it is difficult to determine how far north the sediment catchment area extended during Lycium deposition a late Jurassic arc terrane source with headwaters possibly 10s to 100s km north of the Fish Creek-Vallecito Basin.

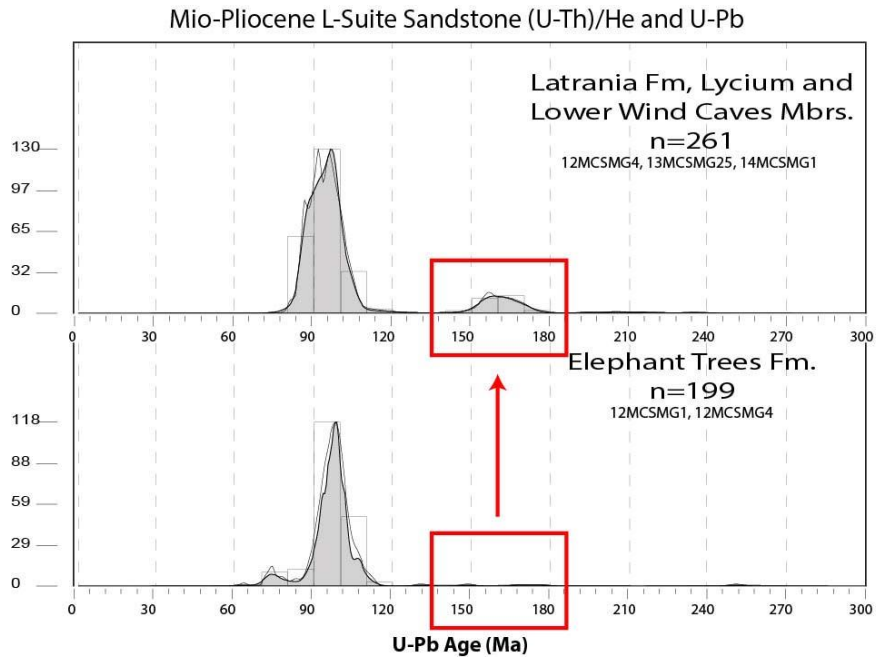

Figure 4-2: U-Pb age distributions and helium ages of samples taken from the Lycium and Elephant Trees formation. Modified from Cloos 2014.

4.2.3 Paleocurrent Indicators

Paleo flow throughout the Lycium turbidites is variable but shows an overall E-SE trend. The variation in paleo current transport directions may be the result of avulsing lobe channels. From the northwest to southeast of the system there is a transition from SW trending paleocurrents to a dominant E-SE direction giving the appearance of a longitudinal flow which curves towards the deepest part of the basin in the southeast.. Measurements by Kerr (1982) taken from unidirectional cross-strata and gravel fabric indicate a general NW flow direction, but more recent measurements (pers. Comm. Elisabeth Steel 2014) suggest an east and northeast dispersal direction for the underlying

Elephant Trees alluvial fan system. These transport directions contrast with that of the overlying marine turbidites. The underlying mass transport complex (lower mega breccia) shows an overall SE transport direction (Abbot et al., 2002).

4.2.4 Summary of Total Provenance

Petrographic data indicate a shared source between the Lycium turbidites and the Elephant trees alluvial fans. This shared source being the Peninsular Range batholith and local plutonic basement. However, detrital zircon U-Pb ages reveal that Lycium sediment could be partly derived from a more northerly source due to the presence of Late Jurassic U-Pb ages not seen in Elephant Trees samples. Zircon of this age may be derived from accreted terranes consisting of Late Jurassic arcs and plutons which are more commonly found north of the Fish Creek-Vallecito Basin. This provenance change might not be easily recognized using petrographic methods as the source terranes for Elephant Trees and Lycium sediment may have similar lithologies. Paleoflow indicators of the Lycium turbidites show an E-SE trend of sediment flow into the basin, differing from the northeastward trend of the underlying alluvial fan system. This transition in transport direction alludes to a possible change in sediment source area within the Peninsular Range Batholith and a likely routing of the Lycium turbidite system along the base of the WSDF footwall. A synthesis of each data type shows that both the alluvial fans and turbidites are sourced from the surrounding Peninsular Range batholith but a secondary more distant source is introduced into the basin with the deposition of marine turbidites.

4.3 LATE MIOCENE PALEOGEOGRAPHY

By combining the sedimentological descriptions with the provenance from this study, Late Miocene sedimentation of the Fish Creek Vallecito Basin can be summarized from a paleogeographic perspective. A hypothetical paleogeographic model has been developed for this area during Late Miocene deposition of the Lycium Member turbidite system (~6.3 to 5.6 Ma). The proposed model is illustrated in Figure 4-3, illustrating sediment dispersal into the basin at two different points in time: 1) Before marine input into the basin (Pre 6.3 Ma) and 2) co-eval with the deposition of the marine turbidites.

The Fish Creek-Vallecito Basin is a part of a series of NW trending basins located in the Basin and Range province (Kerr, 1982). These basins are tectonically controlled, and characterized by half-graben structural geometries with a normal fault bounding an edge of the basin and a back-tipped basement block defining the other edge (Kerr, 1982). In the Fish Creek-Vallecito Basin, the basin is bound by the normal Vallecito Mountain fault in the north and a nameless fault in the southeastern portion which borders the northern side of the Fish Creek Mountains. The half-graben structures in these basins had a significant influence on the sedimentation and paleogeography of the area in the late Miocene.

During the Late Miocene, between 8 and 6.3 Ma, alluvial fans were being shed into the Fish Creek-Vallecito Basin from its margins onto the hanging wall of the West Salton Detachment Fault (Fig. 4-3A). These fans were sourced from the Peninsular Range batholith, specifically the neighboring Vallecito Mountains and shed into the

newly forming rift basin. Around 6.3 Ma, a mass transport complex moving from the NW to SE deposited into the basin creating chaotic topography on the basin floor. Mass transport most likely caused by a large seismic event which instantaneously distributed massive amount of debris into the basin. This flow most likely diverted sediment transport into the basin, translating the dominant sediment dispersal direction from the northeast to E-SE. After the large 'sturzstrom' event, environmental conditions were appropriate to form a thick succession of clean gypsum into the deepest portion of the basin.

At around 6.3 Ma, further rapid marine incursion of the basin occurred with deposition of the Lycium Member turbidites. Within the Lycium, thick amalgamated channels dominate the NW portion of the system and thin towards the southeast implying sediment input from the northwest. The overall bed thickness trend coupled with grain size distribution also reflects this northwesterly sediment input trend indicating a transition from a proximal to distal environment. The clean and organized character of this thick succession of sandy turbidites makes the interpretation of these sediments in terms of subaqueous transitions from alluvial fan deposits at the margin of the basin unlikely. It is more likely that a fluvial and deltaic feeder system (now completely eroded after uplift of the region) was the main turbidity current supply conduit running parallel to the WSDF footwall and generating sand rich turbidite succession that is better sorted than the underlying alluvial fan system. (Fig. 4-3B)

Within the turbidite system, but towards the northwestern margin of the basin there is an influx of large clasts that resemble those seen in the underlying Elephant Trees. These clasts occur in large debris flow beds focused in the northwestern margins of the system and interfinger with sandy turbidite beds. These deposits represent a zone of mixing, with input from both the line-sourced marginal alluvial fans and the point-sourced fluvial to turbidity current feeder into the basin.

Moving south through the system, the environment changes from more proximal to distal show an overall succession thinning. As the lobes enlarged and coalesced they built into a channel-lobe complex prograding into the basin from NW to SE, prograding over the Lower Mega Breccia and Fish Creek Gypsum. In Split Mountain gorge (section 1) there is an abrupt and dramatic increase in thickness of the turbidites, caused at least partly by the chaotic topography created by the underlying lower mega breccia. This mass transport deposit focused the turbidity flows around paleo highs and into paleo lows, creating a ponded turbidite succession.

Based on the results of this study combined with previous work, a comprehensive paleogeographic overview of Lycium deposition was created. Around 6.3 Ma, following the abrupt marine incursion into the basin, a headward eroding fluvial system to the northwest of Fish Creek Basin prograded into the basin, bringing with it sediment from the Peninsular Range batholith as well as possibly from the more northern Sierra Nevada Batholith. Alluvial fans were shed off the basin margins into the deep water creating debris flow lobes interfingering with the sediment supplied from the northwesterly fluvial

feeder draining in an E/SE direction. The turbidites of the system were sourced from the discharge of this axial fluvial system prograding from the NW.. The chaotic topography created by the underlying mega breccia was also a factor in sediment distribution through the basin. Overall, the trend of deposition into the basin at this time is in line with longitudinal deposition along the length the West Salton Detachment fault footwall, indicating that the Lycium turbidites represent the earliest axial marine deposits into the Miocene Gulf of California.

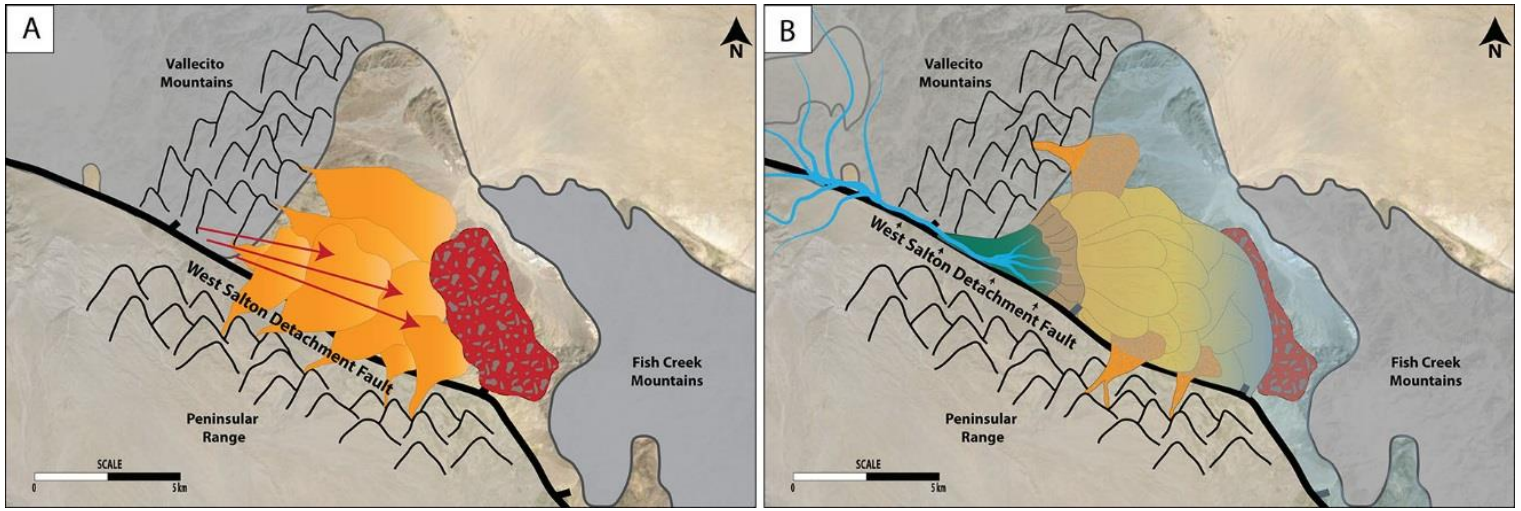

Figure 4-3: A) Paleogeographic interpretation of basin before marine incursion (~6.4-6.3 Ma), Alluvial fans were shedding into the basin from the neighboring Peninsular Ranges and Vallecito Mountains and a sturzstrom deposit entered the basin; B) Paleogeographic interpretation of deposition into the basin from 6.3 Ma to 5.6 Ma. Rapid marine incursion followed by progradation of an axial fluvial feeder system into the basin along the West Salton Detachment fault depositing basin floor fans.

5. CONCLUSIONS

- Five lithologic facies were identified and described in the Lycium Member turbidites of the Fish Creek Vallecito Basin: well-bedded turbidite sandstones (LF-1), thick amalgamated sandstones (LF-2), sandy debris flow beds (LF-3), sandstone dominated heterolithics (LF-4), siltstone dominated heterolithics (Lf-5).
- Four unique facies associations were identified: Channelized turbidites (FA-1), subaqueous alluvial-fan debris-flow lobes (FA-2), sheet turbidites (FA-3) and heterolithic interbedded sandstones and siltstones (FA-4).
- Architectural elements such as: debris flow lobes, turbidite channel complexes, lobe complexes, and lobe fringe were identified throughout the system highlighting a NW to SE trending basin floor fan system.
- Integration of petrographic and detrital zircon provenance along with paleo flow measurements indicate a Peninsular Range and possible additional secondary source for the Lycium Member turbidites. This latter source likely comes from further north where Late Jurassic Igneous rock related to arc accretion is more common.
- A proposed paleogeographic model of Late Miocene deposition in the Fish Creek-Vallecito Basin includes a fault-parallel (WSDF) longitudinal fluvial to turbidity current feeder system prograding from the northwest to the southeast. This fluvial feeder possibly represents the first axial system delivering sediment into the

paleo-Gulf of California.

Appendices

APPENDIX A: POINT COUNT

Point count data with number of points out of 250 listed next to grain type.

SAMPLE #	14-Ly-1	14-Ly-2	14-Ly-3	14-Ly-4	14-Ly-5	14-Ly-6	14-Ly-7	14-Ly-8	14-Ly-9	14-Ly-10	14-Ly-11	14-Ly-12	14-Ly-13	14-Ly-14	13-SMG-25
QUARTZ															
mono.	73	104	66	85	96	81	79	89	86	95	69	90	83	63	77
poly.	1	0	3	3	3	0	5	0	0	0	5	1	1	0	1
Q total	74	104	69	88	99	81	84	89	86	95	74	91	84	63	78
FELDSPAR															
Plagioclase															
fresh/slight alteration	26	27	24	15	34	26	17	25	32	29	63	40	36	28	38
sericitized	19	27	10	13	5	11	13	11	6	7	16	3	4	4	4
replaced	2	0	2	11	13	10	9	10	4	3	3	2	8	10	4
leached	0	0	31	18	9	17	32	15	15	2	14	15	24	20	23
plag. Total	47	54	67	57	61	64	71	61	57	41	96	60	72	62	69
K-spar															
fresh/slight alteration	10	17	23	19	21	16	14	21	16	17	2	17	22	18	19
replaced	34	0	2	5	1	2	1	1	0	3	0	1	1	0	1
leached	0	0	9	5	0	6	4	4	5	0	0	5	1	3	2
K-spar Total	44	17	34	29	22	24	19	26	21	20	2	23	24	21	22
Feldspar Total	91	71	101	86	83	88	90	87	78	61	98	83	96	83	91
ROCK FRAGMENT															
Plutonic RF	1	0	2	0	0	7	2	0	0	2	3	1	1	1	2
Unkown	1	0	0	2	0	0	0	3	3	0	3	1	0	2	1
Total RF	2	0	2	2	0	7	2	3	3	2	6	2	1	3	3
HEAVY MINERALS	0	3	4	4	2	3	1	4	2	1	3	2	5	3	4

SAMPLE #	14-Ly-1	14-Ly-2	14-Ly-3	14-Ly-4	14-Ly-5	14-Ly-6	14-Ly-7	14-Ly-8	14-Ly-9	14-Ly-10	14-Ly-11	14-Ly-12	14-Ly-13	14-Ly-14	13-SMG-25
MICAS															
biotite	37	30	32	32	34	39	23	41	46	27	18	39	22	56	34
muscovite	4	0	0	0	0	0	2	0	0	4	1	1	1	5	1
UKNOWN GRAINS	3	3	3	1	0	0	0	0	0	0	1	0	2	2	1
POROSITY															
primary intergr.	14	16	31	16	0	28	20	23	32	16	15	30	29	14	24
secondary	5	8	11	14	1	4	21	5	5	4	6	1	4	4	5
Porosity Total	19	24	42	30	1	32	41	28	37	20	21	31	33	18	29
CEMENT															
calcite	4	6	0	4	30	3	12	0	0	40	25	0	7	20	1
zeolite	6	1	0	0	0	0	1	0	0	0	0	0	0	0	12
uknown	0	8	0	7	3	0	1	1	0	0	1	1	0	0	0
total cement	10	15	0	11	33	3	14	1	0	40	26	1	7	20	13
FRACTURE															
circumgranular	6	0	0	0	0	0			0	0	4	0	0	0	0
intragranular	4	3	1	0	0	0	1	2	0	1	1	2	4	0	0
Total Points	250	250	250	250	250	250	257	251	250	250	250	250	250	250	250
Quartz %	0.296	0.416	0.276	0.352	0.396	0.324	0.326848	0.354582	0.344	0.38	0.296	0.364	0.336	0.252	0.312
Feldspar %	0.364	0.284	0.404	0.344	0.332	0.352	0.350195	0.346614	0.312	0.244	0.392	0.332	0.384	0.332	0.364
Lithics %	0.008	0	0.008	0.008	0	0.028	0.007782	0.011952	0.012	0.008	0.024	0.008	0.004	0.012	0.012
biotite %	0.148	0.12	0.128	0.128	0.136	0.156	0.089494	0.163347	0.184	0.108	0.072	0.156	0.088	0.224	0.136
IGV%	9.6	12.4	12.4	10.8	13.2	12.4	13.22957	9.561753	12.8	22.4	16.4	12.4	14.4	13.6	14.8
porosity %	7.6	9.6	16.8	12	0.4	12.8	15.95331	11.15538	14.8	8	8.4	12.4	13.2	7.2	11.6
cement %	4	6	0	4.4	13.2	1.2	5.447471	0.398406	0	16	10.4	0.4	2.8	8	5.2
p/k ratio	1.068182	3.176471	1.970588	1.965517	2.772727	2.666667	3.736842	2.346154	2.714286	2.05	48	2.608696	3	2.952381	3.13636364
Plagiocase/feldtotal	0.516484	0.760563	0.663366	0.662791	0.73494	0.727273	0.788889	0.701149	0.730769	0.672131	0.979592	0.722892	0.75	0.746988	0.75824176
Kspar/feldtotal	0.483516	0.239437	0.336634	0.337209	0.26506	0.272727	0.211111	0.298851	0.269231	0.327869	0.020408	0.277108	0.25	0.253012	0.24175824

APPENDIX B: GRAIN SIZE DATA

Grainsize dat: the long axis of 100 grains was measured for each sample.

Sample #	14-Ly-1	14-Ly-2	14-Ly-3	14-Ly-4	14-Ly-5	14-Ly-6	14-Ly-7	14-Ly-8	14-Ly-9	14-Ly-10	14-Ly-11	14-Ly-12	14-Ly-13	14-Ly-14	13-SMG-25
Grainsize (mm)	0.648	0.534	0.451	0.660	0.180	0.278	0.499	0.322	0.352	0.866	1.133	0.569	0.525	0.564	0.483
	0.411	0.403	0.560	0.593	0.368	0.307	0.681	0.245	0.255	0.361	0.645	0.466	0.406	0.493	0.509
	0.297	0.658	0.470	0.552	0.328	0.227	0.667	0.241	0.304	0.311	0.720	0.435	0.185	0.296	0.348
	0.433	0.519	0.311	0.241	0.267	0.194	0.585	0.179	0.395	0.390	0.789	0.814	0.273	0.281	0.237
	0.628	0.667	0.317	0.533	0.268	0.302	0.717	0.188	0.228	0.384	0.839	0.464	0.296	0.199	0.257
	0.545	0.668	0.479	1.326	0.187	0.213	0.550	0.231	0.216	0.356	0.949	0.658	0.226	0.350	0.314
	0.544	0.389	0.494	0.971	0.545	0.205	0.410	0.283	0.191	0.392	0.930	0.422	0.215	0.314	0.283
	0.569	0.593	0.573	0.474	0.173	0.232	0.657	0.250	0.210	0.468	1.071	0.613	0.408	0.235	0.327
	0.402	0.330	0.657	0.566	0.231	0.368	0.510	0.281	0.363	0.422	0.641	0.452	0.266	0.307	0.372
	0.397	0.799	0.539	0.538	0.251	0.174	0.367	0.157	0.316	0.255	0.675	0.433	0.315	0.216	0.475
	0.450	0.599	0.405	0.524	0.293	0.337	0.316	0.165	0.251	0.386	0.835	0.457	0.260	0.252	0.585
	0.783	0.691	0.458	0.272	0.160	0.274	0.769	0.324	0.248	0.292	0.706	0.820	0.353	0.383	0.749
	0.479	0.281	0.578	0.579	0.208	0.353	0.753	0.222	0.262	0.288	0.727	1.195	0.253	0.304	0.629
	0.363	0.531	0.229	0.349	0.292	0.119	0.477	0.268	0.350	0.290	0.476	0.979	0.280	0.280	0.465
	0.337	0.634	0.508	0.789	0.267	0.341	0.485	0.274	0.426	0.226	0.595	0.490	0.313	0.273	0.408
	0.358	0.511	0.568	0.527	0.228	0.205	0.518	0.222	0.395	0.304	0.492	0.687	0.366	0.239	0.433
	0.237	0.376	0.463	0.281	0.332	0.240	0.418	0.294	0.263	0.202	0.396	0.410	0.361	0.248	0.266
	0.493	0.940	0.314	0.379	0.463	0.249	0.883	0.225	0.274	0.224	0.907	0.456	0.186	0.218	0.376
	0.584	0.519	0.359	0.347	0.275	0.215	0.341	0.429	0.380	0.279	0.970	0.427	0.543	0.267	0.360
	0.498	0.470	0.357	0.449	0.228	0.270	0.786	0.317	0.312	0.263	1.522	0.404	0.272	0.280	0.338
	0.335	0.317	0.541	0.453	0.280	0.206	0.539	0.308	0.249	0.253	0.807	0.203	0.433	0.241	0.487
	0.369	0.245	0.393	0.459	0.308	0.270	0.470	0.301	0.169	0.210	0.952	0.855	0.231	0.237	0.462
	0.414	0.395	0.374	0.871	0.267	0.323	0.635	0.304	0.199	0.352	1.424	0.469	0.255	0.316	0.336
	0.395	0.445	0.300	0.768	0.375	0.226	0.728	0.190	0.251	0.275	1.562	0.506	0.333	0.263	0.761
	0.328	0.435	0.380	0.406	0.225	0.224	0.638	0.346	0.314	0.330	0.742	0.383	0.277	0.230	0.339
	0.536	0.386	0.212	0.568	0.224	0.237	0.609	0.340	0.280	0.295	1.196	0.504	0.203	0.407	0.340
	0.790	0.207	0.481	0.507	0.239	0.305	0.451	0.279	0.306	0.357	0.681	0.689	0.250	0.231	0.231
	0.469	0.319	0.334	0.556	0.318	0.244	0.330	0.318	0.238	0.275	0.935	0.707	0.310	0.217	0.216
	0.405	0.363	0.314	0.949	0.456	0.204	0.440	0.318	0.347	0.257	0.946	0.462	0.198	0.327	0.230
	0.254	0.451	0.358	0.899	0.194	0.204	0.336	0.399	0.249	0.276	0.522	0.430	0.201	0.228	0.288
	0.296	0.437	0.302	0.395	0.279	0.269	0.445	0.299	0.300	0.525	0.603	0.344	0.239	0.390	0.288
	0.354	0.409	0.239	0.784	0.230	0.189	0.429	0.373	0.209	0.300	0.505	0.530	0.257	0.196	0.208
	0.471	0.521	0.227	0.860	0.344	0.204	0.770	0.443	0.270	0.326	0.362	0.266	0.253	0.277	0.196
	0.549	0.462	0.348	0.582	0.128	0.184	0.554	0.319	0.228	0.434	0.685	0.290	0.198	0.283	0.235
	0.498	0.370	0.443	0.295	0.195	0.230	0.539	0.196	0.364	0.430	0.365	0.358	0.148	0.364	0.255
	0.319	0.421	0.278	0.810	0.349	0.219	0.488	0.511	0.238	0.630	0.829	0.611	0.243	0.293	0.370
	0.374	0.330	0.203	0.436	0.312	0.231	0.623	0.264	0.366	0.434	0.855	0.712	0.257	0.211	0.438
	0.403	0.374	0.226	0.443	0.382	0.302	0.363	0.399	0.347	0.393	0.598	0.593	0.229	0.197	0.303
	0.313	0.338	0.374	0.493	0.401	0.241	0.456	0.249	0.428	0.356	0.414	1.581	0.292	0.219	0.290
	0.562	0.539	0.313	0.449	0.334	0.250	0.542	0.317	0.374	0.461	0.479	0.540	0.319	0.241	0.359
	0.302	0.399	0.339	0.444	0.259	0.199	0.347	0.366	0.251	0.345	0.378	0.383	0.333	0.351	0.471
	0.408	0.308	0.371	0.626	0.283	0.401	0.682	0.223	0.295	0.539	0.611	0.392	0.245	0.274	0.252
	0.322	0.491	0.353	0.394	0.235	0.144	0.593	0.233	0.249	0.259	0.597	0.277	0.235	0.263	0.355
	0.266	0.538	0.317	0.381	0.384	0.206	0.487	0.206	0.276	0.372	0.918	0.623	0.187	0.251	0.302
	0.469	0.606	0.342	0.455	0.263	0.263	0.477	0.295	0.199	0.221	0.768	0.449	0.241	0.283	0.307
	0.501	0.342	0.292	0.346	0.314	0.192	0.356	0.347	0.269	0.271	0.644	0.286	0.181	0.264	0.238
	0.588	0.794	0.222	0.517	0.285	0.238	0.570	0.232	0.179	0.235	0.631	0.553	0.194	0.246	0.419
	0.569	0.472	0.236	0.606	0.293	0.242	0.410	0.254	0.215	0.304	0.614	0.324	0.262	0.209	0.325
	0.344	0.376	0.293	0.771	0.266	0.224	0.293	0.234	0.185	0.284	0.701	0.295	0.443	0.212	0.219
	0.404	0.355	0.165	0.804	0.269	0.238	0.677	0.354	0.187	0.336	0.429	0.380	0.173	0.244	0.330
	0.650	0.257	0.273	0.723	0.236	0.325	0.790	0.200	0.415	0.233	0.466	0.290	0.258	0.244	0.476
	0.180	0.355	0.398	0.392	0.353	0.160	0.486	0.577	0.200	0.323	0.411	0.391	0.228	0.189	0.665
	0.334	0.887	0.223	0.393	0.325	0.215	0.267	0.213	0.263	0.213	1.004	0.379	0.355	0.261	0.375
	0.262	0.381	0.254	0.547	0.218	0.195	0.436	0.252	0.333	0.328	1.022	0.421	0.263	0.297	0.219
	0.457	0.429	0.295	0.531	0.181	0.338	0.434	0.238	0.249	0.308	0.747	0.338	0.321	0.275	0.332
	0.364	0.243	0.223	0.455	0.327	0.215	0.383	0.257	0.267	0.207	0.343	0.321	0.208	0.216	0.311
	0.629	0.359	0.418	0.423	0.294	0.137	0.320	0.238	0.181	0.286	0.270	0.603	0.439	0.211	0.270
	0.369	0.615	0.320	0.290	0.242	0.183	0.469	0.184	0.276	0.253	0.368	0.502	0.366	0.290	0.289

Sample #	14-Ly-1	14-Ly-2	14-Ly-3	14-Ly-4	14-Ly-5	14-Ly-6	14-Ly-7	14-Ly-8	14-Ly-9	14-Ly-10	14-Ly-11	14-Ly-12	14-Ly-13	14-Ly-14	13-SMG-25
Grainsize (mm)	0.406	0.400	0.233	0.379	0.239	0.247	0.500	0.422	0.359	0.446	0.637	0.307	0.226	0.168	0.176
	0.669	0.259	0.286	0.312	0.176	0.195	0.570	0.257	0.306	0.262	0.497	0.305	0.291	0.293	0.295
	1.003	0.335	0.353	0.229	0.315	0.176	0.432	0.399	0.242	0.333	0.404	0.211	0.231	0.167	0.279
	0.297	0.926	0.341	0.316	0.214	0.260	0.400	0.336	0.310	0.230	0.402	0.232	0.279	0.351	0.419
	0.380	0.308	0.234	0.452	0.229	0.207	0.512	0.377	0.328	0.299	0.640	0.440	0.257	0.194	0.397
	0.454	0.266	0.200	0.450	0.161	0.231	0.566	0.396	0.264	0.253	0.318	0.311	0.243	0.409	0.240
	0.340	0.453	0.273	0.506	0.323	0.229	0.428	0.299	0.248	0.224	0.290	0.503	0.209	0.383	0.258
	0.565	0.675	0.246	0.298	0.342	0.358	0.416	0.269	0.274	0.227	0.244	0.316	0.254	0.225	0.263
	0.602	0.364	0.276	0.245	0.221	0.352	0.240	0.325	0.252	0.410	0.359	0.347	0.373	0.158	0.257
	0.494	0.237	0.183	0.410	0.207	0.341	0.384	0.313	0.223	0.228	0.422	0.357	0.290	0.247	0.268
	0.509	0.409	0.204	0.287	0.230	0.209	0.314	0.275	0.338	0.361	0.293	0.351	0.312	0.257	0.302
	0.529	0.300	0.167	0.368	0.286	0.267	0.293	0.186	0.358	0.334	0.516	0.341	0.213	0.218	0.382
	0.618	0.263	0.199	0.586	0.239	0.378	0.446	0.197	0.195	0.333	0.429	0.300	0.296	0.277	0.710
	0.675	0.329	0.237	0.471	0.187	0.198	0.398	0.189	0.286	0.357	0.537	0.291	0.305	0.239	0.386
	0.450	0.531	0.222	0.417	0.208	0.379	0.373	0.215	0.379	0.457	0.487	0.334	0.435	0.253	0.248
	0.400	0.300	0.293	0.382	0.241	0.198	0.506	0.259	0.282	0.318	0.771	0.603	0.365	0.278	0.291
	0.530	0.366	0.365	0.421	0.430	0.231	0.351	0.211	0.215	0.313	0.815	0.379	0.283	0.334	0.259
	0.933	0.277	0.572	0.382	0.216	0.344	0.507	0.299	0.178	0.353	0.381	0.304	0.243	0.325	0.351
	0.461	0.381	0.452	0.392	0.276	0.207	0.502	0.257	0.218	0.321	0.343	0.272	0.180	0.179	0.507
	0.451	0.348	0.264	0.373	0.176	0.296	0.408	0.228	0.214	0.516	0.333	0.464	0.218	0.222	0.470
	0.285	0.387	0.333	0.428	0.249	0.137	0.576	0.249	0.350	0.279	0.267	0.273	0.176	0.257	0.328
	0.920	0.474	0.328	0.288	0.242	0.173	0.464	0.216	0.162	0.223	0.250	0.554	0.255	0.187	0.354
	0.382	0.308	0.395	0.419	0.212	0.199	1.329	0.244	0.292	0.457	0.492	0.379	0.212	0.200	0.666
	0.527	0.646	0.265	0.547	0.308	0.197	0.450	0.215	0.290	0.295	0.357	0.338	0.272	0.168	0.374
	0.657	0.335	0.318	0.471	0.269	0.267	0.273	0.203	0.201	0.342	0.498	0.457	0.288	0.375	0.258
	0.432	0.361	0.293	0.630	0.290	0.333	0.766	0.225	0.166	0.270	0.564	0.278	0.510	0.212	0.282
	0.256	0.280	0.333	0.327	0.127	0.274	0.407	0.231	0.228	0.437	0.311	0.328	0.304	0.262	0.212
	0.483	0.249	0.470	0.533	0.204	0.367	0.501	0.322	0.419	0.201	0.440	0.357	0.319	0.206	0.273
	0.377	0.312	0.157	0.642	0.180	0.207	0.346	0.329	0.377	0.277	0.299	0.283	0.326	0.219	0.175
	0.342	0.208	0.257	0.405	0.238	0.129	0.315	0.212	0.190	0.270	0.657	0.349	0.196	0.257	0.247
	0.483	0.153	0.274	0.338	0.280	0.247	0.358	0.224	0.305	0.200	0.277	0.485	0.249	0.154	0.220
	0.562	0.286	0.298	0.301	0.319	0.225	0.338	0.235	0.283	0.245	0.441	0.553	0.312	0.316	0.304
	0.668	0.384	0.259	0.344	0.323	0.196	0.301	0.252	0.241	0.384	0.431	0.290	0.470	0.220	0.208
	0.589	0.474	0.312	0.150	0.638	0.150	0.408	0.336	0.195	0.319	0.322	0.196	0.377	0.142	0.372
	0.397	0.570	0.280	0.356	0.181	0.467	0.445	0.309	0.450	0.320	0.411	0.322	0.255	0.216	0.244
	0.781	0.374	0.178	0.346	0.231	0.297	0.485	0.327	0.234	0.420	0.305	0.246	0.282	0.194	0.226
	0.547	0.281	0.214	0.300	0.248	0.184	0.297	0.218	0.269	0.289	0.448	0.433	0.354	0.283	0.260
	0.426	0.257	0.352	0.364	0.216	0.234	0.384	0.324	0.233	0.189	0.269	0.366	0.302	0.260	0.279
	0.394	0.358	0.437	0.249	0.260	0.163	0.566	0.350	0.366	0.178	0.453	0.240	0.388	0.366	0.292
	0.277	0.197	0.236	0.284	0.258	0.263	0.421	0.223	0.292	0.256	0.260	0.244	0.217	0.230	0.153
	0.319	0.478	0.390	0.441	0.238	0.209	0.274	0.396	0.214	0.313	0.277	0.285	0.324	0.388	0.365
	0.513	0.253	0.238	0.417	0.281	0.222	0.636	0.254	0.225	0.255	0.417	0.350	0.224	0.271	0.400
Average	0.467	0.424	0.333	0.483	0.271	0.244	0.491	0.281	0.277	0.324	0.600	0.445	0.285	0.265	0.343

APPENDIX C: MEASURED SECTION

Vertical measure sections, listed from NW to SE across the field area. A reference map is provided below, with the Lycium turbidites highlighted in yellow.

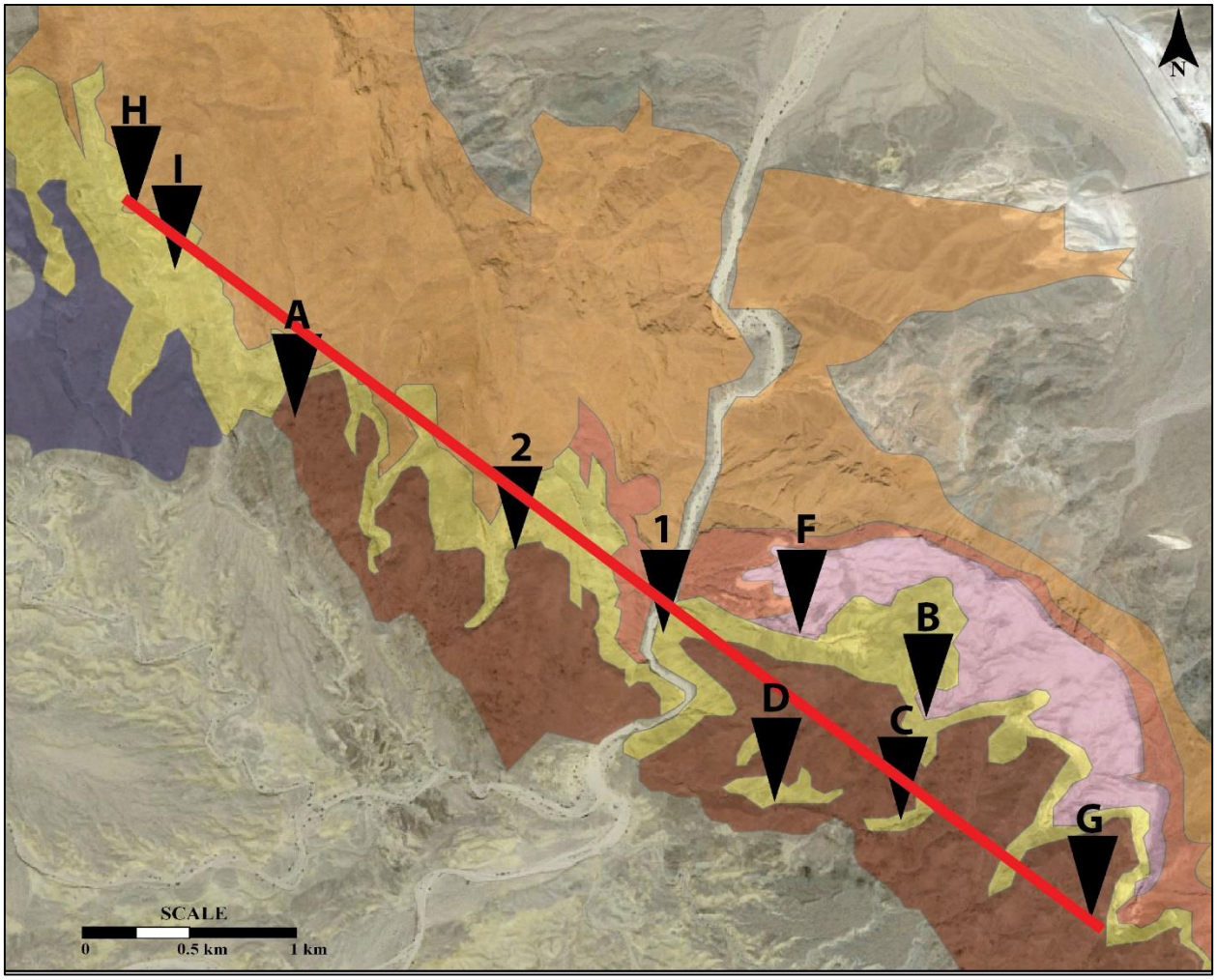

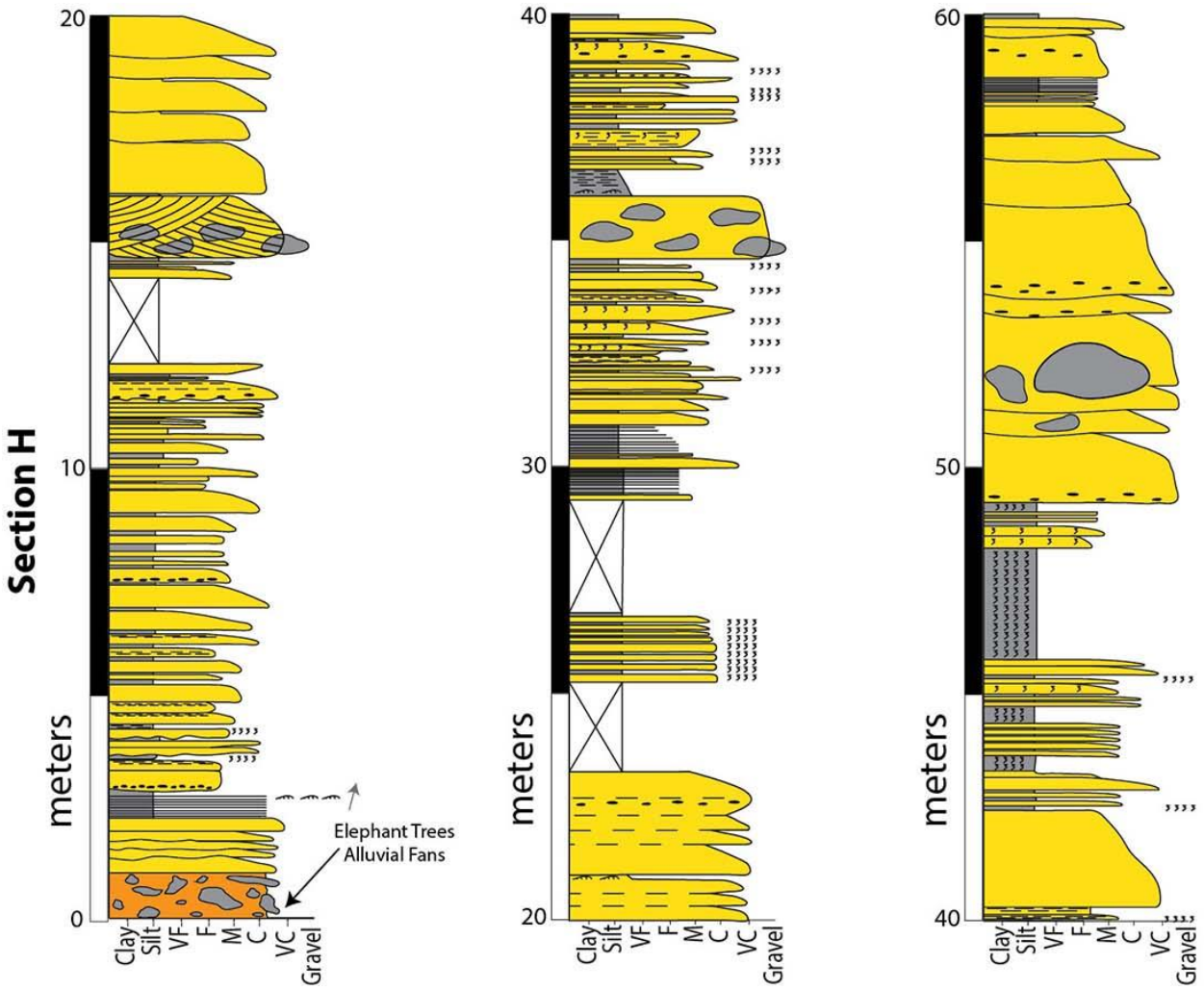

Section H
Latitude: 33.018793°
Longitude: -116.142418°

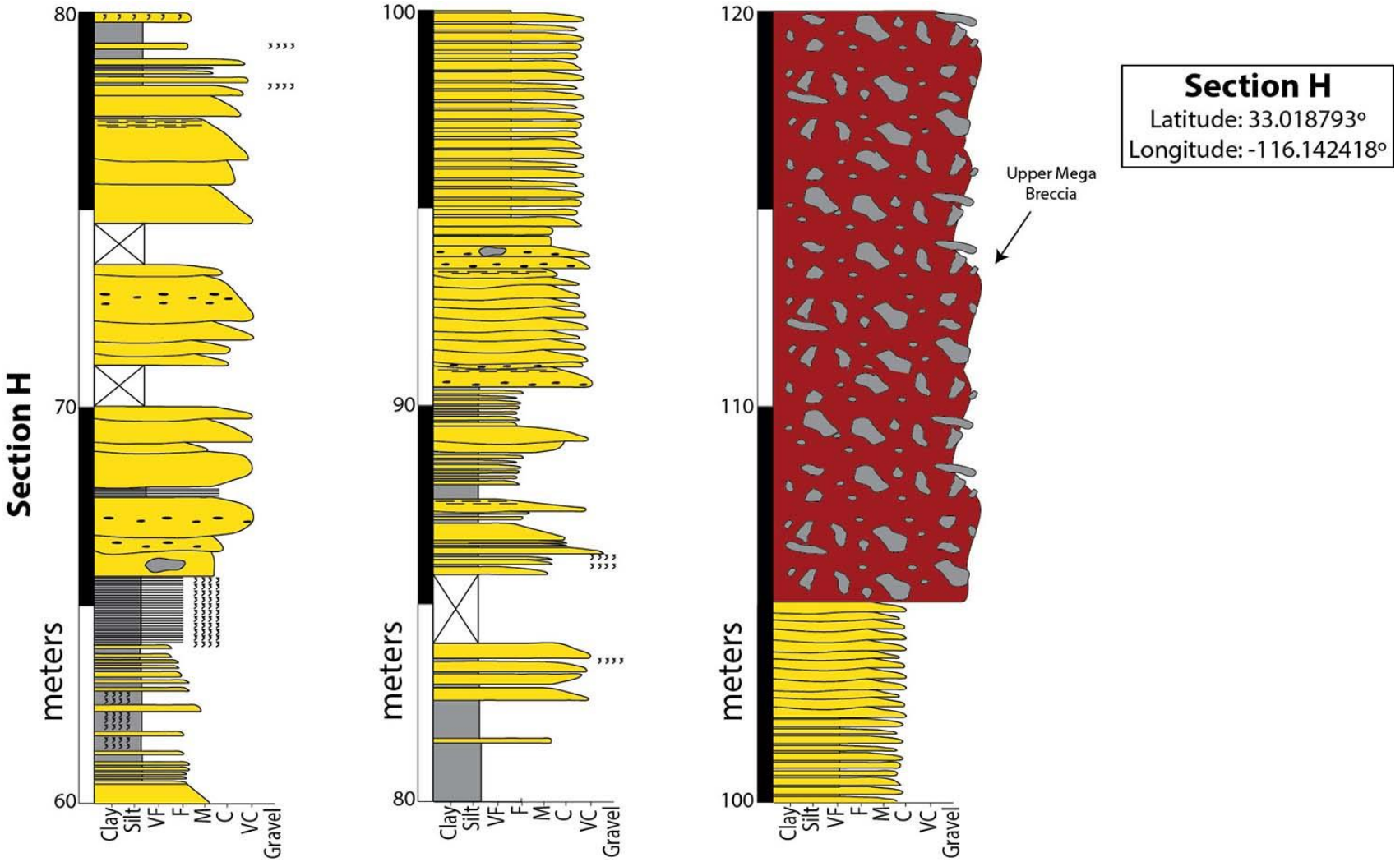
Section H
80
70
60
meters
Clay
Silt
VF
F
M
C
VC
Gravel
100
90
80
meters
Clay
Silt
VF
F
M
C
VC
Gravel
120
110
100
meters
Upper Mega Breccia
Clay
Silt
VF
F
M
C
VC
Gravel
Section H
Latitude: 33.018793°
Longitude: -116.142418°

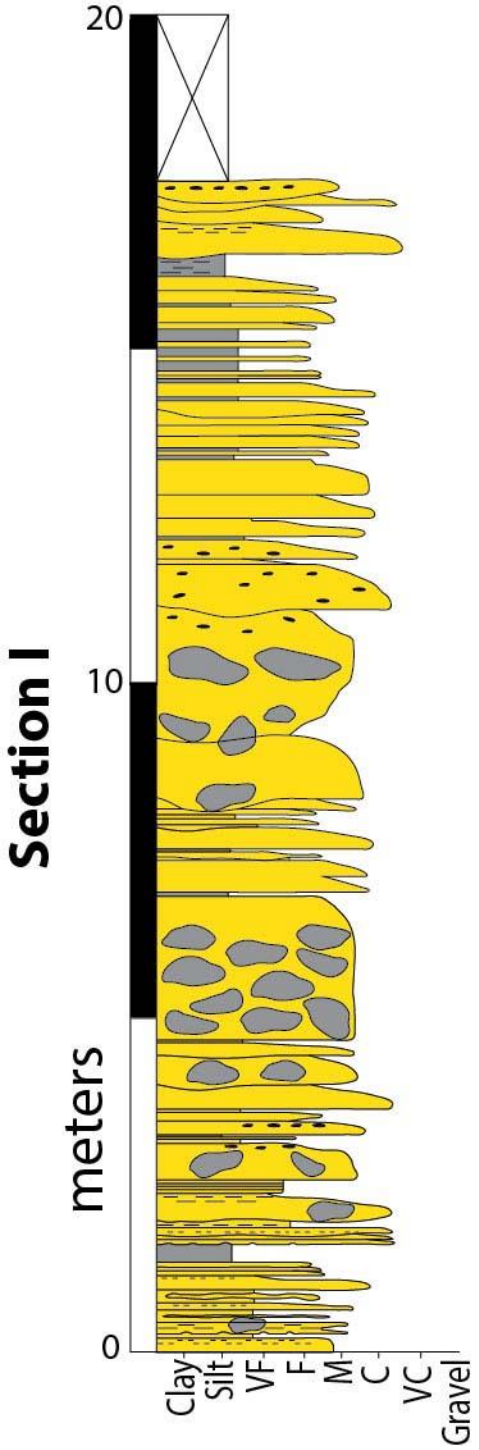

Section I
Latitude: 33.016980°
Longitude: -116.141266°

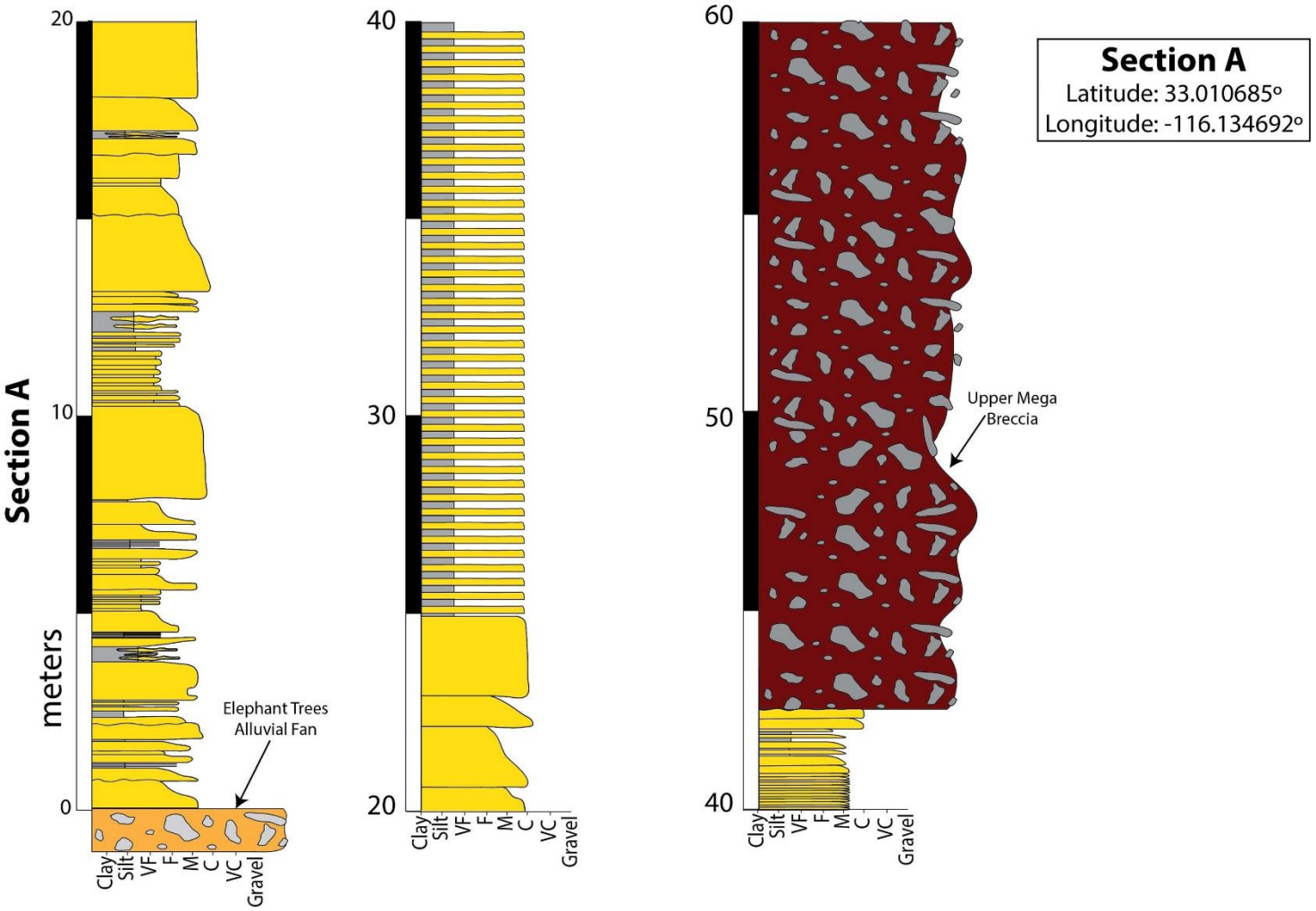
Section A
meters
0
10
20
30
40
50
60
Elephant Trees
Alluvial Fan
Upper Mega
Breccia
Clay
Silt
VF
F
M
C
VC
Gravel
Section A
Latitude: 33.010685°
Longitude: -116.134692°

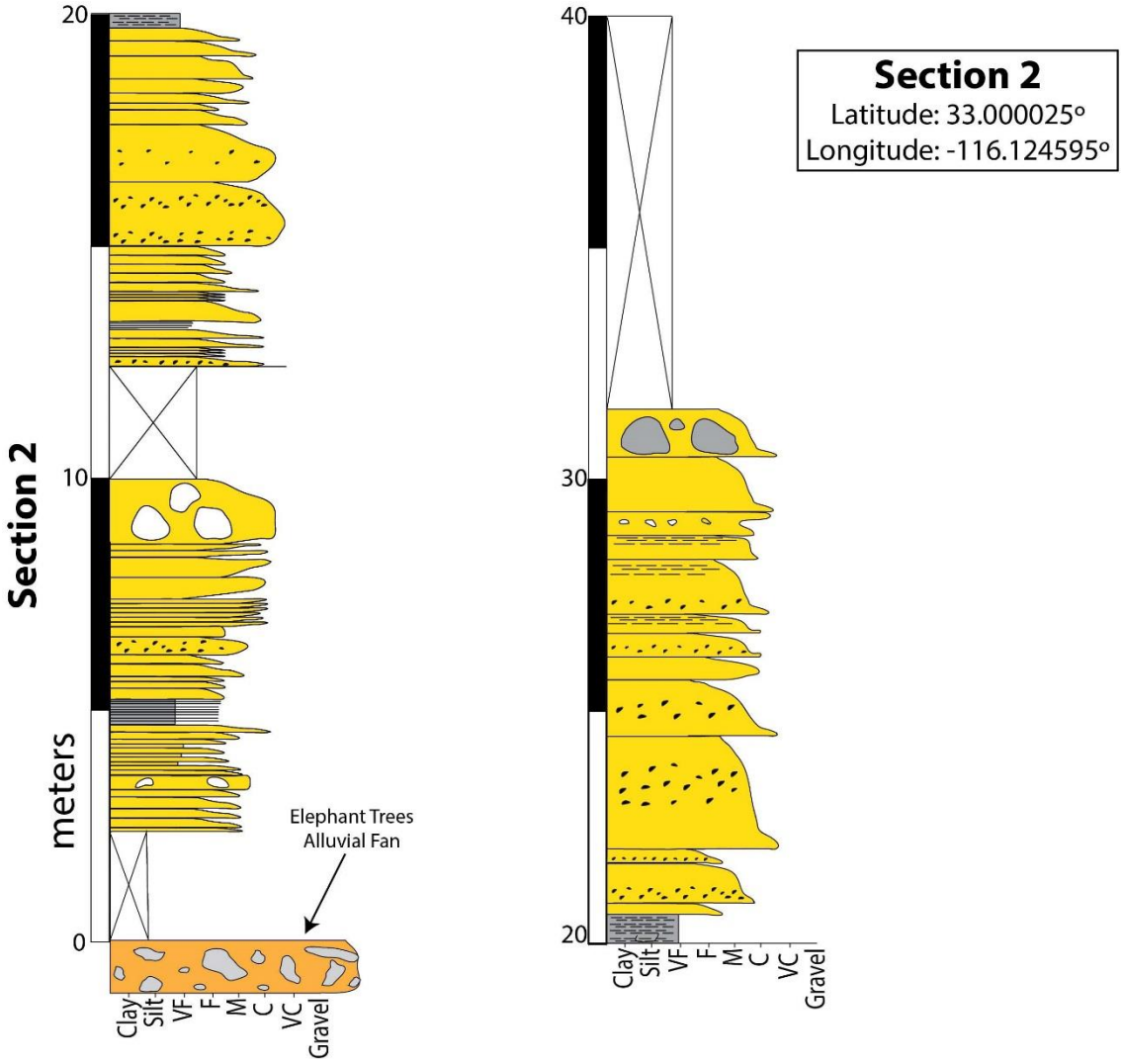
Section 2
Latitude: 33.000025°
Longitude: -116.124595°
Section 2
meters
20
10
0
40
30
20
Elephant Trees
Alluvial Fan
Clay
Silt
VF
F
M
C
VC
Gravel

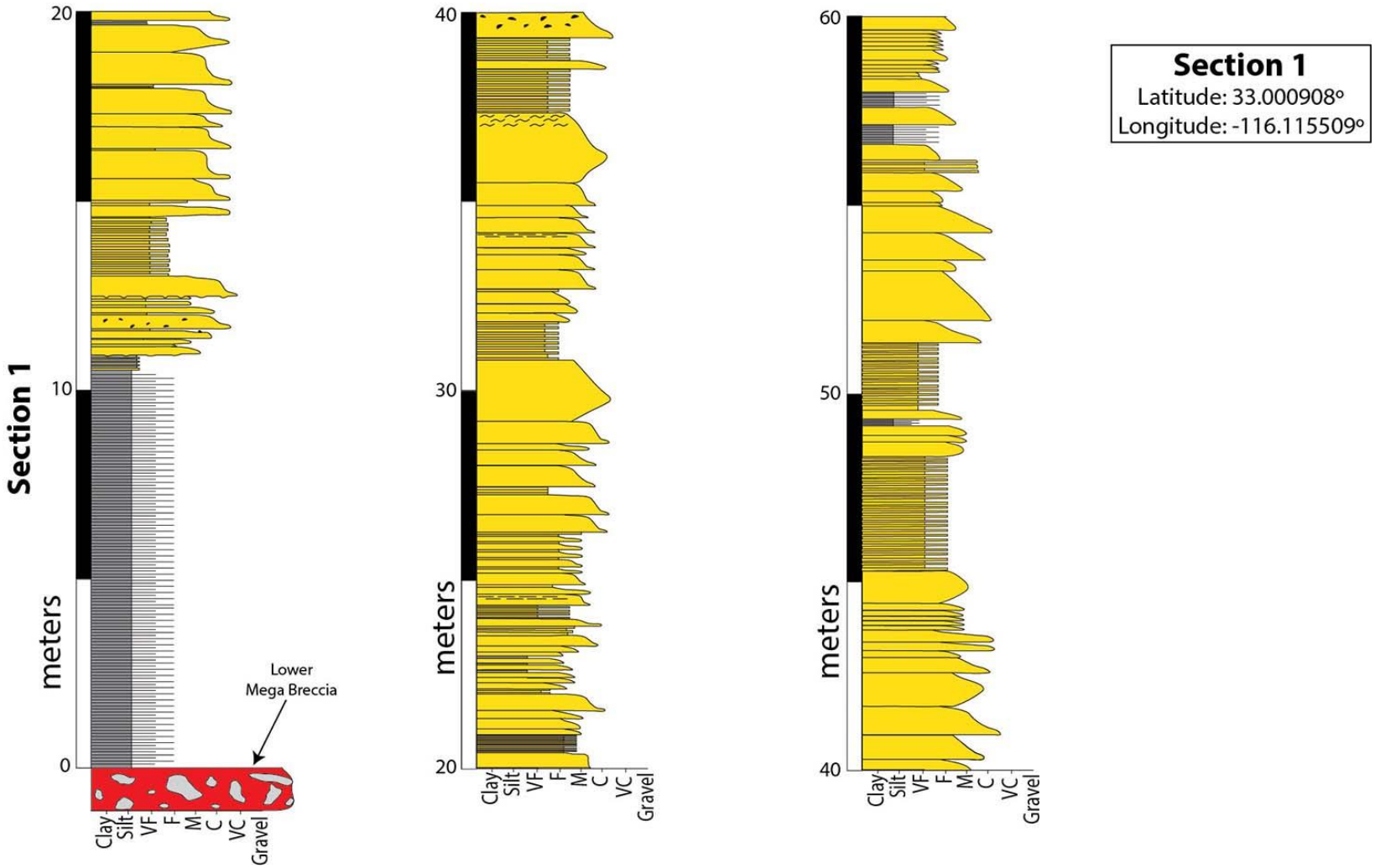
Section 1
meters
20
10
0
Lower
Mega Breccia
Clay
Silt
VF
F
M
C
VC
Gravel
40
30
20
60
50
40
Section 1
Latitude: 33.000908°
Longitude: -116.115509°

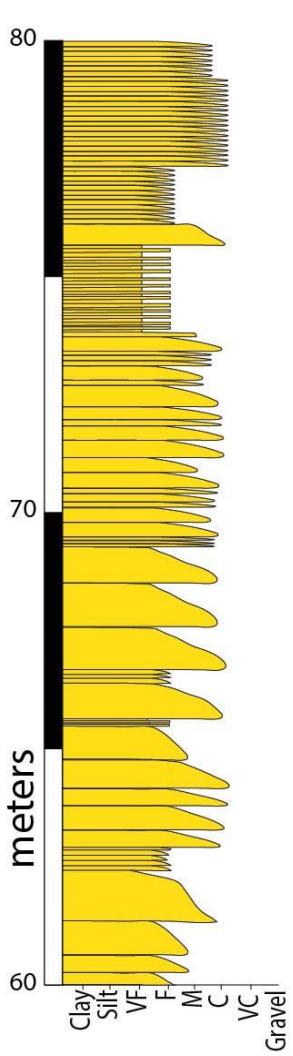

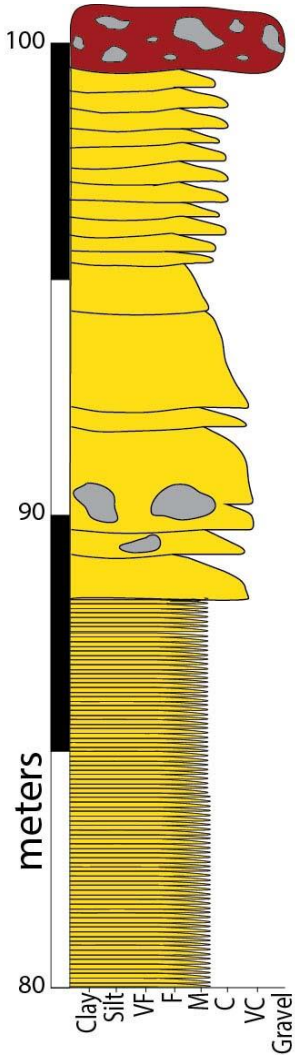

Section 1
Latitude: 33.000908°
Longitude: -116.115509°

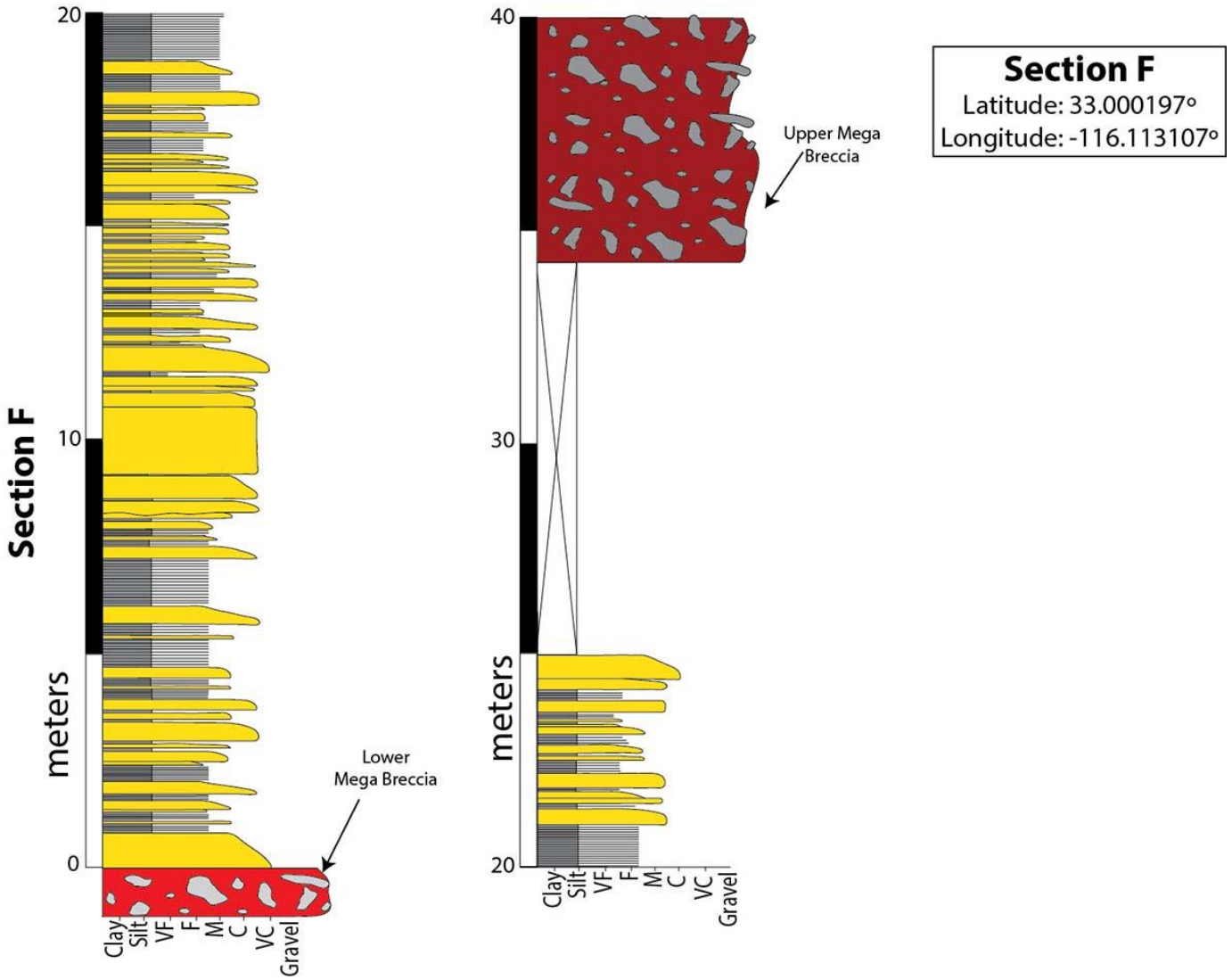
Section F
meters
20
10
0
Lower
Mega Breccia
Clay
Silt
VF
F
M
C
VC
Gravel
40
30
20
Upper Mega
Breccia
Clay
Silt
VF
F
M
C
VC
Gravel
Section F
Latitude: 33.000197°
Longitude: -116.113107°

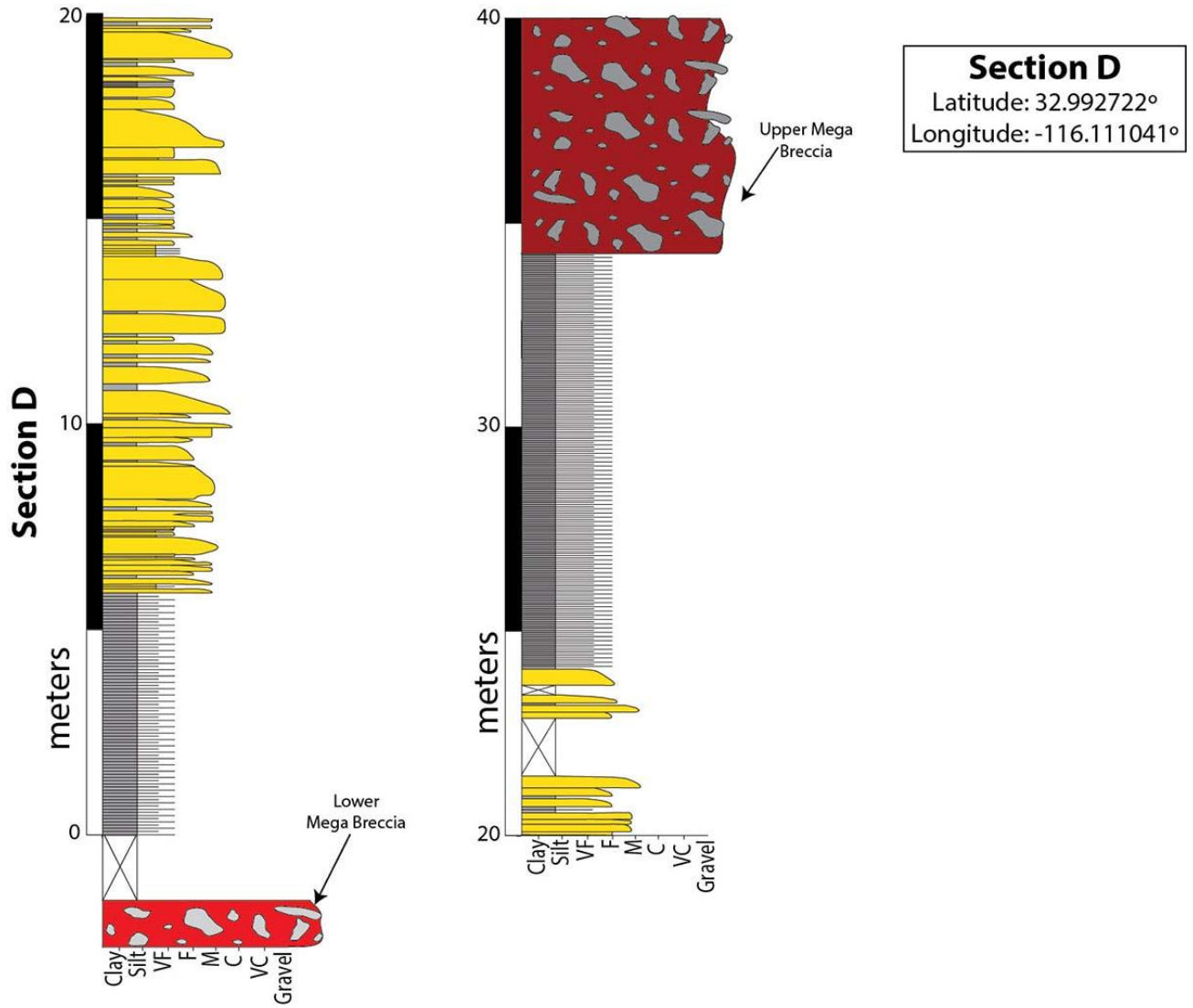
Section D
meters
0
10
20
30
40
Lower
Mega Breccia
Upper Mega
Breccia
Clay
Silt
VF
F
M
C
VC
Gravel
Section D
Latitude: 32.992722°
Longitude: -116.111041°

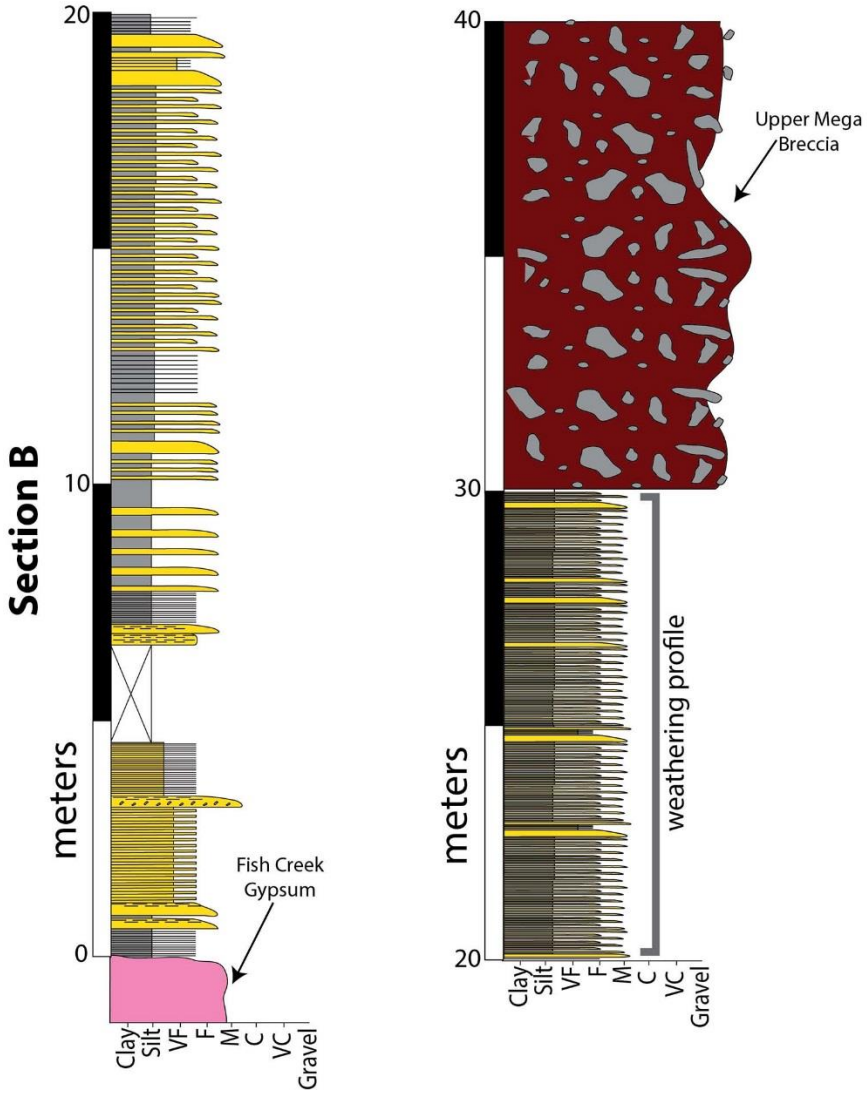

Section B
Latitude: 32.995129°
Longitude: -116.103289°

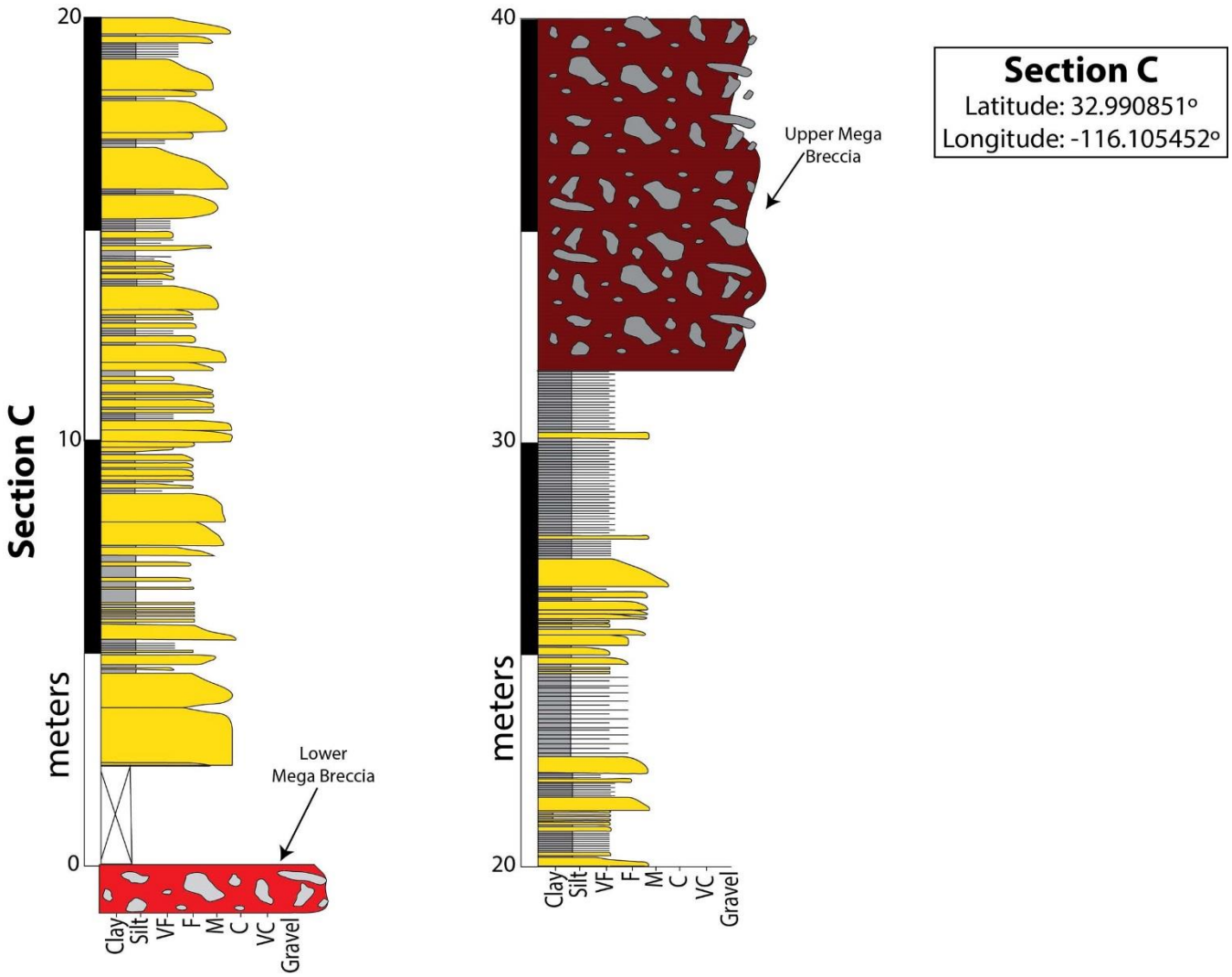

Section C
Latitude: 32.990851°
Longitude: -116.105452°

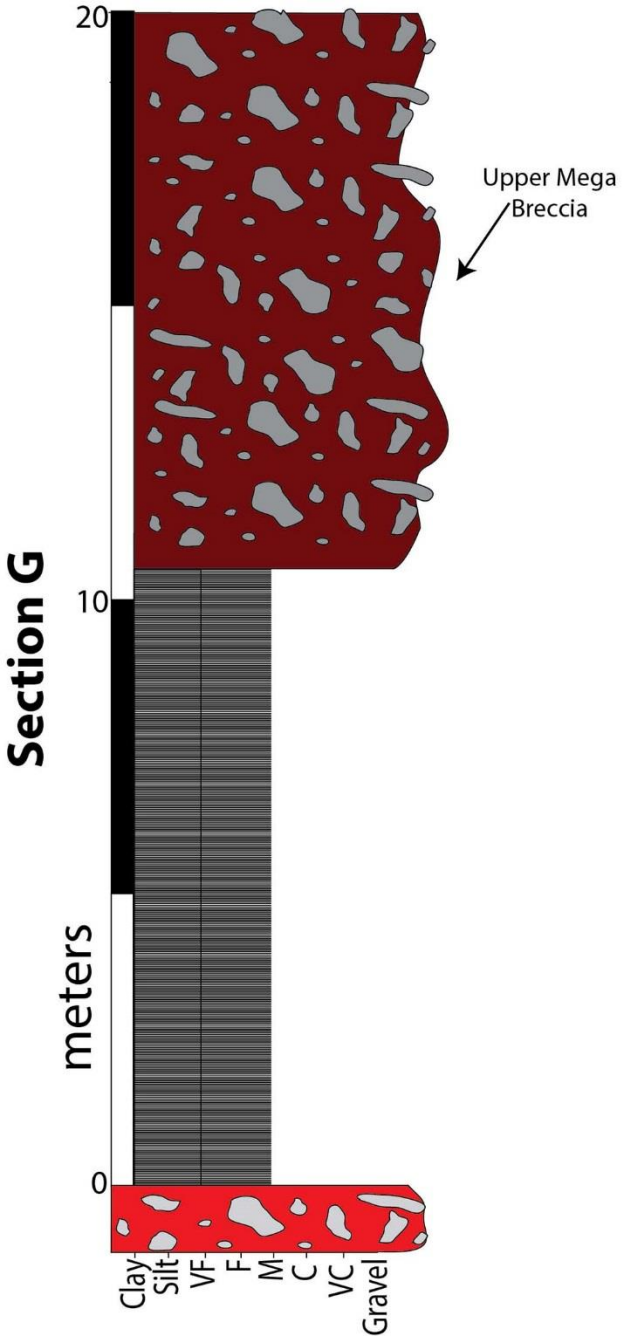

Section G
Latitude: 32.990851°
Longitude: -116.105452°

References

Abbott, Patrick L et al. 2002. "Anza-Borrego Desert State Park , California." XV: 379–400.

Abreu, Vitor, Morgan Sullivan, Carlos Pirmez, and David Mohrig. 2003. "Lateral Accretion Packages (LAPs): An Important Reservoir Element in Deep Water Sinuous Channels." *Marine and Petroleum Geology* 20(6-8): 631–48. http://linkinghub.elsevier.com/retrieve/pii/S026481720300134X (February 27, 2015).

Axen, Gary J., and John M. Fletcher. 1998. "Late Miocene-Pleistocene Extensional Faulting, Northern Gulf of California, Mexico and Salton Trough, California." *International Geology Review* 40(3): 217–44. http://www.tandfonline.com/doi/abs/10.1080/00206819809465207 (March 7, 2015).

Cecil, MR et al. 2012. "Magmatic Growth and Batholithic Root Deevlopment in the Northern Sierra Nevada, California." *Geosphere* 8: 592–606.

Chapin, MA, P Davies, JL Gibson, and HS Pettingill. 1994. "Reservoir Architecture of Turbidite Sheet Sandstones in Laterally Extensive Outcrops, Ross Formation, Western Ireland." *Submarine Fans and Turbidite Systems*: 53–68.

Cloos, Michael Ethan. "Detrital Zircon U-Pb and (U-Th)/ He Geo-Thermochronometry and Submarine Turbidite Fan Development in the Mio-Pliocene Gulf of California , Fish Creek-Vallecito Basin , Southern California APPROVED BY SUPERVISING COMMITTEE :"

Dean, Marlene A. 1988. "Genesis, Mineralogy and Stratigraphy of the NEogene Fish Creek Gypsum, Southwestern Salton Trough, California."

Dickinson, WR. 1985. "Interpreting Provenance Relations from Detrital Modes of Sandstones." *Provenance of Arenites*: 333–61.

Dorsey, R. J. 2010. "Sedimentation and Crustal Recycling along an Active Oblique-Rift Margin: Salton Trough and Northern Gulf of California." *Geology* 38(5): 443–46. http://geology.gsapubs.org/cgi/doi/10.1130/G30698.1 (November 5, 2014).

Dorsey, Rebecca J. et al. 2007. "Chronology of Miocene–Pliocene Deposits at Split Mountain Gorge, Southern California: A Record of Regional Tectonics and Colorado River Evolution." *Geology* 35(1): 57. http://geology.gsapubs.org/cgi/doi/10.1130/G23139A.1 (November 5, 2014).

Dorsey, RJ, Housen, BA, Janecke, SU, Fanning, M and Spears, ALF 2011. "Stratigraphic Record of Basin Development within the San Andreas Fault System: Late Cenozoic Fish Creek-Vallecito Basin, Southern California." *Bulletin of the Geological Society of America* 123(5): 771–93. http://gsabulletin.gsapubs.org/cgi/doi/10.1130/B30168.1 (November 5, 2014).

Dorsey, Rebecca J., Gary J. Axen, Thomas C. Peryam, and Mary E. Kairouz. 2012. "Initiation of the Southern Elsinore Fault at ~1.2 Ma: Evidence from the Fish Creek-Vallecito Basin, Southern California." *Tectonics* 31(2): n/a–n/a. http://doi.wiley.com/10.1029/2011TC003009 (March 7, 2015).

Ehrenberg, S. (1995). Measuring Sandstone Compaction From Modal Analyses of Thin Sections: How to Do It and What The Results Mean. *Journal of Sedimentary Research*, *A65*(2), 369–379.

Folk, R.L. 1980. *Petrology of Sedimentary Rocks*. Austin, TX: Hemphill Publishing Company.

Galloway, W E. 1998. "Siliciclastic Slope and Base-of-Slope Depositional Systems: Component Facies, Stratigraphic Architecture, and Classification." *AAPG Bulletin* 82 (1998)(4): 569–95. http://search.datapages.com/data/doi/10.1306/1D9BC5BB-172D-11D7-8645000102C1865D.

Gardner, Michael H et al. 2003. "Stratigraphic Process-Response Model for Submarine Channels and Related Features from Studies of Permian Brushy Canyon Outcrops, West Texas." *Marine and Petroleum Geology* 20(6-8): 757–87. http://linkinghub.elsevier.com/retrieve/pii/S0264817203001260 (March 19, 2015).

Gazzi, P. 1966. "Le Arenarie Del Flysch Sopracretaceo dell'Appennino Modenese: Correlazioni Con Il Flysch Di Monghidoro." *Mineralogica e Petrografica Acta 12:69 97*.

Grove, M, O Lovera, and M Harrison. 2003. "Late Cretaceous Cooling of the East-Central Peninsular Ranges Batholith (33^ oN): Relationship to La Posta Pluton Emplacement, Laramide Shallow Subduction, and Forearc Sedimentation." *Special Papers-Geological Society of America*: 355–80.

Grundvåg, Sten-Andreas, Erik P. Johannessen, William Helland-Hansen, and Piret Plink-Björklund. 2014. "Depositional Architecture and Evolution of Progradationally Stacked Lobe Complexes in the Eocene Central Basin of Spitsbergen" ed. Peter Talling. *Sedimentology* 61(2): 535–69. http://doi.wiley.com/10.1111/sed.12067 (February 26, 2015).

Hampton, Monty A. 1979. “Buoyancy in Debris Flows.” *SEPM Journal of Sedimentary Research* Vol. 49(3): 753–58. http://jsedres.sepmonline.org/cgi/doi/10.1306/212F7838-2B24-11D7-8648000102C1865D.

Haughton, Peter D. W., Simon P. Barker, and William D. McCaffrey. 2003. “ Debrites in Sand-Rich Turbidite Systems - Origin and Significance.” *Sedimentology* 50(3): 459–82. http://doi.wiley.com/10.1046/j.1365-3091.2003.00560.x.

Hiscott, RN, and GV Middleton. 1980. “Fabric of Coarse Deep-Water Sandstones Tourelle Formation, Quebec, Canada.” *Journal of Sedimentary Petrology* 50(3): 703–22.

Johnson, SD, S Flint, D Hinds, and H De Ville Wickens. 2001. “Anatomy , Geometry and Sequence Stratigraphy of Basin ¯ Oor to Slope Turbidite Systems , Tanqua Karoo , South Africa.”

Van de Kamp, P.C. 1973. “Holocene Continental Sedimentation in the Salton Basin , California : A Reconnaissance.” (March): 827–48.

Kane, I. a., and a. S. M. Ponten. 2012. “Submarine Transitional Flow Deposits in the Paleogene Gulf of Mexico.” *Geology* 40(12): 1119–22. http://geology.gsapubs.org/cgi/doi/10.1130/G33410.1 (December 9, 2014).

Kerr, D.R. 1982. “Early Neogene Continental Sedimentation, Western Salton Trough, California.” San Diego State University.

Kerr, Dennis R. 1984. “Early Neogene Continental Sedimentation in the Vallecito and Fish Creek Mountains, Western Salton Trough, California.” *Sedimentary Geology* 38: 217–46.

Lien, Trond, Roger G. Walker, and Ole J. Martinsen. 2003. “Turbidites in the Upper Carboniferous Ross Formation, Western Ireland: Reconstruction of a Channel and Spillover System.” *Sedimentology* 50(1): 113–48. http://doi.wiley.com/10.1046/j.1365-3091.2003.00541.x.

Lowe, Donald R. 1982. “SEDIMENT GRAVITY FLOWS : II . DEPOSITIONAL MODELS WITH SPECIAL REFERENCE TO THE DEPOSITS OF HIGH-DENSITY TURBIDITY CURRENTS L A Reasonably Clear Picture Has Emerged in Recent Years of the Gravity-Driven Processes That Deliver and Redistribute Coarse Sedim.” 52(1).

Lundegard, P. D. (1992). Sandstone Porosity Loss- A "Big Picture" View of the Importance of compaction. *Journal of Sedimentary Petrology*, *62*(2), 250–260.

McLean, H, and DG Howell. 1985. "Blanca Turbidite System, California." *Submarine Fans and Turbidite Systems*: 167–72.

Merriam, Richard, and Orville L Bandy. 1965. "IN COLORADO DELTA REGION 1." 35(4): 911–16.

Mutti, Emiliano, and WR Normark. 1987. "Comparing Examples of Modern and Ancient Turbidite Systems: Problems and Concepts." *Marine Clastic Sedimentology: Concepts and Case Studies*: 1–38.

Plink-Björklund, Piret, Donatella Mellere, and Ron J Steel. 2001. "TURBIDITE VARIABILITY AND ARCHITECTURE OF SAND-PRONE , DEEP-WATER SLOPES : EOCENE CLINOFORMS IN THE CENTRAL BASIN , SPITSBERGEN." *Journal of Sedimentary Research* 71(6): 895–912.

Rahl, JM et al. 2003. "Combined Single-Grain (U-Th)/He and U/Pb Dating of Detrital Zircons from the Navajo Sandstone, Utah." *Geology* 31(9): 761–64.

Reading, Harold G, and Marcus Richards. "Turbidite Systems in Deep-Water Basin Margins Classified by Grain Size and Feeder System 1." 792–822.

Rotzien, J O N R, and Donald R Lowe. 2014. "PROCESSES OF SEDIMENTATION AND STRATIGRAPHIC ARCHITECTURE OF DEEP-WATER BRAIDED LOBE COMPLEXES : THE PLIOCENE REPETTO AND PICO FORMATIONS , VENTURA BASIN , U . S . A ." (Cartwright 1928): 910–34.

Shirvell, Catherine R., Daniel F. Stockli, Gary J. Axen, and Marty Grove. 2009. "Miocene-Pliocene Exhumation along the West Salton Detachment Fault, Southern California, from (U-Th)/He Thermochronometry of Apatite and Zircon." *Tectonics* 28(2): n/a–n/a. http://doi.wiley.com/10.1029/2007TC002172 (November 5, 2014).

Silver, LT, and B Chappell. 1988. "The Peninsular Ranges Batholith; and Insight into the Evolution of the Cordilleran Batholiths of Southwestern North America." *Transactions of the Royal Society of Edinburgh: Earth Sciences* 79: 105–21.

Talling, Peter J., Douglas G. Masson, Esther J. Sumner, and Giuseppe Malgesini. 2012. "Subaqueous Sediment Density Flows: Depositional Processes and Deposit Types." *Sedimentology* 59(7): 1937–2003. http://doi.wiley.com/10.1111/j.1365-3091.2012.01353.x (December 8, 2014).

Winker, Charles D, and Susan M Kidwell. 1996. *Stratigraphy of a Marine Rift Basin: Neogene of the Western Salton Trough, California*.

Winker, Charles David. 1987. "Neogene Stratigraphy of the Fish Creek-Vallecito Section, Southern California: Implications for Early History of the Norther Gulf of California and Colorado Delta." University of Arizona.

Vita

Sarah Bateman was born in Orlando, FL in 1990. She graduate from Lake Brantley High School in 2008. In August of 2013, she graduate from the University of Florida in Gainesville, FL with a Bachelor of Science in Geology. She attended the University of Texas at Austin in August of 2013 to pursue a Master of Science in Geological Sciences.

Permanent email address: sarahbateman@utexas.edu

This thesis was typed by the author.